Forschungszentrum Jülich
in der Helmholtz-Gemeinschaft

Institut für Kernphysik

Study of pion-nucleon scattering up to 1.9 GeV through a coupled-channels meson-nucleon model

Ashot Gasparyan

Jül-4015

Study of pion-nucleon scattering up to 1.9 GeV through a coupled-channels meson-nucleon model

Ashot Gasparyan

Berichte des Forschungszentrums Jülich ; 4015
ISSN 0944-2952
Institut für Kernphysik Jül-4015
D 5 (Diss., Bonn, Univ., 2002)

Zu beziehen durch: Forschungszentrum Jülich GmbH · Zentralbibliothek
D-52425 Jülich · Bundesrepublik Deutschland
☎ 02461/61-5220 · Telefax: 02461/61-6103 · e-mail: zb-publikation@fz-juelich.de

Abstract

In the present work we study the πN induced reactions in a coupled-channels approach in the range of c.m. energies from the πN threshold up to 1.9 GeV. A meson-exchange model, which includes the channels πN, ηN, as well as three effective $\pi\pi N$ channels namely ρN, $\pi\Delta$, and σN is constructed. Within this framework we systematically investigate the background (non resonant) contributions in the elastic πN scattering for all partial waves with $J \leq 3/2$ and achieve a good agreement with the data at small energies having only a few free parameters. This background also proves to be consistent with the data at higher energies, and this agreement allowed us to include a number of the N^* and Δ resonances, and to describe the πN data in the whole energy range considered. Simultaneously, a reasonable agreement with the data is obtained for the total $\pi N \to \rho N$ and total and differential $\pi N \to \eta N$ transition cross sections. The importance of higher partial waves for those reactions is emphasized. The connection of the πN dynamics in the S_{11} partial wave to the reaction $\pi N \to \eta N$ is discussed.

Contents

Chapter 1

Introduction

1.1 Strong interactions at medium energies

One of the main problems related to the physics of the standard model is to connect the realization of the strong interactions at low and medium energies to the underlying theory, namely Quantum Chromo Dynamics (QCD). The dynamical degrees of freedom of this theory are quarks and gluons – objects that carry the so-called color charge. At extremely high energies QCD can be well studied applying perturbative methods. However at low and medium energies the appropriate degrees of freedom are the physically observable states – colorless mesons and baryons. This is due to the phenomenon called confinement. There is a wealth of data available for reactions involving mesons and baryons in many reaction channels. A detailed study of those data including the analysis of the resonances in various systems should bring us closer to an understanding of the confining mechanism and the non perturbative regime of QCD.

One of the reactions studied very intensively is pion–nucleon scattering. The available data show rich structures pointing to many baryonic resonances. Actually, the analysis of the πN system was so far one of the best sources for the information on those resonances. Some very interesting patterns could be observed. E.g. there is a resonance in the P_{11} partial wave (the so-called Roper resonance) that is hard to understand in terms of standard quark models. However, within a meson exchange model, that will be discussed in detail below, it was possible to explain

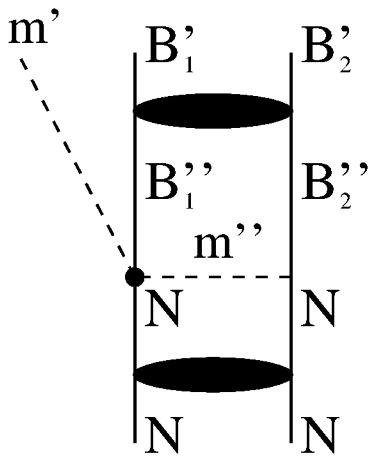

Figure 1.1: Typical diagram corresponding to the m''-meson exchange contribution to the m'-meson production process in NN collisions. Ellipsis denote the initial NN interaction and the interaction of two baryons B_1' and B_2' in the final state.

this particular resonance as being due to the interaction of the nucleon with the surrounding pion cloud alone, thus not having a three quark core (for a detailed discussion c.f. [1]). Naturally the question arises, if there are other resonances that could be generated dynamically, since an understanding of the nature of the resonances may shed light on the mechanism of the confinement. Of course, for such an investigation it is crucial to properly treat the background contributions.

A detailed knowledge of the πN elastic and inelastic scattering is also important when studying the processes of meson production in various reactions. E.g. one of the main mechanisms that is believed to contribute to the meson production amplitude in NN collisions can be represented by the diagram, shown in fig. 1.1, where the produced meson can be π, η, K (associated with $\Lambda(\Sigma)$), and so on. These reactions are of specific interest, because many accurate experiments on them have been carried out recently and are being carried out at the moment and these data provide a rich testing ground for the validity of the meson-exchange picture (see e.g. [2]). In order to have a consistent description of such processes one has to apply meson-baryon (solid dot in fig. 1.1) and baryon-baryon (ellipses) models, in which the off-shell extension of the amplitudes is done in the same framework. Investigations along this line were carried out, e.g., for the reactions

$NN \to NN\pi$ [3] and $NN \to NN\eta$ [4].

The aim of our present work is to start with the existing Jülich πN model and improve it in such a way that it enables one to describe the transition processes from πN to the channels like ηN, $K\Lambda$, $K\Sigma$, ωN. This requires, of course, a simultaneous description of the πN elastic channel at corresponding energies and explicit inclusion of all relevant N^* and Δ resonances, besides those which are generated dynamically by the model.

1.2 Theoretical models of the πN reactions

The low energy πN scattering can be systematically studied by means of the chiral perturbation theory [5], which represents the application of the effective field theoretical methods to the strong interactions at low energies. However, a treatment within this approach is limited to energies close to the πN threshold. In particular, when the phase shift in some partial wave starts to exceed $\sim 20°$ the perturbative methods do not work and a unitarization procedure is needed.

The simplest models describing πN processes in the resonance region are separable models [6–8]. Those models treat each partial wave independently, and, therefore, should be considered as parameterizations of the πN data rather than providing us with a dynamical understanding of the reaction. One should note here, however, that such models can generate resonances dynamically via the solution of the scattering equation. There are also studies that use the lowest order chiral Lagrangian as a separable kernel of the scattering equation [9–11]. One of the latest works in this direction is by Inoue et al. [11]. The authors consider S-wave scattering in the system of coupled channels πN, $\pi\pi N$, and ηN. The lowest S-wave resonances are generated dynamically. However, such methods can hardly reveal the real structure of resonances, when only one partial wave is considered.

Another class of models is based on the so-called K-matrix approximation [12–16]. In this case one uses the Born term for the K-matrix, that still leads to a unitary T-matrix. In this approach one can treat different partial waves simultaneously. However, the possibility to generate resonant states dynamically is lost. From the various studies along this line we would like to mention specifically a quite recent work [16], which describes πN induced reactions in all important channels mentioned above over a wide energy range.

Finally, there exist meson exchange models of the πN interaction [17–21]. They preserve some features of the effective field theories (in the sense that they are based on the effective Lagrangian formalism, and the potential derived from this is consistent with the symmetries of the underlying theory namely QCD), but at the same time allow one to include non-perturbative effects via infinite iterations of the meson-exchange potential. Note that in meson-exchange models the background (which represents the non-resonant contributions, e.i. t and u channel exchanges) is rather well constrained in the sense, that it contributes to all partial waves. Therefore adjusting the background for each partial wave individually is impossible. The existing meson-exchange models, however, either do not extend to the resonance energies (except may be for $\Delta(1232)$) or do not take into account all relevant channels.

1.3 Jülich πN model

The Jülich πN model was originally constructed to describe elastic πN data not far from threshold [22]. One of the main novelties of the model was treating the σ and ρ-meson t-channel exchanges as correlated pion pairs exchange, using the dispersion relations technique. Later the model was extended to higher energies by including several inelastic channels namely three effective $\pi\pi N$ channels (σN, ρN, and $\Delta\pi$) and the ηN channel [1,23]. The treatment of correlated $\pi\pi$-exchange was made more consistent and transparent in ref. [24]. The possibility of generating resonances dynamically was also systematically studied. It turned out, that only one of them, namely the Roper resonance, can be understood in this way in the framework of the Jülich πN model [1,23]. Other resonances like $S_{11}(1535)$, $S_{11}(1650)$, $D_{13}(1520)$, and $\Delta(1232)$ had to be included explicitly.

Unfortunately, a straightforward extension of the model to even higher energies by proceeding in the same way, namely by introducing further resonances (in other partial waves) and by including additional channels proved to be impossible due to several reasons. First of all the existing background in some partial waves was incompatible with the data in the sense that it did not reproduce the experimental phase shifts well above the position of the resonance, as it should. Therefore, the parameters of the model have to be readjusted in such a way that the background provides already a good qualitative reproduction of the πN phase shifts over the extended energy range, and allow one to include resonances.

The second problem was a strong influence of the $N^*(1650)$ resonance on the low energy S_{11} phase shift. In fact it gave the main contribution to the S_{11} even at threshold, which is, of course, unphysical. Moreover, this artificial strong influence of the resonance tail makes the results very sensitive to the details of other contributions, and therefore is rather impractical if one wants to change something in the model.

Another drawback of the existing πN model is an unsatisfactory description of the inelasticity parameter in the S_{11} partial wave, and the simultaneous overestimation of the $\pi N \to \eta N$ cross section close to the ηN threshold. These two related problems are believed to be due to insufficiencies in the treatment of the $\pi\pi N$ channel and we will show in this thesis that they can be solved by introduction of additional strength in the $\pi\pi N$ channel in the S_{11}.

Note that the S_{11} partial wave is of particular importance, because it plays a very significant role for the ηN and $K\Lambda$ channels close to their thresholds. For $\pi N \to \eta N$ as well as $\pi N \to K\Lambda$ experimental information on the transition cross sections and also differential cross sections and polarization observables are available. An analysis of those data within our model requires a consistent description of the S_{11} πN partial wave in the relevant energy range. Moreover, a detailed knowledge of the resonance structures in the ηN channel is needed if one wishes to describe the η production in NN collisions, including the isospin dependence of the cross section and angular distributions [4]. The $\pi N \to K\Lambda(\Sigma)$ transition amplitude plays an important role in studies of $\Lambda(\Sigma)$ production in NN collisions. It enters into the rescattering diagram of the type shown in fig. 1.1 with the pion as exchange particle m''. The interference of this pion-rescattering contribution with the K-exchange graph is crucial when considering the cross section ratio $\sigma(pp \to pK\Lambda)/\sigma(pp \to pK\Sigma)$ [25,26]. The energy dependence of this ratio should depend strongly on the details of the $\pi N \to K\Lambda(\Sigma)$ amplitudes [27].

In the present work we remedy the above-mentioned deficiencies of the present πN Jülich model. For the time being, apart from the $\pi\pi N$ channel (described effectively via the σN, ρN, and $\Delta\pi$ channels) only the ηN channel is taken into account. However, the inclusion of the $K\Lambda$ channel (and possibly ωN and $K\Sigma$) is expected to be straightforward within the new improved model.

The work is organized as follows. In chapter 2 the main ingredients of our the πN model are described. Chapter 3 is devoted to the details of the treatment of the correlated two-pion exchange. The problems related to 3-body intermediate states are discussed in chapter 4. In chapter 5 we present the results of the model for the πN elastic scattering, and also for the $\pi N \to \rho N$ and $\pi N \to \eta N$ transitions. The main part ends with the chapter 6, where we make some concluding remarks.

Chapter 2

Description of the Model

In this chapter we survey the formalism of the coupled channel meson exchange model for πN induced two particle reactions. We start with the channels that are relevant in the energy region we are interested in. Then we derive the Lippmann-Schwinger equation for the scattering amplitude. Finally we construct the effective potential from the phenomenological Lagrangian.

2.1 Open channels

The πN scattering remains a purely elastic process (with respect to strong interactions) up to the two pion production threshold. If we go higher in energy then more inelastic channels open (fig. 2.1). All these production processes contribute to the inelasticity of the πN scattering amplitude.

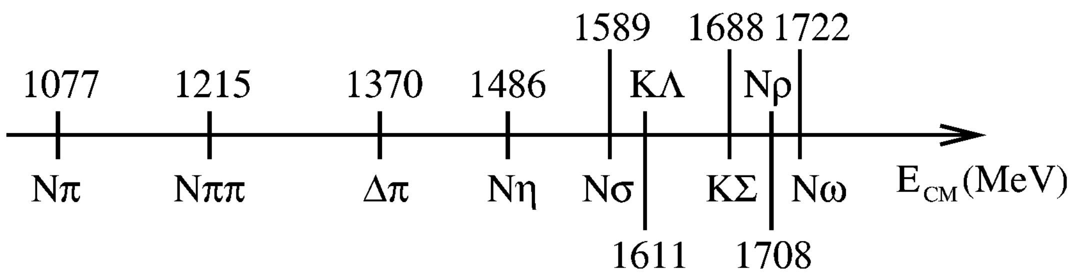

Figure 2.1: Open channels coupled to πN system in the energy range under consideration.

Our goal is to describe the πN data in a rather wide energy range: from the πN threshold up to the η production threshold and beyond. Therefore in order to have intrinsic consistency we build a coupled channels model i.e. we consider all diagonal and non-diagonal transitions between various channels simultaneously. In this work the following channels are taken into account: πN, $\pi\Delta$, ηN, σN and ρN.

Although one of the most important inelastic channels is the $\pi\pi N$ channel it is rather complicated to treat it explicitly due to the necessity to deal with three body dynamics. Instead we model this channel by effective two body channels [28].

The σN channel is introduced to allow for the strong S-wave $\pi\pi$ correlation in the $\pi\pi N$ system. This effective channel in particular has a sizable impact on the P_{11} partial wave. One should note that the nominal σN threshold shown in fig. 2.1 has no physical meaning, because the two pion mass distribution produced by the effective σ-meson is very broad. Thus, this channel gets important almost from the very $\pi\pi N$ threshold. The channels $\pi\Delta$ and ρN reflect the correlations in the πN and $\pi\pi$ subsystems, corresponding to the excitations of Δ and ρ resonances respectively. Similar to the situation with the σN channel, the influence of the ρN channel extends to somewhat lower energies than its nominal threshold, due to the large width of the ρ meson.

We are not able to compute any observable for the unstable particles like Δ, or σ in the initial or final state (only for ρ it can be done). This is due to some technical subtleties which are discussed in chapter 4. But nevertheless one can have them as intermediate states, thereby providing a contribution to the πN inelasticities.

Although we do not compare our results to any $\pi\pi N$ data we need several effective 2-body channels since they have different energy dependence. E.g. the structures in those πN amplitudes that can be described by the $\pi\Delta$ channel can not be reproduced by the ρN channel and so on. The isospin structure of those channels is also different, e.g. σN is a pure $I = 1/2$ state, whereas $\pi\Delta$ as well as ρN have $I = 1/2$ and also $I = 3/2$ components.

On the other hand for reactions like $\pi N \to \eta N$, $K\Lambda$, $K\Sigma$, ωN one can calculate any observable within the approach used in the present work. Therefore they can be compared to available experimental data which imposes additional constraints on the model. At present only the lowest channel, namely ηN is included.

2.2 Effective Lagrangian

The effective Lagrangian approach is very popular and useful in low energy hadronic physics. The basic idea of this method is the following. The QCD Lagrangian, which is believed to describe strong interactions of particles, is written in terms of quark and gluon as degrees of freedom. However, it is known that in the low energy regime QCD is highly non-perturbative. The appropriate degrees of freedom at this energy scale are the physical states: mesons and baryons. Therefore one constructs a Lagrangian in terms of these physical degrees of freedom but at the same time maintains the symmetries of the underlying fundamental theory. An approximate symmetry group of the QCD Lagrangian is (chiral) $SU(2) \times SU(2)$ (that means that the Lagrangian is invariant under the independent isospin rotation of left and right-handed quark fields). Thus this symmetry is used as a guideline when constructing the effective Lagrangian.

Since we want to incorporate vector mesons in our model, such as $\rho, a_1, \ldots$, we need a Lagrangian including vector fields. There are detailed studies of a general form of effective Lagrangians involving vector mesons consistent with chiral symmetry (e.g. [29], [30]). For our purposes we take the Lagrangian in a simple form suggested by Wess and Zumino in [31]. Here we shortly explain the approach used when constructing this Lagrangian. We follow the notations of [31].

One starts with the nonlinear σ model. The basic ingredients are the pion ($\vec{\phi}$) and nucleon (N) fields . It is convenient to introduce auxiliary fields: $\xi = \vec{\phi}\vec{\tau}/F_\pi$ and $\psi = [(1+i\gamma_5\xi)/(1+\xi^2)^{1/2}]N$ where $\vec{\tau}$ are the usual τ matrices (cf. appendix C), and $F_\pi = 93$ MeV is the pion decay constant. By a chiral transformation they transform in the following way:

$$N \rightarrow e^{i\beta} N \tag{2.1}$$

$$\xi \rightarrow e^{i\beta} \xi e^{-i\beta} \tag{2.2}$$

$$\psi \rightarrow e^{i\alpha\gamma_5} \psi \tag{2.3}$$

$$\frac{1-i\gamma_5\xi}{1+i\gamma_5\xi} \rightarrow e^{-i\alpha\gamma_5} \frac{1-i\gamma_5\xi}{1+i\gamma_5\xi} e^{-i\alpha\gamma_5} \tag{2.4}$$

where $\alpha = \vec{\alpha}\vec{\tau}$ and $\beta = \vec{\beta}\vec{\tau}$ are the parameters of the axial and vector $SU(2)$ transformations, respectively. The simplest chiral invariant Lagrangian has the form:

$$\mathcal{L} = \bar{\psi}\gamma_\mu i\partial_\mu\psi - m_N\bar{N}N \tag{2.5}$$

Vector mesons are introduced by gauging this model. The procedure is economical in the sense that it minimizes the number of parameters. Gauging means that one allows the parameters α and β to be coordinate-dependent. To preserve the invariance of the Lagrangian one has to introduce a vector gauge field

$$\rho_\mu = \vec{\rho}_\mu\vec{\tau} \tag{2.6}$$

and an axial gauge field

$$a_\mu = \vec{a}_\mu\vec{\tau}. \tag{2.7}$$

These fields correspond to the physical ρ and a_1 mesons. Then an infinitesimal gauge transformation takes the form

$$\delta\rho_\mu = i[\beta, \rho_\mu] + (2/g)\partial_\mu\beta, \tag{2.8}$$
$$\delta a_\mu = i[\beta, a_\mu] \tag{2.9}$$

for the vector transformation and

$$\delta a_\mu = i[\alpha, \rho_\mu] + (2/g)\partial_\mu\alpha, \tag{2.10}$$
$$\delta\rho_\mu = i[\alpha, a_\mu] \tag{2.11}$$

for the axial transformation. Here the coupling constant $g \equiv g_\rho \equiv g_{\rho\pi\pi} = 2g_{\rho NN}$ is related to F_π via the KSFR relation [32], [33] $F_\pi = (\sqrt{2}m_\rho/g)$. The invariants of this gauge group are constructed in the usual way, via covariant derivatives and field strength tensors. The Wess-Zumino Lagrangian contains three parts: one, which is fully gauge invariant, the mass terms of the vector mesons, which are only globally $SU(2) \times SU(2)$ invariant, and a pion mass term which possesses only isospin symmetry.

The complete Wess-Zumino Lagrangian is rather lengthy. Thus we only take from it those terms which are relevant for us, namely the πNN, ρNN, $\rho\pi\pi$, $a_1\rho\pi$

vertices, the $\pi\pi NN$ and $\pi\rho NN$ contact terms, and so on. The whole list of the interaction terms of our effective Lagrangian is given in appendix B.

Let us consider the free parameters that are present in the Lagrangian of [31]. The $\rho\pi\pi$ coupling is given by

$$\mathcal{L}_{\rho\pi\pi} = -g_\rho(\vec{\pi} \times \partial_\mu \vec{\pi}) \cdot \vec{\rho}^\mu + (\frac{1}{2} - \kappa)(\partial_\mu \vec{\pi} \times \partial_\nu \vec{\pi}) \cdot (\partial^\mu \vec{\rho}^\nu - \partial^\nu \vec{\rho}^\mu). \tag{2.12}$$

where the parameter κ is arbitrary, i.e. not constrained by symmetries. We make the simple choice $\kappa = 1/2$, that eliminates the second term in (2.12). One should emphasize that all other parameters in the Wess-Zumino Lagrangian are fixed, and related to each other.

Note that the whole approach described in [31] is applicable in the case of $SU(3)$ flavor symmetry, i.e. one can construct interaction terms involving, for example, the η meson in the same way.

Let us mention some other interaction vertices which are included into the Lagrangian and not present in [31]. All terms containing Δ and σ are taken over from [34]. The ωNN vertex is constructed in the same way as the ρNN vertex except for the isospin structure, whereas the structure of the $\omega\rho\pi$ term is taken from [35]. For the $a_0\pi\eta$ vertex we choose a scalar coupling. For couplings of heavy N^* and Δ resonances to the meson-baryon system we take the simplest structures that provide a reasonable description of data. The coupling constants at those additional vertices are mostly extracted from the literature, but some of them remain free. They are listed in chapter 5.

2.3 TOPT and scattering equation

In the present work we use the formalism of the so-called Time Ordered ("old fashioned", non-covariant) Perturbation Theory (TOPT) [36–38] to obtain the effective potential and the scattering amplitude of the πN induced reactions. The advantage of this approach over the covariant one is that all integrals to be computed are explicitly three dimensional, which reduces greatly the complications of the numerical calculations (mostly because of a simpler singularity structure).

Of course this is only true when simplifying assumptions about the potential are made, which are discussed later in this section.

First of all TOPT is based on the Hamiltonian approach. A Hamiltonian density is obtained from the Lagrangian by means of a Legendre transformation

$$\mathcal{H} = \sum_j \frac{\delta \mathcal{L}}{\delta \dot{\Phi}_j} \dot{\Phi}_j - \mathcal{L}, \tag{2.13}$$

where the Φ_j denote all the fields entering into the Lagrangian. Then $\mathcal{H}$ is to be expressed in terms of Φ_j and the canonical conjugates $\Pi_j = \frac{\delta \mathcal{L}}{\delta \dot{\Phi}_j}$:

$$\mathcal{H} = \mathcal{H}^0 - \mathcal{L}_{\text{int}} + \mathcal{H}_{\text{ct}}. \tag{2.14}$$

Here one divides $\mathcal{H}$ into a free particle part $\mathcal{H}^0$ and an interacting part which contains non-covariant TOPT contact terms $\mathcal{H}_{\text{ct}}$. Those appear, if the interaction terms of Lagrangian $\mathcal{L}_{\text{int}}$ depend on time derivatives of fields $\dot{\Phi}_j$, or if there are non-dynamical fields in $\mathcal{L}$, such as zeroth component of vector field [39]. The Hamiltonian is obtained from its density performing the spatial integration:

$$H = \int \mathcal{H}(x) d^3x = H^0 + H_I \tag{2.15}$$

Again we divide H into free and interacting parts. The scattering matrix in terms of the interaction Hamiltonian has the form

$$S = \lim_{t \to \infty, t_0 \to -\infty} \hat{U}(t, t_0), \tag{2.16}$$

where $\hat{U}(t,t_0) = e^{iH_0 t} e^{-iH(t-t_0)} e^{-iH_0 t_0}$ is the evolution operator in the interaction representation. Taking into account the energy conservation in the transition from the initial state i to the final state f one can define the $\mathcal{T}$-operator by

$$S_{fi} \equiv \delta_{fi} - i(2\pi)\delta(E_f - E_i)\mathcal{T}_{fi}. \tag{2.17}$$

Here δ_{fi} denotes the unit matrix, E_i and E_f are the initial and final energies respectively. At this stage $\mathcal{T}$ is defined on energy shell.

Our goal is to reduce the problem to a 2-body scattering equation since we are interested only in 2-body transition amplitudes. We present here a simplified schematic derivation, omitting all the subtleties of quantum field theory. Nevertheless this formal derivation does not miss the physical content of the considered approach. It is known (see e.g. [40]) that $\mathcal{T}$ can be written in the following form:

$$\mathcal{T} = H_I + H_I \frac{1}{E - H + i\epsilon} H_I = H_I + H_I \frac{1}{E - H_0 - H_I + i\epsilon} H_I \tag{2.18}$$

Performing some formal manipulations and expanding $\mathcal{T}$ into a power series in H_I, assuming that the latter is a small perturbation, one gets:

$$\mathcal{T} = H_I \frac{1}{1 - \mathcal{G} H_I} = H_I + H_I \mathcal{G} H_I + H_I \mathcal{G} H_I \mathcal{G} H_I + \dots \tag{2.19}$$

where

$$\mathcal{G} = \frac{1}{E - H_0 + i\epsilon} = \sum_n \frac{|n\rangle\langle\, n\,|}{E - E_n + i\epsilon} \tag{2.20}$$

is the Green's function of free particle states. The summation in the r.h.s. is performed over all possible multi-particle states, and the sum Σ denotes the integration over the continuum and the summation over discrete variables.

The perturbation series (2.19) can be related to a set of diagrams, where the matrix elements of H_I –as usual– correspond to the vertices. The rules relating a diagram and the corresponding matrix element are similar to the standard Feynman rules (see e.g. [41]), with the slight differences, described in section 2.4.

Since we are interested only in 2-body initial and final states, it is convenient to isolate also the 2-body intermediate states, reducing the problem to an effective 2-body equation. We define

$$\mathcal{G} = \tilde{\mathcal{G}} + \mathcal{G}^{(2)}, \tag{2.21}$$

where

$$\tilde{\mathcal{G}} = \sum_{\tilde{n}} \frac{|\tilde{n}\rangle\langle\, \tilde{n}\,|}{E - E_{\tilde{n}} + i\epsilon}; \; \mathcal{G}^{(2)} = \sum_{n^{(2)}} \frac{\left|n^{(2)}\right\rangle\left\langle\, n^{(2)}\,\right|}{E - E_{n^{(2)}} + i\epsilon}. \tag{2.22}$$

Here the sum over $n^{(2)}$ includes now only 2-particle intermediate states, the sum over $\tilde{n}$ contains the rest. Then we have

$$\begin{aligned} \mathcal{T} &= H_I(1 - (\tilde{\mathcal{G}} + \mathcal{G}^{(2)})H_I)^{-1} = H_I \left(\left(1 - \mathcal{G}^{(2)} H_I \frac{1}{1 - \tilde{\mathcal{G}} H_I}\right) \left(1 - \tilde{\mathcal{G}} H_I\right) \right)^{-1} \\ &= H_I \frac{1}{1 - \tilde{\mathcal{G}} H_I} \left(1 - \mathcal{G}^{(2)} H_I \frac{1}{1 - \tilde{\mathcal{G}} H_I}\right)^{-1} = \mathcal{V} \frac{1}{1 - \mathcal{G}^{(2)} \mathcal{V}}. \end{aligned} \tag{2.23}$$

Here we define the effective potential operator in the following way:

$$\mathcal{V} = H_I \frac{1}{1 - \tilde{\mathcal{G}} H_I} = H_I \sum_{k=0}^{\infty} \left(\sum_{\tilde{n}} \frac{|\tilde{n}\rangle\langle \tilde{n} \,|\, H_I}{E - E_{\tilde{n}} + i\epsilon} \right)^k . \tag{2.24}$$

Eq. (2.18) - (2.24) can be generalized to the off-shell case, i.e. when $E \neq E_i \neq E_f$. For this off-shell $\mathcal{T}$ one can derive from (2.24) the equation:

$$\mathcal{T} = \mathcal{V} + \mathcal{V}\mathcal{G}^{(2)}\mathcal{T} \tag{2.25}$$

or in matrix notation

$$\mathcal{T}_{fi} = \mathcal{V}_{fi} + \sum_j \frac{\mathcal{V}_{fj}\mathcal{T}_{ji}}{E - E_j + i\epsilon}. \tag{2.26}$$

Now all states i, f, j are two-body ones, and the sum Σ stands for the integration over the 3-momenta of the particles $\vec{q}_1$ and $\vec{q}_2$ ($\int d^3q_1 d^3q_2$; we use a normalization $\langle \vec{q} \,|\, \vec{q}\,' \rangle = \delta(\vec{q} - \vec{q}\,')$) and summation over the type of the particles and the spin variables. The energy in the intermediate system is a sum of baryon and meson on-shell energies $E_j = E_{q_1} + \omega_{q_2} = \sqrt{M_B + q_1^2} + \sqrt{m_M + q_2^2}$, where M_B and m_M are baryon and meson masses, respectively.

The matrix element $\mathcal{V}_{fi}$, as seen from (2.24) can be easily interpreted as a set of all two-particle irreducible diagrams, i.e. those that cannot be disconnected by cutting off two of their internal lines. Its calculation will be considered in the subsequent section.

To make a final step to obtain a scattering equation let us choose the system of reference to be the center of mass system of two particles, that is natural for our problem. In this system the total momenta of initial and final particles $\vec{p}_1 + \vec{p}_2 = \vec{p}_3 + \vec{p}_4 = \vec{0}$. Making use of the momentum conservation the reaction matrix T and the potential matrix V are introduced:

$$\begin{aligned}\langle \vec{p}_4, \vec{p}_3, \lambda_3, \lambda_4, \mu, I, I_3 \,|\, \mathcal{T}(\mathrm{E}) \,|\vec{p}_1, \vec{p}_2, \lambda_1, \lambda_2, \nu, I, I_3\rangle \\ = \delta(\vec{p}_1 + \vec{p}_2 - \vec{p}_3 - \vec{p}_4) T^I_{\mu\nu}(E, \vec{k}', \lambda', \vec{k}, \lambda)\end{aligned} \tag{2.27}$$

$$\begin{aligned}\langle \vec{p}_4, \vec{p}_3, \lambda_3, \lambda_4, \mu, I, I_3 \,|\, \mathcal{V}(\mathrm{E}) \,|\vec{p}_1, \vec{p}_2, \lambda_1, \lambda_2, \nu, I, I_3\rangle \\ = \delta(\vec{p}_1 + \vec{p}_2 - \vec{p}_3 - \vec{p}_4) V^I_{\mu\nu}(E, \vec{k}', \lambda', \vec{k}, \lambda)\end{aligned} \tag{2.28}$$

Here $\vec{k} = \vec{p}_1 = -\vec{p}_2$ and $\vec{k}' = \vec{p}_3 = -\vec{p}_4$. The different 2-particle channels (πN, ηN,...) are marked by indices μ and ν. In addition to them we have an isospin index I. It is convenient to work in the isospin basis, since V and T are diagonal in total isospin I and its projection I_3 and are independent of I_3, because of isospin conservation in the strong interactions. The treatment of spin states is done in helicity basis, which is very convenient when dealing with a relativistic two-body problem [42]. The corresponding helicities of initial and final particles are λ_1, λ_2, λ_3, λ_4, or, for shortness λ and λ'. After that equation (2.26) takes the form

$$T^I_{\mu\nu}(\vec{k}',\lambda',\vec{k},\lambda) = V^I_{\mu\nu}(\vec{k}',\lambda',\vec{k},\lambda)+ \\ \sum_\gamma\sum_{\lambda''}\int d^3k'' V^I_{\mu\gamma}(\vec{k}',\lambda',\vec{k}'',\lambda'')\frac{1}{Z-E_\gamma(k'')+i\epsilon}T^I_{\gamma\nu}(\vec{k}'',\lambda'',\vec{k},\lambda). \quad (2.29)$$

Henceforth we omit the dependence of V and T on the center of mass energy which is denoted here by Z. Equations (2.29), (2.25), (2.26) have the same form as the well known Lippmann-Schwinger equation ([43]).

Because of rotational invariance of the strong interactions and, as a consequence, angular momentum conservation, states with a fixed angular momentum J decouple in the Lippmann-Schwinger equation. Moreover, since the total angular momentum J is a sum of the orbital angular momentum L and the total spin of the system S, there may be only a limited number of states with fixed L coupled to each other. Because of this reason one usually solves the equation in the JLS basis, where it takes the form of a one dimensional integral equation:

$$\langle L'S'k'|T^{IJ}_{\mu\nu}|LSk\rangle = \langle L'S'k'|V^{IJ}_{\mu\nu}|LSk\rangle+ \\ \sum_{\gamma,L''S''}\int k''^2dk''\langle L'S'k'|V^{IJ}_{\mu\gamma}|L''S''k''\rangle\frac{1}{Z-E_\gamma(k'')+i\epsilon}\langle L''S''k''|T^{IJ}_{\gamma\nu}|LSk\rangle. \quad (2.30)$$

The details of the transformation from plain-wave helicity basis to JLS basis are described in Appendix D.

Note that close to any production threshold the production amplitude is proportional to $k'^{(L')}$, where "prime" denotes the produced system, and consequently inclusion of only the lowest partial waves is sufficient if one wants to calculate observables like the $\pi N \to \eta N$ cross section. Thus we restrict ourselves to partial waves with $J \leq 3/2$. Of course, with such a restriction one cannot hope to describe the elastic πN cross section far from the πN threshold. Instead we have to use the existing partial wave analysis [44, 45] to constrain the parameters of the model.

2.4 Construction of the potential

As has been stated before the effective potential (2.24) contains an infinite set of two particle irreducible diagrams, because intermediate states can consist of an arbitrary number of particles. In practice of course one has to truncate this series. In our potential we only kept those diagrams that contain 3 or less particles in the intermediate state. This leads to the following classification of different contributions.

- Diagrams with three body intermediate states. Those correspond to t-channel exchange of $\pi, \rho, \sigma, \omega, a_1$ mesons and u-channel nucleon and Δ exchanges. The treatment of ρ and σ exchanges in the $\pi N \to \pi N$ potential differs from the general picture, because in this case we consider those mesons as correlated $\pi\pi$ pairs. Chapter 3 is dedicated to this question.
- Contact terms. There are 2 sources of contact terms: those which arise from the Wess-Zumino Lagrangian for vector mesons, and non-covariant TOPT contact terms.
- Diagrams with one particle in the intermediate state, or pole graphs. Except for the nucleon pole graph they all correspond to s-channel resonance contributions. The first two types of diagrams represent in this sense "background" contribution.

All diagrams can be computed using the standard Feynmann rules [41]. The difference from the covariant approach is that the zeroth components of the momenta of intermediate particles entering into vertices have to be put on mass shell, and the propagators have the form following from (2.24), i.e $\frac{1}{Z-E_1-E_2-E_3}$ for t and u-exchange diagrams, and $\frac{1}{Z-M_{res}}$ for resonance graphs. Here E_1, E_2, E_3 and M_{res}

are the on-shell energies of the intermediate particles and a resonance, respectively. In the latter case the on-shell center of mass energy is equal to the mass of the resonance.

Notice that both t as well as u exchange diagrams always appear in pairs, because in the intermediate state one can emit either a particle or its antiparticle (even if they coincide). These are the so-called first and second time orderings. For example, if there is u-exchange by a baryon B'' in the transition between two baryon-meson states Bm and $B'm'$ via the intermediate state $B''mm'$, one always gets in addition an intermediate $B\bar{B}''B'$ state. Or in the case of t-exchange by a meson m'' there appear two intermediate states $B'm''m'$ and $B\bar{m}''m$. The sum of the two time ordering is equal to the Feynmann expression for a given diagram if initial and final particles are on mass shell. When these two expressions are not equal there is always a corresponding TOPT contact term, that restores the equivalence.

All the diagrams which constitute the potential are depicted in fig. 2.2-2.8. Pole graphs are shown separately in fig. 2.8. Their specific feature is that each of the resonances contributes only to one particular partial wave. In principle resonances can couple to all Bm channels allowed by quantum numbers, but for practical reason we introduce bare couplings only to those channels on which they have physical impact. The expressions corresponding to every diagram are presented in appendix B.

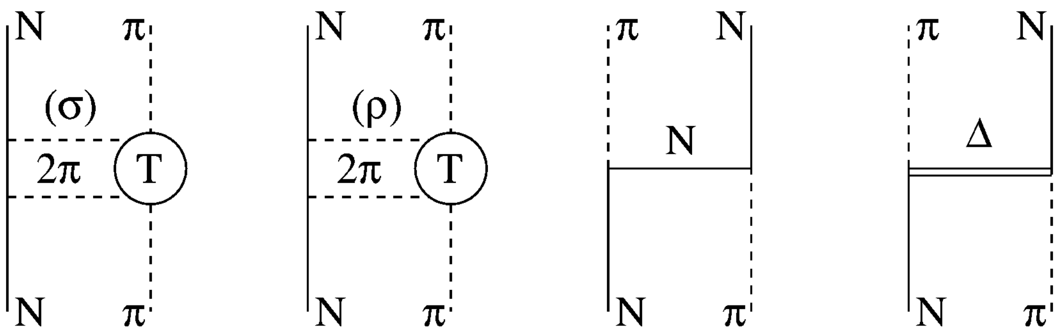

Figure 2.2: Diagrams entering into elastic πNpotential.

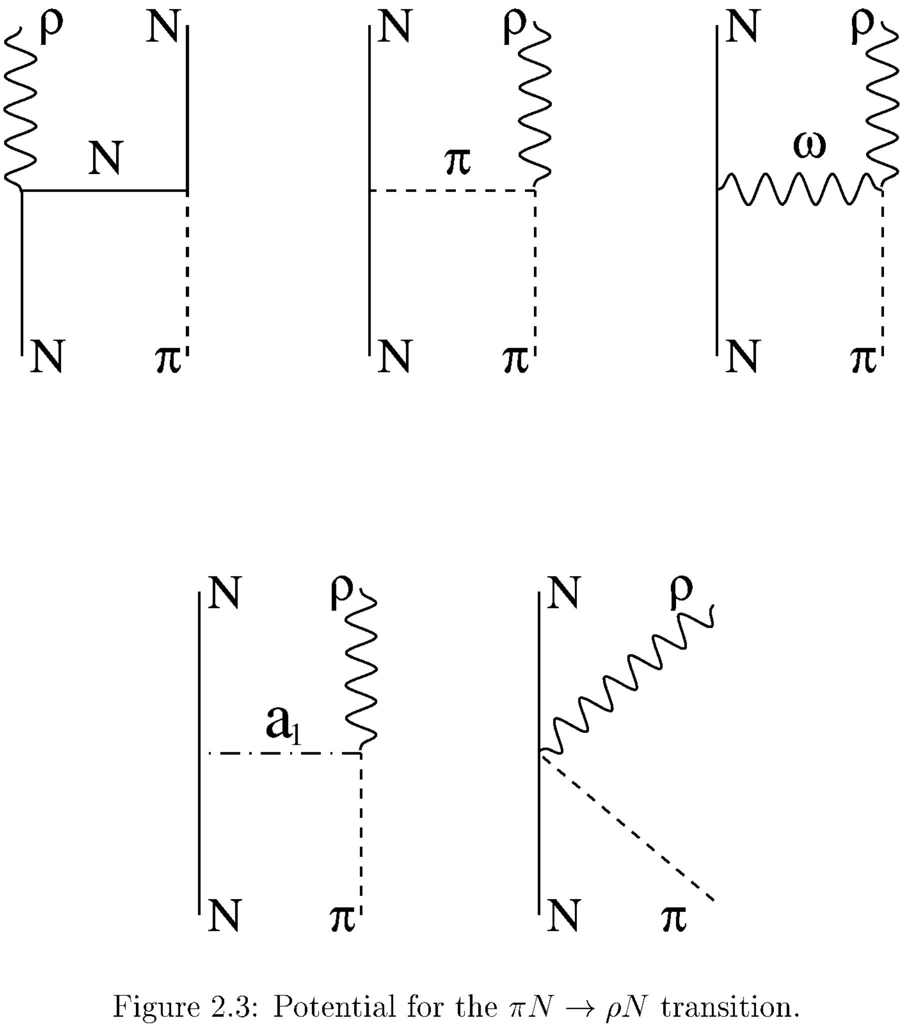

Figure 2.3: Potential for the $\pi N \to \rho N$ transition.

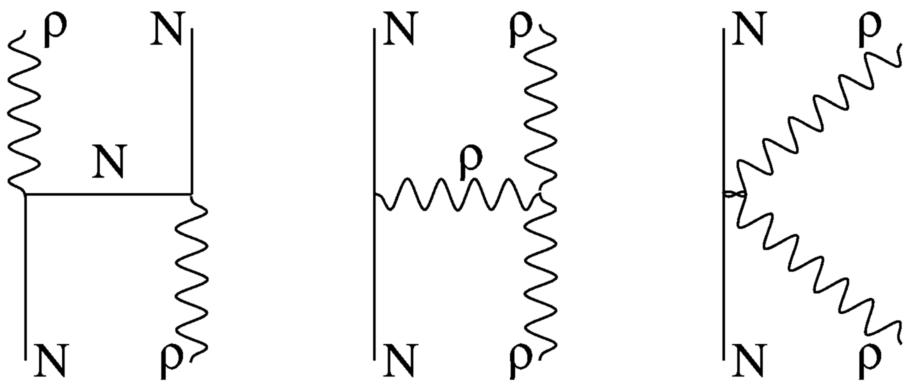

Figure 2.4: The $\rho N \to \rho N$ graphs.

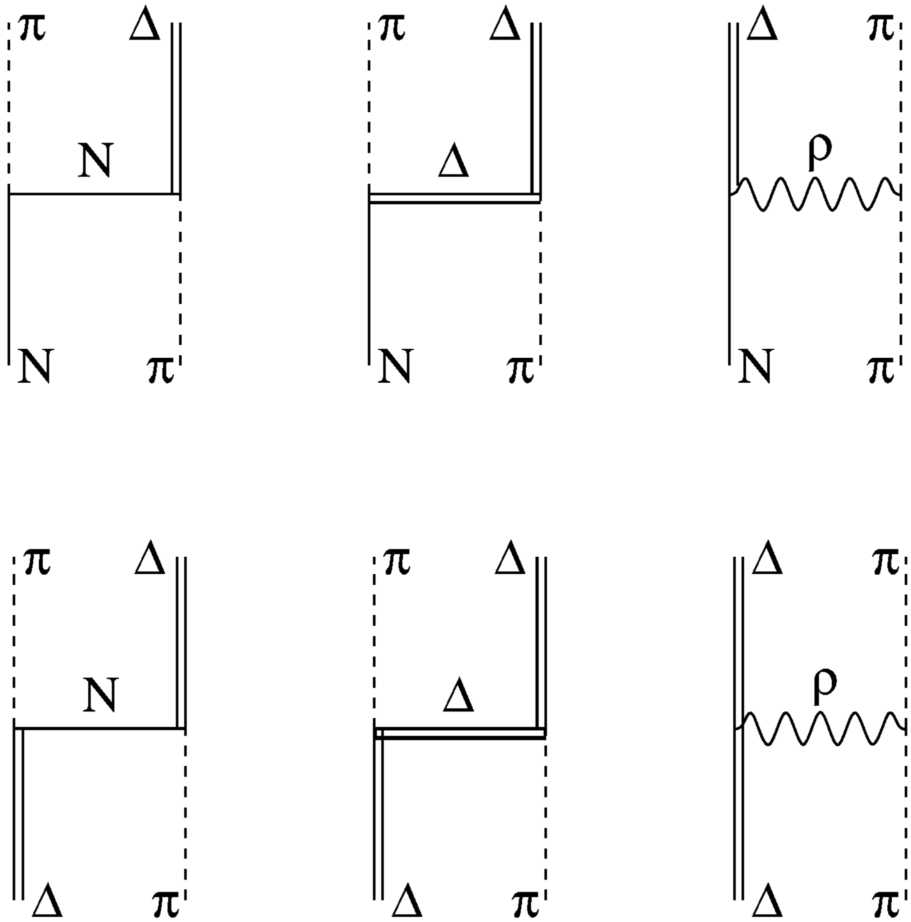

Figure 2.5: Diagrams of $\pi N \to \pi\Delta$ and $\pi\Delta \to \pi\Delta$ potential.

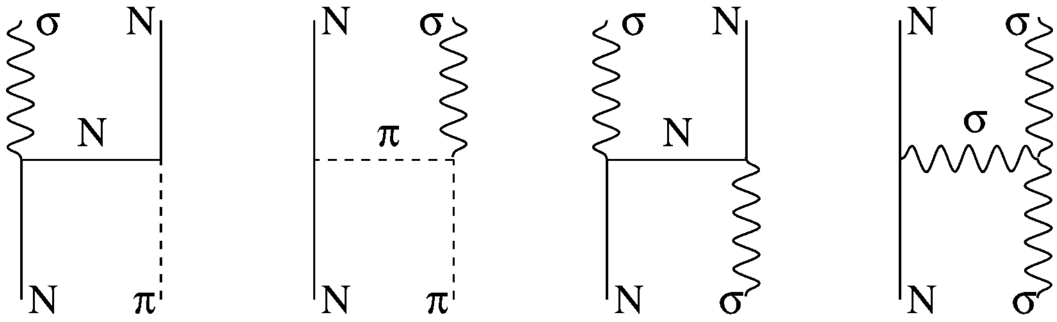

Figure 2.6: Transitions $\pi N \to \sigma N$ and $\sigma N \to \sigma N$.

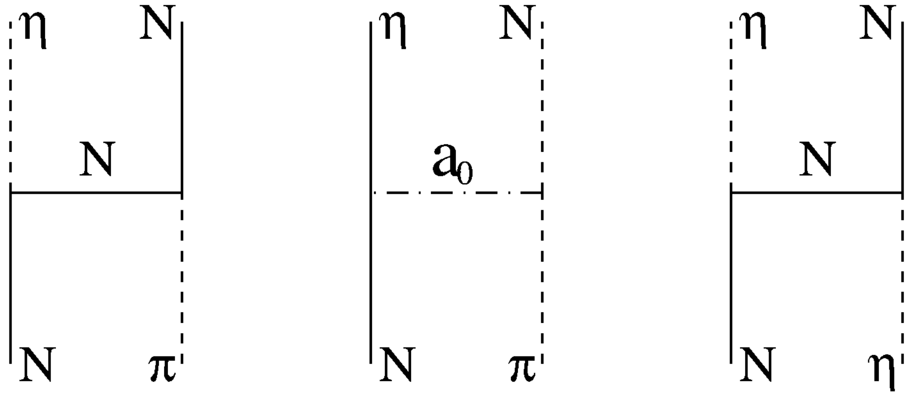

Figure 2.7: The $\pi N \to \eta N$ and $\eta N \to \eta N$ potentials.

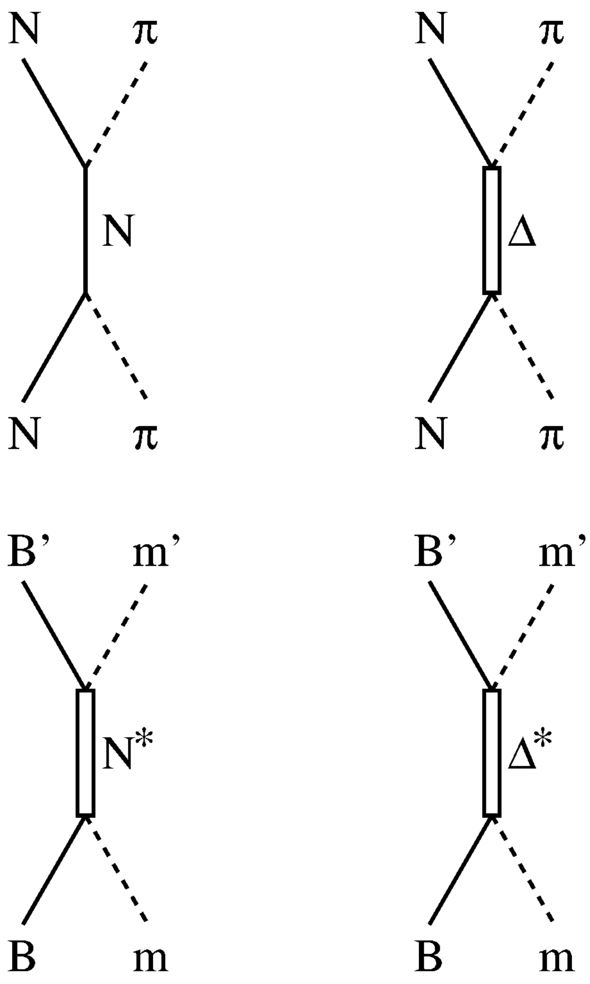

Figure 2.8: Pole graphs.

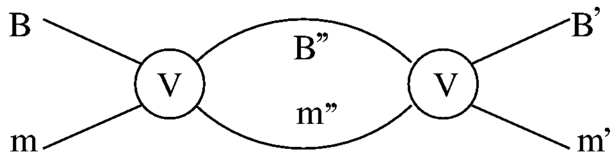

Figure 2.9: Second iteration of the Lippmann-Schwinger equation.

2.5 Form factors

The Lippmann-Schwinger equation (2.30) is an ordinary integral equation which is a very well known mathematical object (see e.g. [46]). This equation is well defined and there are established methods for its numerical treatment when its kernel is compact [46, 47] in (generalized) Hilbert space. The kernel of eq. (2.30) is nothing but

$$\frac{\langle L'S'k'|V^{IJ}_{\mu\gamma}|L''S''k''\rangle k''^2}{Z - E_\gamma(k'') + i\epsilon}. \tag{2.31}$$

This operator is compact under the condition that the partial wave potential drops with k'' quickly enough [48]. However, it is easy to see that the potential, calculated directly from the diagrams of figs. 2.2-2.8 in the way described in section 2.4, rises with k''.

To formulate this problem in a different way one can consider a perturbation series for eq. (2.30). Then already an integral, coming from the second iteration of the Lippmann-Schwinger equation, corresponding to the diagram shown in fig. 2.9, is divergent. The divergency of the integral comes from its high momentum part. Processes related to this regime are in no way a subject of our investigations, and cannot be determined by the potential that we use. That is why it is customary to introduce form factors that suppress contribution to the integral from k'' higher then some cutoff mass Λ. In our model those Λ's have values of a typical hadron scale of order of 1 GeV, varying from one particular type of the form factor to another. In a sense those form factors parameterize the unknown high momentum physics. Another way to think of them is that they reflect the extended structure of hadrons (at least in the case of a t-channel exchange) corresponding to a size of the hadron determined by $1/\Lambda$ [49].

Below, we give the expressions for the form factors, corresponding to different kinds of diagrams.

- For the t and u-channel exchanges we use conventional monopole ($n = 1$) or dipole ($n = 2$) form factors at each vertex

$$F(q) = \left(\frac{\Lambda^2 - m_x^2}{\Lambda^2 + \vec{q}^{\,2}}\right)^n, \tag{2.32}$$

  where m_x is the mass and $\vec{q}$ is the momentum of the exchanged particle (Note that for correlated $\pi\pi$-exchange we apply a different regularization, described in chapter 3). A dipole type is used when ρ or Δ are present at the vertex to suppress additional powers of momentum, otherwise the monopole type proves to be sufficient.

- One exception from the previous case is the u-channel nucleon exchange diagram in the $\pi N \to \pi N$ potential. Here we modify the monopole form factor in such a way that it is normalized to one at the Cheng-Dashen point (where $\vec{q}^{\,2} = ((m_N^2 - m_\pi^2)/m_N)^2 - m_N^2$)

$$F(q) = \frac{\Lambda^2 - m_N^2}{\Lambda^2 - ((m_N^2 - m_\pi^2)/m_N)^2 + \vec{q}^{\,2}}. \tag{2.33}$$

  The importance of the Cheng-Dashen point for the low energy πN scattering is explained in chapter 3

- For pole graphs the form factor is given by

$$F(k')F(k) = \left(\frac{\Lambda^4 + m_R^4}{\Lambda^4 + (E_3(k') + \omega_4(k'))^4}\right)^{n_f} \left(\frac{\Lambda^4 + m_R^4}{\Lambda^4 + (E_1(k) + \omega_2(k))^4}\right)^{n_i} \tag{2.34}$$

  where E_1, ω_2 (E_3, ω_4) are on-shell energies of incoming (outgoing) particles with c.m. momentum k (k'), and m_R is the mass of the resonance (or the nucleon mass in the case of the nucleon pole). There are two reasons why this type of cutoff was introduced

  - it is normalized to one at the position of the resonance
  - it does not increase too fast at small values of k, as some other types do [50] (see fig. 2.10 for an example of a pole graph form factor).

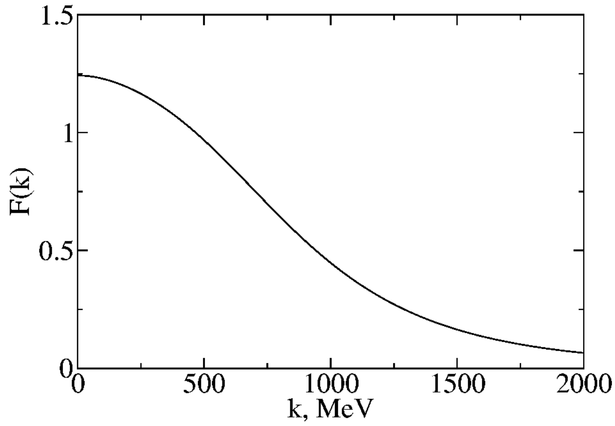

Figure 2.10: Form factor $F(k)$ at the $N^*(1535)N\pi$ vertex as a function of the πN c.m. momentum. The cutoff mass is $\Lambda = 2$ GeV.

We choose $n_{i,f} = 1$ when particles can couple to the resonance only in s or p wave, and $n_{i,f} = 2$ when they can couple in d or f waves.

- The form factor for the contact terms of Wess-Zumino Lagrangian is taken to be of the form

$$F(k,k') = \left(\frac{\Lambda^2 - m_4^2}{\Lambda^2 + \vec{k}'^2} \frac{\Lambda^2 - m_2^2}{\Lambda^2 + \vec{k}^2} \right)^2, \tag{2.35}$$

dependent only on the s-channel variables k, k', since in this case there is no exchanged particle. The masses of incoming and outgoing mesons are denoted as m_2 and m_4.

We treat cutoff masses as free parameters of our model. However one should note, that only some of them have a crucial impact on a quality of the results.

2.6 Resonances

Resonances play an important role in πN scattering. In this section we derive a physically transparent form of the solution of the Lippmann-Schwinger equation in the presence of resonances that will prove very useful in many applications.

First of all let us write the Lippmann-Schwinger equation in JLS basis (2.30) in matrix form:

$$T = T + VGT. \tag{2.36}$$

Here, as in (2.30), the matrix multiplication means an integration over the c.m. momentum in the intermediate state and a summation over the channel index, L, and S ($\sum_{\gamma,L''S''}\int k''^2 dk''$). The potential V consist of the sum of a pole and a non-pole part $V = V^P + V^{NP}$. Note that since each pole graph contributes only to the state with a particular J and isospin, V^P can be written in factorizable form (at the moment we assume only one resonance in a given partial wave)

$$\langle L'S'k'|V^P_{\mu\nu}|LSk\rangle = \frac{\tilde{v}^{L'S'}_\mu(k')v^{LS}_\nu(k)}{Z - M_0}, \tag{2.37}$$

where M_0 is a bare mass of the resonance, v and $\tilde{v}$ are the bare vertex functions for incoming and outgoing particles (including form factors of the type (2.34). From the hermiticity of the Lagrangian follows $\tilde{v} = v^\dagger$ (The explicit expressions for $v^{LS}_\nu(k)$ corresponding to various resonances are given in appendixB). We will look for a solution of (2.36) in the form $T = T^P + T^{NP}$, where T^{NP} is the solution of the equation

$$T^{NP} = T^{NP} + V^{NP}GT^{NP}. \tag{2.38}$$

We can now rewrite eq. (2.36) as

$$(1 - V^{NP}G)T^P = V^P(1 + GT^{NP}) + V^PGT^P. \tag{2.39}$$

We will need also the formal solution of (2.38) to eliminate V^{NP} from (2.39):

$$T^{NP} = \frac{1}{1 - V^{NP}G}V^{NP}; \tag{2.40}$$

$$1 + T^{NP}G = \frac{1}{1 - V^{NP}G} \Rightarrow 1 - V^{NP}G = \frac{1}{1 + T^{NP}G}. \tag{2.41}$$

Introducing the auxiliary quantities $T' = (1 + T^{NP}G)^{-1}T^P$ and $V' = V^P(1 + T^{NP}G)$ we obtain an equation for T'

$$T' = V' + V'GT'. \tag{2.42}$$

The reason why we introduced these quantities is that V' is separable in the initial and final momenta, and therefore eq. (2.42) belongs to a class of equations with a degenerate kernel and can be integrated in a closed form (see e.g. [46]). Indeed

$$\langle L'S'k'|V'_{\mu\nu}|LSk\rangle = \frac{\tilde{v}_\mu^{L'S'}(k')f_\nu^{LS}(k)}{Z-M_0}, \tag{2.43}$$

where the dressed vertex functions f_ν are given as

$$\begin{aligned} f_\nu^{LS}(k) &= v_\nu^{LS}(k) \\ &+ \sum_{\gamma,L''S''}\int k''^2dk''v_\gamma^{L''S''}(k'')\frac{1}{Z-E_\gamma(k'')+i\epsilon}\langle L''S''k''|T_{\gamma\nu}^{NP}|LSk\rangle, \end{aligned} \tag{2.44}$$

or diagrammatically:

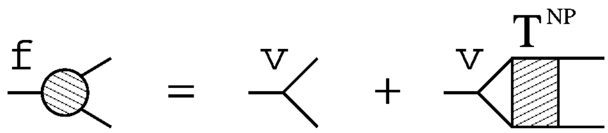

It is important to emphasize, that even if the bare coupling of some state to the resonance is zero ($v_\nu^{LS}(k)=0$), the dressed one will be finite (though maybe small).

We will follow the standard procedure of solving equations with a degenerate kernel [46]. Let us write eq. (2.42) restoring all sums and integrals

$$\begin{aligned} \langle L'S'k'|T'_{\mu\nu}|LSk\rangle &= \frac{\tilde{v}_\mu^{L'S'}(k')f_\nu^{LS}(k)}{Z-M_0} \\ &+\frac{\tilde{v}_\mu^{L'S'}(k')}{Z-M_0}\sum_{\gamma,L''S''}\int k''^2dk''f_\gamma^{L''S''}(k'')\frac{1}{Z-E_\gamma(k'')+i\epsilon}\langle L''S''k''|T'_{\gamma\nu}|LSk\rangle \\ &= \frac{\tilde{v}_\mu^{L'S'}(k')}{Z-M_0}(f_\nu^{LS}(k)+A_\nu^{LS}(k)), \end{aligned} \tag{2.45}$$

with

$$\begin{aligned} A_\nu^{LS}(k) &= \sum_{\gamma,L''S''}\int k''^2dk''f_\gamma^{L''S''}(k'')\frac{1}{Z-E_\gamma(k'')+i\epsilon}\langle L''S''k''|T'_{\gamma\nu}|LSk\rangle \\ &= \frac{f_\nu^{LS}(k)+A_\nu^{LS}(k)}{Z-M_0}\sum_{\gamma,L''S''}\int k''^2dk''f_\gamma^{L''S''}(k'')\tilde{v}_\gamma^{L''S''}(k'') \\ &= \frac{\Sigma(Z)}{Z-M_0}(f_\nu^{LS}(k)+A_\nu^{LS}(k)). \end{aligned} \tag{2.46}$$

The self-energy $\Sigma(Z)$ of the resonance is defined as

$$\Sigma(Z) = \sum_{\gamma,LS}\int k^2dkf_\gamma^{LS}(k)\tilde{v}_\gamma^{LS}(k). \tag{2.47}$$

The diagrams corresponding to this definition are:

$\Sigma(Z)$=

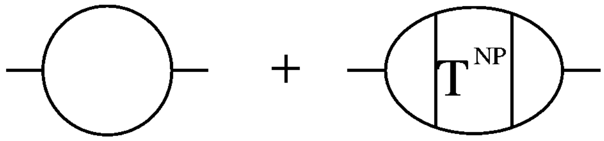

Now, performing some trivial algebra we get

$$A_\nu^{LS}(k) = \frac{\Sigma(Z)}{Z - M_0 - \Sigma(Z)} f_\nu^{LS}(k); \; \langle L'S'k'|T'_{\mu\nu}|LSk\rangle = \frac{\tilde{v}_\mu^{L'S'}(k') f_\nu^{LS}(k)}{Z - M_0 - \Sigma(Z)}. \quad (2.48)$$

Therefore we arrive at the final answer for T:

$$\langle L'S'k'|T_{\mu\nu}|LSk\rangle = \langle L'S'k'|T_{\mu\nu}^{NP}|LSk\rangle + \frac{\tilde{f}_\mu^{L'S'}(k') f_\nu^{LS}(k)}{Z - M_0 - \Sigma(Z)}, \quad (2.49)$$

where we used the fact that $T^P = (1 + T^{NP}G)T'$ and defined dressed vertex function for outgoing particles

$$\tilde{f}_\nu^{LS}(k) = \tilde{v}_\nu^{LS}(k)$$
$$+ \sum_{\gamma, L''S''} \int k''^2 dk'' \langle LSk|T_{\gamma\nu}^{NP}|L''S''k''\rangle \frac{1}{Z - E_\gamma(k'') + i\epsilon} \tilde{v}_\gamma^{L''S''}(k''), \quad (2.50)$$

or in diagrammatic language:

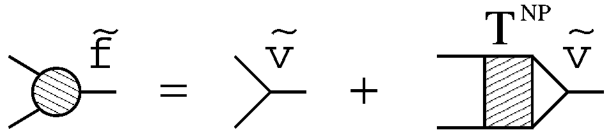

Eq. (2.49) has a form analogous to the famous Breit-Wigner formula [51] for the resonance scattering. The physical characteristics of the resonance (mass and width) are determined by the position of a zero of the denominator $Z - M_0 - \Sigma(Z)$ in the complex plane. In this work we do not try to determine physical masses and partial widths of resonances but rather fit bare quantities to the data. The procedure of fitting the resonance parameters is simplified when using eq. (2.49), because then changing coupling constants becomes a purely algebraic transformation. One only needs to calculate once the dressed vertex functions and the self-energy, that can be expressed purely in terms of the non-pole T-matrix.

Finally, let us generalize eq. (2.49) to the case of two resonances in one partial wave(relevant e.g. in the S_{11} partial wave). Then the resonance potential is given by

$$\langle L'S'k'|V_{\mu\nu}^P|LSk\rangle = \sum_{i=1,2} \frac{\tilde{v}_{\mu,i}^{L'S'}(k') v_{\nu,i}^{LS}(k)}{Z - M_{0,i}}. \quad (2.51)$$

The definitions of $f_{\nu,i}^{LS}(k)$, $\tilde{f}_{\nu,i}^{LS}(k)$, $A_{\nu,i}^{LS}(k)$ are obvious. The analogs of eqs. (2.45) and (2.46) are

$$\langle L'S'k'|T'_{\mu\nu}|LSk\rangle = \sum_{i=1,2} \frac{\tilde{v}_{\mu,i}^{L'S'}(k')}{Z-M_{0,i}}(f_{\nu,i}^{LS}(k)+A_{\nu,i}^{LS}(k)); \tag{2.52}$$

$$A_{\nu,i}^{LS}(k) = \sum_{j=1,2} \frac{\Sigma_{ij}(Z)}{Z-M_{0,j}}(f_{\nu,j}^{LS}(k)+A_{\nu,j}^{LS}(k)), \tag{2.53}$$

where $\Sigma^{ij}(Z)$ denotes the self-energy matrix

$$\Sigma_{ij}(Z) = \sum_{\gamma,LS}\int k^2 dk f_{\gamma,i}^{LS}(k)\tilde{v}_{\gamma,j}^{LS}(k). \tag{2.54}$$

By solving the system of linear equations (2.53) is straightforward to get the expression for T

$$\begin{aligned}
&\langle L'S'k'|T_{\mu\nu}|LSk\rangle = \langle L'S'k'|T_{\mu\nu}^{NP}|LSk\rangle \\
&+\frac{\tilde{f}_{\mu,1}^{L'S'}(k')f_{\nu,1}^{LS}(k)(Z-M_{0,2}-\Sigma_{22})+\tilde{f}_{\mu,2}^{L'S'}(k')f_{\nu,2}^{LS}(k)(Z-M_{0,1}-\Sigma_{11})}{(Z-M_{0,1}-\Sigma_{11})(Z-M_{0,2}-\Sigma_{22})-\Sigma_{12}\Sigma_{21}} \\
&+\frac{\tilde{f}_{\mu,1}^{L'S'}(k')f_{\nu,2}^{LS}(k)\Sigma_{12}+\tilde{f}_{\mu,2}^{L'S'}(k')f_{\nu,1}^{LS}(k)\Sigma_{21}}{(Z-M_{0,1}-\Sigma_{11})(Z-M_{0,2}-\Sigma_{22})-\Sigma_{12}\Sigma_{21}}.
\end{aligned} \tag{2.55}$$

Note that all integrals appearing in this section can be performed along the complex contour as explained in chapter 4.

2.7 Nucleon pole

The formalism of the previous section can be also applied to the nucleon s-channel pole amplitude which provides an important contribution to the P_{11} partial wave. The only difference in case of the nucleon pole is that we cannot consider all bare parameters as free, because the πNN coupling constant $f_{\pi NN}$ as well as the nucleon mass m_N are known physical quantities. Here we show, how one can implement those constraints in our approach. Here we follow the approach of ref. [52].

Let us write again the pole part of eq. (2.49) for the case of the nucleon pole

$$T_{\pi N}(k',k) = \frac{\tilde{f}^{P_{11}}(k')f^{P_{11}}(k)}{Z-M_0-\Sigma(Z)}, \tag{2.56}$$

assuming that we already calculated the non-pole T-matrix. In the energy region below the πN threshold the non-pole T-matrix and the two-body Green's function $(Z - E_\gamma(k'') + i\epsilon)^{-1}$ are real (there are no open channels), and therefore the vertex functions $f(k)$ and $\tilde{f}(k)$ are purely imaginary (because of the kinematical P-wave factor) and equal. The self-energy $\Sigma(Z)$ is also real for the same reasons. Note that, since we have the nucleon pole potential only in one channel, the vertex functions $f(k)$ are proportional to the bare πNN coupling constant $f^B_{\pi NN}$, and one can write

$$f^{P_{11}}(k) = f^B_{\pi NN} f_1(k), \ \Sigma(Z) = (f^B_{\pi NN})^2 \Sigma_1(Z) \tag{2.57}$$

where f_1 and Σ_1 depend only on the non-pole T-matrix (and on the πNN cutoff mass, but we assume that it is already fixed). Now, let us demand that eq. (2.56) has a pole at $Z = m_N$

$$m_N - M_0 - \Sigma(m_N) = 0. \tag{2.58}$$

Then, in the vicinity of the pole, eq. (2.56) is given by

$$T_{\pi N} = \frac{(f^B_{\pi NN} f_1(k_0))^2}{\left(1 - \dfrac{\partial \Sigma(m_N)}{\partial Z}\right)(Z - m_N)}, \tag{2.59}$$

where k_0 is the c.m. momentum of the πN system at the pole $k_0^2 = \dfrac{m_\pi^2(m_\pi^2 - 2m_N^2)}{4m_N^2}$. The structure of $T_{\pi N}$ at the nucleon pole defines the physical coupling constant $f_{\pi NN}$ through

$$T_{\pi N} = \frac{v(k_0)^2}{Z - m_N}, \tag{2.60}$$

with

$$v = \sqrt{3}\frac{f_{\pi NN}}{m_\pi \sqrt{4\pi}} \frac{k_0}{\sqrt{2\pi}} \frac{E_N(k_0) + \omega_\pi(k_0) + m_N}{\sqrt{E_N(k_0)\omega_\pi(k_0)(E_N(k_0) + m_N)}} \tag{2.61}$$

(see appendix B). Thus, we have an equation for $f^B_{\pi NN}$:

$$\frac{(f^B_{\pi NN} f_1(k_0))^2}{1 - (f^B_{\pi NN})^2 \dfrac{\partial \Sigma_1(m_N)}{\partial Z}} = v(k_0)^2 \tag{2.62}$$

The solution of this equation,

$$f^B_{\pi NN} = \frac{1}{\sqrt{f_1(k_0)^2/v(k_0)^2 + \partial\Sigma_1(m_N)/\partial Z}}, \tag{2.63}$$

and the nucleon bare mass

$$M_0 = m_N - (f^B_{\pi NN})^2 \Sigma_1(m_N) \tag{2.64}$$

have to be taken as input for the calculations.

Here one should note that we do not include nucleon pole graphs in other channels, like e.g. ρN or ηN. This should be a good approximation since those channels open quite far from the position of the nucleon pole. Consequently, their effect would be just an additional renormalization of the bare parameters.

2.8 Self-energies of σ and ρ mesons and Δ-isobar

As was stated before, we have three effective channels σN, ρN, and $\pi\Delta$ that represent the $\pi\pi N$ channel. Each of them consists of a stable and an unstable particle. In order to take into account the possibility of the decay of σ, ρ and Δ into the $\pi\pi$ and πN systems, respectively, we follow the procedure described in ref. [23]. The idea is to modify the 2-body Green's function of the effective 3-body states, introducing the self-energy, in a way similar to that, described in section 2.6. The modified propagators take the form [1, 23]

$$\begin{aligned}
G_{\pi\Delta}(Z,k) &= \frac{1}{Z - \sqrt{m_\pi^2 + k^2} - \sqrt{(m^0_\Delta)^2 + k^2} - \Sigma_\Delta(Z_\Delta)}, \\
G_{\sigma N}(Z,k) &= \frac{1}{Z - \sqrt{m_N^2 + k^2} - \sqrt{(m^0_\sigma)^2 + k^2} - \Sigma_\sigma(Z_\sigma)}, \\
G_{\rho N}(Z,k) &= \frac{1}{Z - \sqrt{m_N^2 + k^2} - \sqrt{(m^0_\rho)^2 + k^2} - \Sigma_\rho(Z_\rho)}.
\end{aligned} \tag{2.65}$$

The self-energies are calculated within a simple model, which includes only the interaction vertices corresponding to the decay of the σ, ρ and Δ states. The effective Lagrangian of this model is given by

$$\begin{aligned}
\mathcal{L}_{\sigma\pi\pi} &= g_{\sigma\pi\pi} m_\pi \vec{\phi}_\pi \vec{\phi}_\pi \phi_\sigma, \\
\mathcal{L}_{\rho\pi\pi} &= -g_{\rho\pi\pi} (\vec{\pi} \times \partial^\mu \vec{\pi}) \vec{\rho}^\mu, \\
\mathcal{L}_{\Delta\pi N} &= \frac{f_{N\Delta\pi}}{m_\pi} \bar{\Delta}^\mu \vec{T}^\dagger \partial_\mu \vec{\pi} \Psi_N.
\end{aligned} \tag{2.66}$$

Then the T matrix in each (σ, ρ or Δ) channel has only the resonance part and can be written as (see section2.6)

$$T = \frac{v v^\dagger}{Z - m_0 - \Sigma}, \tag{2.67}$$

where the self-energy Σ is calculated in a standard way, e.g.

$$\Sigma_\Delta(Z_\Delta) = \int q^2 dq \frac{v_{N\Delta\pi}(q)[v_{N\Delta\pi}(q)]^\dagger}{Z_\Delta - E_N(q) - \omega(q)}, \tag{2.68}$$

and similarly for the σ and ρ self-energies. Here q denotes the c.m. momentum in the πN subsystem. The vertex functions corresponding to the Lagrangian (2.66) with the form factors taken from [1, 23] have the following form

$$v^{\sigma\pi\pi}(q) = \frac{\sqrt{3} g_{\sigma\pi\pi} m_\pi}{2\pi \omega_\pi(q) \sqrt{\omega_\sigma^0(k)}} \frac{\Lambda_{\sigma\pi\pi}^2}{\Lambda_{\sigma\pi\pi}^2 + q^2}, \tag{2.69}$$

$$v^{\rho\pi\pi}(q) = \frac{g_{\rho\pi\pi}}{2\pi\sqrt{3}} \frac{k}{\omega_\pi(q) \sqrt{\omega_\rho^0(k)}} \frac{\Lambda_{\rho\pi\pi}^2 + m_\rho^2}{\Lambda_{\rho\pi\pi}^2 + 4\omega_\pi(q)^2}, \tag{2.70}$$

where $\omega_\sigma^0(k) = \sqrt{(m_\sigma^0)^2 + k^2}$, $\omega_\rho^0(k) = \sqrt{(m_\rho^0)^2 + k^2}$ with bare masses m_σ^0 and m_ρ^0. The $\Delta\pi N$ vertex function is the same as in the Δ pole diagram in appendixB.

The T-matrix in eq. (2.67) has to be evaluated in the rest frame of the unstable particle ($k = 0$). Then the parameters of the effective Lagrangian (2.66) are fitted to the empirical data. These parameters are collected in table 2.1. The results of the fit are shown in figs. 2.11,2.12. To take into account the effect of a moving resonance (the Δ, say) one fixes the energy Z_Δ in eq. (2.68) as follows

$$Z_\Delta = Z - \omega_\pi(k) - E_\Delta^{kin}(k) = Z - \omega_\pi(k) - (\sqrt{(m_\Delta^0)^2 + k^2} - m_\Delta^0), \tag{2.71}$$

i.e. subtracting from the total c.m. energy Z the energy of the spectator pion and the kinetic energy of the Δ isobar. The generalization to the case of the σ and ρ mesons is straightforward.

σ	$g_{\sigma\pi\pi}$	9.5
	Λ_σ	1500 MeV
	m^0_σ	900 MeV
ρ	$g^2_{\rho\pi\pi}/(4\pi)$	2.9
	Λ_ρ	1800 MeV
	m^0_ρ	911 MeV
Δ	$f^2_{N\Delta\pi}/(4\pi)$	0.36
	Λ_Δ	1500 MeV
	m^0_Δ	1415 MeV

Table 2.1: Parameters of σ, ρ, and Δ pole potentials.

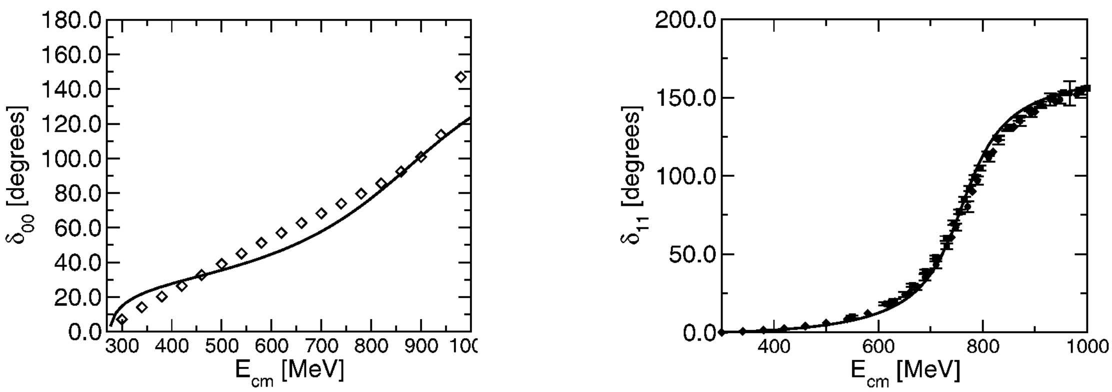

Figure 2.11: The $\pi\pi$ phase shifts for the scalar-isoscalar and vector-isovector partial waves. The data are from [53–55].

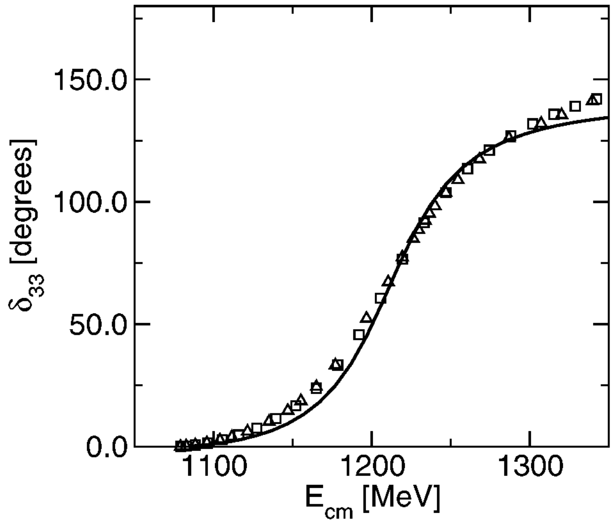

Figure 2.12: The πN phase shift for the P_{33} partial wave. The data are from [44, 45].

Chapter 3

Correlated two pion exchange potential

The picture that the σ meson represent a correlated $\pi\pi$ exchange is very successful. Within this scheme it is possible to simultaneously and consistently describe $\pi\pi$ data as well as the intermediate range attraction of NN scattering. The latter was implemented by a dispersive analysis of πN and $\pi\pi$ data [49, 56–58].

Since the treatment of the correlated $\pi\pi$ exchange by means of dispersion relations is successful in the case of NN interactions, it makes sense to apply the same idea to πN scattering. This was realized in Jülich πN model [22, 24]. Using a dispersion theoretical approach allows one to reduce the number of free parameters and largely to fix σ and ρ exchange contributions by experimental data. Without such constrains those contributions are almost arbitrary. This is reflected in the discrepancy among the πN models considering σ and ρ as stable particles [12, 17–19], where the corresponding contributions differ in many details, including the sign of the σ exchange potential.

In this chapter we derive the correlated $\pi\pi$-exchange potential for elastic πN scattering in the scalar-isoscalar (σ) and vector-isovector (ρ) channel using a dispersion relations technique. As an input for dispersion relations we use a model describing the $N\bar{N} \to \pi\pi$ transition, which fits rather well the "quasi-empirical" $N\bar{N} \to \pi\pi$ amplitude obtained in [59–61] by analytic continuation of πN and $\pi\pi$ data into the unphysical region. Then we discuss the σ and ρ exchange contributions in

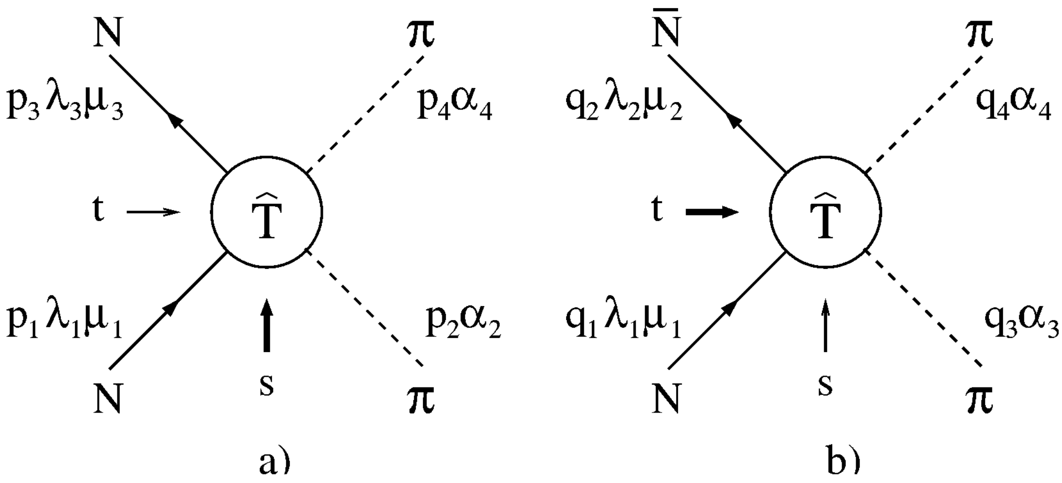

Figure 3.1: Notations for a) s ($\pi N \to \pi N$) channel and b) t ($N\bar{N} \to \pi\pi$) channel processes, p and q denote the four momenta of the particles, μ and α are the isospin indices, and λ is the helicity of nucleon and antinucleon.

more detail.

3.1 Dispersion relation for partial wave amplitude

We start with the definition of the T-matrix describing the processes $\pi N \to \pi N$ and $N\bar{N} \to \pi\pi$ (in the same way as in section 2.3) relating it to the S-matrix:

$$S_{fi} = \delta_{fi} - i(2\pi)\delta^{(4)}(P_f - P_i)T_{fi} \tag{3.1}$$

where P_i and P_f are the total four-momenta of the incoming and outgoing systems of the corresponding reactions (cf. fig. 3.1). The s ($\pi N \to \pi N$) and t ($N\bar{N} \to \pi\pi$) channel reactions are related to each other due to crossing symmetry. In order to take this into account it is convenient to introduce an operator $\hat{T}$, acting in isospin space and in the space of Dirac spinors, in such a way that the s-channel amplitude can be written as

$$T_s(p_3, p_4; p_1, p_2) = \frac{1}{(2\pi)^3}\frac{1}{\sqrt{2\omega_{p_2}2\omega_{p_4}}}\bar{u}(\vec{p}_3, \lambda_3)\xi^\dagger(\mu_3)\zeta^\dagger(\alpha_4)\hat{T}(s,t)u(\vec{p}_1, \lambda_1)\xi(\mu_1)\zeta(\alpha_2). \tag{3.2}$$

Here ξ and ζ stand for the isospin wave functions of nucleon and pion, respectively, $u(\vec{p},\lambda)$ and $\bar{u}(\vec{p},\lambda)$ are Dirac spinors defined in appendix A with momentum $\vec{p}$ and helicity λ. The kinematical pre-factor containing $\omega_{p_{2,4}} = \sqrt{\vec{p}_{2,4}^{\,2} + m_\pi^2}$ was introduced so that $\hat{T}$ is identical to the conventional invariant amplitude. The Mandelstam variables are defined as

$$\begin{aligned} s &= (p_1 + p_2)^2, \\ t &= (p_1 - p_3)^2, \\ u &= (p_1 - p_4)^2. \end{aligned} \tag{3.3}$$

Only two of them are independent because of the identity $s+t+u = 2m_N^2 + 2m_\pi^2$, thus $\hat{T}$ depends only on s and t. Isospin invariance leads to the decomposition of $\hat{T}$ into

$$\hat{T}(s,t) = \hat{T}^{(+)}(s,t) - \hat{T}^{(-)}(s,t)\vec{\tau}\vec{t}. \tag{3.4}$$

where $\vec{\tau}$ and $\vec{t}$ are the isospin operators for nucleon and pion, defined in appendix C.

The spin structure of the operator $\hat{T}$ can be reduced to two invariant amplitudes A and B, making use of parity conservation in strong interactions

$$\hat{T}^{(\pm)} = -(A^{(\pm)}(s,t) + \gamma^\mu Q_\mu B^{(\pm)}(s,t)), \tag{3.5}$$

where $Q = \frac{1}{2}(p_2 + p_4)$.

The amplitude in the t channel is given by

$$\begin{aligned} &T_t(q_3, q_4, q_1, q_2) = \\ &\qquad \frac{1}{(2\pi)^3} \frac{1}{\sqrt{2\omega_{p_2} 2\omega_{p_4}}} \bar{v}(\vec{q}_2,\lambda_2)\xi^\dagger(\mu_2)\zeta^\dagger(\alpha_3)\hat{T}(s,t)u(\vec{q}_1,\lambda_1)\xi(\mu_1)\zeta(\alpha_4). \end{aligned} \tag{3.6}$$

Here $v(\vec{q}_2,\lambda_2)$ is the Dirac spinor of the antinucleon. Crossing symmetry tells us that $\hat{T}$ in (3.6) is the same as in (3.2) but with Mandelstam variables

$$\begin{aligned} s &= (q_1 - q_3)^2 = -p_t^2 - q_t^2 + 2p_t q_t \cos(\theta_t), \\ t &= (q_1 + q_2)^2 = 4(p_t^2 + m_N^2) = 4(q_t^2 + m_\pi^2), \\ u &= (q_1 - q_4)^2 = -p_t^2 - q_t^2 - 2p_t q_t \cos(\theta_t), \end{aligned} \tag{3.7}$$

and eq. (3.4) also holds with $Q = \frac{1}{2}(q_4 - q_3)$. We introduced the initial and final c.m. momenta for the $N\bar{N} \to \pi\pi$ reaction $p_t = |\vec{q}_1|, q_t = |\vec{q}_3|$ and the scattering angle θ_t. Notice that physical regions of s, t, u in (3.3) and (3.7) are totally different, and, therefore, the equivalence of the $\hat{T}$ in (3.6) and (3.2) should be understood as an analytic continuation of $\hat{T}$ in both variables s and t. Making such a continuation is possible if one assumes the Mandelstam's representation for the A and B amplitudes [62]. A simultaneous extention of s and t into the complex plain allows one to write a dispersion relation for partial wave amplitudes.

In order to isolate the σ and ρ contributions we perform a t channel partial wave decomposition for A and B

$$A^{(\pm)}(s,t) = \sum_J \frac{1}{2}(2J+1)P_J(x)A^{(\pm)}(t), \tag{3.8}$$

$$B^{(\pm)}(s,t) = \sum_J \frac{1}{2}(2J+1)P_J(x)B^{(\pm)}(t), \tag{3.9}$$

where $P_J(x)$ are the conventional Legendre polynomials. The argument $x = \cos(\theta_t)$ can be expressed in terms of s and t from (3.7) as

$$x = \frac{s + \frac{1}{2}t - m_N^2 - m_\pi^2}{2(\frac{t}{4} - m_N^2)^{1/2}(\frac{t}{4} - m_\pi^2)^{1/2}} = \frac{s + \frac{1}{2}t - m_N^2 - m_\pi^2}{2p_t q_t}, \tag{3.10}$$

The Pauli principle applied to two pions in the t channel requires

$$A^{(\pm)}(s,t) = \pm A^{(\pm)}(u,t) \tag{3.11}$$

$$B^{(\pm)}(s,t) = \mp B^{(\pm)}(u,t) \tag{3.12}$$

Taking into account that $s \leftrightarrow u$ means $x \leftrightarrow -x$, this implies that for J even

$$A_J^{(-)} = B_J^{(+)} = 0,$$

whereas for J odd

$$A_J^{(+)} = B_J^{(-)} = 0,$$

Therefore the isospin index $(\pm)$ can be suppressed, because it is uniquely defined by J.

The quantities A_J, B_J still contain kinematical singularities. To get rid of them one has to introduce new functions $f_\pm^J$ [63]

$$\begin{aligned} f_+^J(t) &= \frac{1}{8\pi}\left(\frac{-p_t^2}{(p_t q_t)^J}A_J + \frac{m_N}{(2J+1)(p_t q_t)^{J-1}}((J+1)B_{J+1} + JB_{J-1})\right), \\ f_-^J(t) &= \frac{1}{8\pi}\frac{\sqrt{J(J+1)}}{2J+1}\frac{1}{(p_t q_t)^{J-1}}(B_{J-1} - B_{J+1}), \end{aligned} \tag{3.13}$$

where the lower index $\pm$ denotes the helicity of the $N\bar{N}$ state ($\lambda_1 = \pm\frac{1}{2}, \lambda_2 = \frac{1}{2}$). The invariant amplitude is then expressed via $f_\pm^J$ as

$$\begin{aligned} A^{(\pm)}(s,t) &= \frac{8\pi}{p_t^2}\sum_J \frac{1}{2}(2J+1)(p_t q_t)^J \\ &\quad \times \left(\frac{m_N}{\sqrt{J(J+1)}} x P_J'(x) f_-^J(t) - P_J(x) f_+^J(t)\right), \end{aligned} \tag{3.14}$$

$$B^{(\pm)}(s,t) = 8\pi \sum_J \frac{1}{2}(2J+1)\frac{(p_t q_t)^{J-1}}{\sqrt{J(J+1)}} P_J'(x) f_-^J(t), \tag{3.15}$$

with $P_J'(x) = \frac{d}{dx}P_J(x)$. The sum for $A^{(+)}$ and $B^{(-)}$ is performed over even J and the sum for $A^{(+)}$ and $B^{(-)}$ over odd J. The contributions from correlated two pion exchange corresponding to σ and ρ exchanges are contained in the terms of (3.14) with $J = 0$ and $J = 1$ respectively (note that $f_-^{J=0}(t) = 0$).

Now let us discuss the analytic properties of the amplitudes $f_\pm^J$. As stated before they are free of kinematical singularities, but there are dynamical ones coming from the unitarity constrains. The functions $f_\pm^J(t)$ are analytic in the whole complex t-plain apart form two cuts along the real axis [63, 64]. The first cut runs from $-\infty$ to $a = 4m_\pi^2\left(1 - \frac{m_\pi^2}{4m_N^2}\right)$. This cut is generated by s channel nucleon pole and u channel nucleon exchange, and also by many particle s and u channel singularities. The second cut running from $4m_\pi^2$ to ∞ arises from singularities due to the intermediate $\pi\pi$ state in the reaction $N\bar{N} \to \pi\pi$ and higher t cannel intermediate states ($4\pi, N\bar{N}, \dots$). Then the dispersion relation for the amplitudes $f_\pm^J$ for $J \neq 0$ reads

$$f_\pm^J(t) = \frac{1}{\pi}\int_{-\infty}^{a} \frac{Imf_\pm^J(t')dt'}{t' - t - i\epsilon} + \frac{1}{\pi}\int_{4m_\pi^2}^{\infty} \frac{Imf_\pm^J(t')dt'}{t' - t - i\epsilon}. \tag{3.16}$$

For $J = 0$, since $f_+^0(t)/p_t^2$ remains finite at $p_t = 0$, one can formulate the dispersion relation for $f_+^0(t)/p_t^2 = f_+^0(t)/(\frac{t}{4} - m_N^2)$ instead of $f_+^0(t)$ itself [22, 63]

$$\frac{f_+^0(t)}{p_t^2} = \frac{1}{\pi}\int\limits_{-\infty}^{a} \frac{Im f_+^0(t')}{t' - t - i\epsilon}\frac{1}{\left(\frac{t'}{4} - m_N^2\right)}dt' + \frac{1}{\pi}\int\limits_{4m_\pi^2}^{\infty} \frac{Im f_+^0(t')}{t' - t - i\epsilon}\frac{1}{\left(\frac{t'}{4} - m_N^2\right)}dt'. \quad (3.17)$$

Since we are interested only in the $\pi\pi$-exchange contribution, left-hand cuts in (3.16), (3.17) do not produce a relevant contribution and we will skip them. Henceforth we will omit limits of integration assuming an integration along the right-hand cut, unless specified otherwise. The invariant amplitudes related to σ and ρ exchanges now take the form

$$\begin{aligned}
A_\sigma^{(+)}(s,t) &= -\frac{4\pi}{p_t^2} f_+^0(t) = -16\int \frac{Im f_+^0(t')dt'}{(t'-t)(t'-4m_N^2)}, \\
B_\sigma^{(+)}(s,t) &= 0, \qquad (3.18)\\
A_\rho^{(-)}(s,t) &= 12\pi\frac{q_t x}{p_t}\left(\frac{m_N}{\sqrt{2}} f_-^1(t) - f_+^1(t)\right) \\
&= 12\frac{s + \frac{1}{2}t - m_N^2 - m_\pi^2}{t - 4m_N^2}\left(\sqrt{2}m_N\int \frac{Im f_-^1(t')dt'}{t'-t} - 2\int \frac{Im f_+^1(t')dt'}{t'-t}\right) \\
B_\rho^{(-)}(s,t) &= 6\sqrt{2}\pi f_-^1(t) = 6\sqrt{2}\int \frac{Im f_-^1(t')dt'}{t'-t} \qquad (3.19)
\end{aligned}$$

Now s and t can be taken in the physical region for s channel, i.e. $s \geq (m_N + m_\pi), t \leq 0$.

The expressions (3.18) and (3.19) look rather similar to the exchange of spin 0 and spin 1 mesons with their masses ($\sqrt{t'}$) smeared from two pion threshold to infinity and coupling constants proportional to $Im(f_\pm^J(t'))$. We will discuss this analogy in more detail in the subsequent sections.

3.2 The $N\bar{N} \to \pi\pi$ model

To perform the integration along the right-hand cut in (3.18), (3.19) one needs the amplitudes of the $N\bar{N} \to \pi\pi$ reaction $f_+^0(t)$, $f_\pm^1(t)$ (or at least their imaginary parts) in the region $t \geq 4m_\pi^2$. This region is unphysical as long as we are below $N\bar{N}$ threshold ($t \leq 4m_N^2$). These amplitudes are given in ref. [61] where they were obtained by the analytic continuation of both πN and $\pi\pi$ data (the method is described in [59,60]). However, we do not use this quasi-empirical data explicitly but instead utilize a dynamical model [65] which describes them quite well. This allows one to avoid some double counting problems, described below.

Fig. 3.2 shows the results of the $N\bar{N} \to \pi\pi$ model for the real and imaginary parts of the amplitudes $f^0_+(t), f^1_\pm(t)$ as compared to the data from [61].

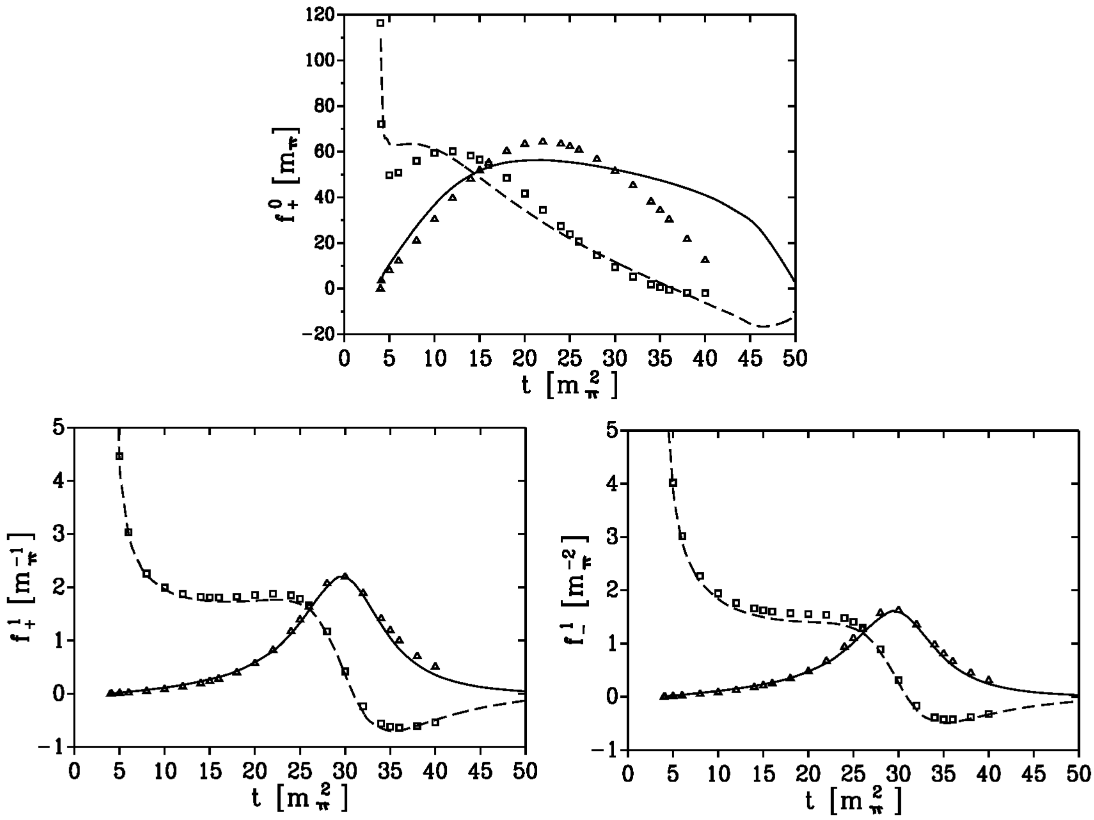

Figure 3.2: Partial wave $N\bar{N} \to \pi\pi$ amplitudes, corresponding to σ and ρ channels given by the model of ref. [65] . Solid and dashed lines denote real and imaginary parts of the amplitudes. The data are from [61].

The model of ref. [65] is based on the meson exchange picture with coupled channels $N\bar{N}, \pi\pi, K\bar{K}$. The resulting $N\bar{N} \to \pi\pi$ amplitude contain among others a contribution from the box diagram (fig. 3.3(a)). The same diagram shows up in the $\pi N \to \pi N$ amplitude through the solution of the Lippmann-Schwinger equation as a second iteration of the $\pi N \to \rho N$ potential (fig. 3.3(b)). This leads to

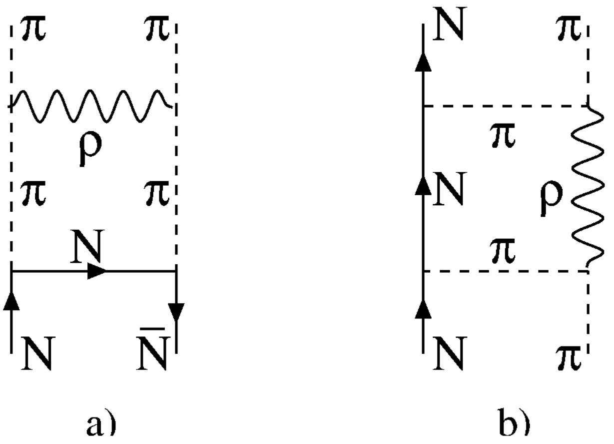

Figure 3.3: Box diagrams in a) $N\bar{N} \to \pi\pi$ model and b) $\pi N \to \pi N$ model leading to double counting.

double counting. To avoid this we subtract the box contribution from the total $N\bar{N} \to \pi\pi$ amplitude and use the resulting amplitude T_{corr} (cf. fig. 3.4) as an input for dispersion relations. The difference between the total $N\bar{N} \to \pi\pi$ ampli-

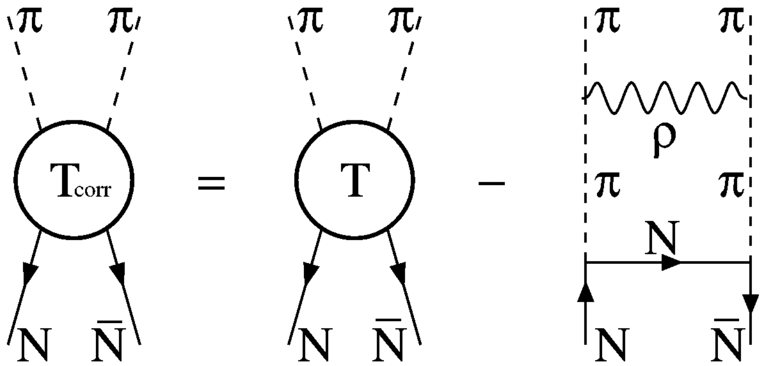

Figure 3.4: Amplitude used in the dispersion relations is obtained from the total amplitude by a subtraction of the box diagram to avoid double counting.

tude and the subtracted one is shown on fig. 3.5. Luckily for $f^1_\pm$ this difference is completely invisible, and for f^0_+ it is quite small. This is an indication that the model dependence of the contribution from the correlated $\pi\pi$-exchange is not significant. Note also that it turns out, that due to the suppression factors $1/t', 1/t'^2$ in the integrands of (3.18), (3.19), the integrals can be truncated at $t_c = 50m_\pi^2$

provided $|t|$ is not too large [22].

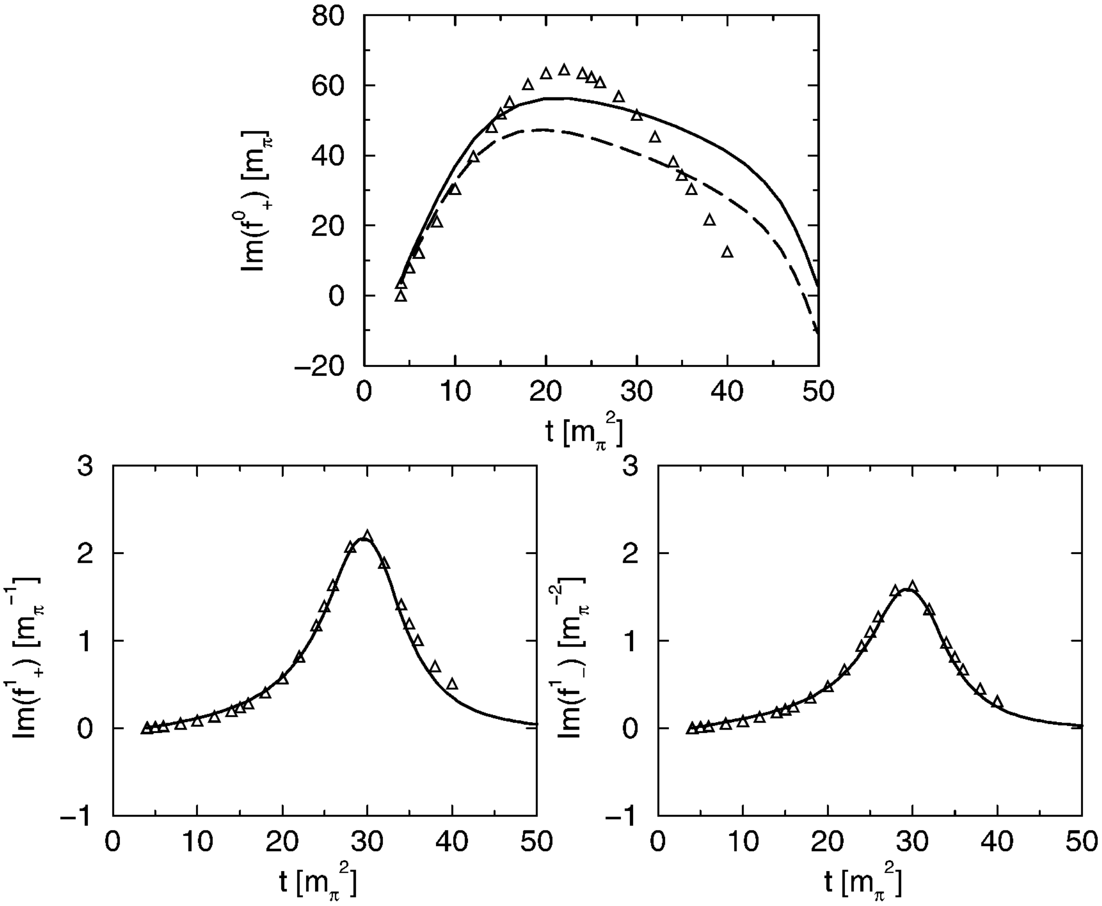

Figure 3.5: Difference between the total $N\bar{N} \rightarrow \pi\pi$ amplitudes (solid line) and with subtracted box diagram (dashed line). Triangles correspond to quasi-empirical data from ref. [61]

3.3 The σ exchange potential

The integral (3.18) for A_σ^+ results in a strongly attractive contribution. There is a way to constrain this quantity from the low energy theorems for πN scattering. They have to do with the forward amplitude D

$$D(\nu, \nu_B^2, p_2^2, p_4^2) = A + \nu B, \tag{3.20}$$

where $\nu \equiv (s-u)/4m_N$, $\nu_B \equiv (t-2m_\pi^2)/4m_N$. One of the low energy relations requires [66] that the on-shell isoscalar amplitude at the unphysical point ($\nu = 0, \nu_B = 0, p_2^2 = m_\pi^2, p_4^2 = m_\pi^2$), called Cheng-Dashen point, is given by

$$D^+(0,0,m_\pi^2,m_\pi^2) = \Sigma/F_\pi^2 \tag{3.21}$$

(The limit $\nu \to 0, \nu_B \to 0$ is taken first by setting $\nu_B = 0$, then the nucleon s and u channel pole terms cancel each other.) Here $\Sigma \simeq 60MeV$ [67] is an important physical quantity related to the pion nucleon σ-term (see e.g. [68]). If one calculates the contribution to $D^+(0,0,m_\pi^2,m_\pi^2)$ from a sigma exchange, using (3.18)

$$D_\sigma^{(+)} = A_\sigma^{(+)}(t=2m_\pi^2) = -16\int_{4m_\pi^2}^{t_c} \frac{Imf_+^0(t')dt'}{(t'-2m_\pi^2)(t'-4m_N^2)}, \tag{3.22}$$

then the result for Σ has the correct sign but is much too large. To resolve this problem we apply a method proposed in [22]. The point here is that the separation of f_0^+/p_t^2 into parts having only left-hand and only right-hand singularities is not unique, so one can redefine them in such a way that Σ will have a required value. The idea is to write a dispersion relation with a subtraction at the Cheng-Dashen point $t_{CD} = 2m_\pi^2$

$$\begin{aligned}
&\frac{f_+^0(t)}{\left(\frac{t}{4}-m_N^2\right)} - \frac{f_+^0(2m_\pi^2)}{\left(\frac{1}{2}m_\pi^2 - m_N^2\right)} = \\
&\frac{t-2m_\pi^2}{\pi}\int_{-\infty}^{a} \frac{Imf_+^0(t')}{(t'-t-i\epsilon)\left(\frac{t'}{4}-m_N^2\right)(t'-2m_\pi^2)}dt' \\
&+\frac{t-2m_\pi^2}{\pi}\int_{4m_\pi^2}^{\infty} \frac{Imf_+^0(t')}{(t'-t-i\epsilon)\left(\frac{t'}{4}-m_N^2\right)(t'-2m_\pi^2)}dt',
\end{aligned} \tag{3.23}$$

that is totally equivalent to (3.17). Leaving out the contribution from left-hand cut we define the σ-exchange amplitude as

$$A_\sigma^+(t) = A_0 - 16(t-2m_\pi^2)\int_{4m_\pi^2}^{t_c} \frac{Imf_+^0(t')}{(t'-t)(t'-4m_N^2)(t'-2m_\pi^2)}dt', \tag{3.24}$$

where $A_0 = -4\pi f_+^0(2m_\pi^2)/(\frac{1}{2}m_\pi^2 - m_N^2)$ is a constant which we treat as a free parameter. The definition (3.24) is of course now different from A_σ^+ in (3.18).

The second term in (3.24) is exactly zero at the Cheng-Dashen point, so A_0 should not be too large to describe low energy πN data. Notice that other diagrams also produce some contribution to the isoscalar πN amplitude and therefore to Σ.

The expression for the on-shell potential corresponding to σ exchange is obtained from (3.24) going back through eqs. (3.5), (3.4), (3.2)

$$V_\sigma(\vec{k}',\lambda',\vec{k},\lambda) = -\kappa\bar{u}(\vec{p}_3,\lambda_3)u(\vec{p}_1,\lambda_1) \times \left[A_0 - 16(t-2m_\pi^2)\int_{4m_\pi^2}^{t_c} \frac{Im f_+^0(t')}{(t'-t)(t'-4m_N^2)(t'-2m_\pi^2)}dt'\right], \quad (3.25)$$

where $\kappa = \frac{1}{(2\pi)^3}\frac{1}{\sqrt{2\omega_2 2\omega_4}}, \omega_2 \equiv \omega_{p_2}, \omega_4 \equiv \omega_{p_4}$.

Now let us discuss how one proceeds to construct the off-shell potential to be used in the Lippmann-Schwinger equation [24, 69]. In order to be as close as possible to the TOPT concept, first, consider the potential produced by the exchange of a stable σ with mass m_σ whose interaction is described by the Lagrangian

$$\mathcal{L} = -g_{NN\sigma}\bar{\Psi}\Psi\sigma + \frac{g_{\sigma\pi\pi}}{2m_\pi}\partial_\mu\vec{\pi}\partial^\mu\vec{\pi}\sigma. \quad (3.26)$$

Then the potential is given by (see Appendix B)

$$V_\sigma^{st}(m_\sigma^2) = \kappa\frac{g_{\sigma\pi\pi}}{2m_\pi}g_{NN\sigma}(-2p_{2_\mu}p_4^\mu)\frac{1}{2\omega_q}\left(\frac{1}{Z-E_q-E_3-\omega_2}+\frac{1}{Z-E_q-E_1-\omega_4}\right)$$
$$\times\bar{u}(\vec{p}_3,\lambda_3)u(\vec{p}_1,\lambda_1) = \kappa\frac{g_{\sigma\pi\pi}}{2m_\pi}g_{NN\sigma}(-2p_{2_\mu}p_4^\mu)P_\sigma(t,m_\sigma^2)\bar{u}(\vec{p}_3,\lambda_3)u(\vec{p}_1,\lambda_1), \quad (3.27)$$

where we introduced a TOPT σ propagator

$$P_\sigma(t,m_\sigma^2) = \frac{1}{2\omega_q}\left(\frac{1}{Z-E_q-E_3-\omega_2}+\frac{1}{Z-E_q-E_1-\omega_4}\right). \quad (3.28)$$

Taking into account that on energy shell $P_\sigma(t,m_\sigma^2) = \frac{1}{t-m_\sigma^2}$ and $-2p_{2_\mu}p_4^\mu = t-2m_\pi^2$, one can rewrite (3.25) as

$$V_\sigma(\vec{k}',\lambda',\vec{k},\lambda) = V_0 + \frac{1}{\pi}\int dm_\sigma^2\rho_\sigma(m_\sigma^2)V_\sigma^{st}(m_\sigma^2), \quad (3.29)$$

where

$$V_0 = -\kappa\bar{u}(\vec{p}_3,\lambda_3)u(\vec{p}_1,\lambda_1)A_0, \quad (3.30)$$

and

$$\rho_\sigma(m_\sigma^2 \equiv t') = -16\pi \frac{Imf_+^0(t')}{(t'-4m_N^2)(t'-2m_\pi^2)} \frac{2m_\pi}{g_{\sigma\pi\pi}g_{NN\sigma}}. \tag{3.31}$$

Hence we obtained a potential corresponding to a an exchange of the σ meson (with derivative coupling (3.26) to pions), however not with a fixed mass, but distributed in a wide range of masses, weighted by the spectral function $\rho_\sigma(m_\sigma^2)$. And there is a contact term V_0 in addition. The explicit form of (3.29) is

$$\begin{aligned} V_\sigma(\vec{k}', \lambda', \vec{k}, \lambda) &= V_0 - 16\kappa\bar{u}(\vec{p}_3, \lambda_3)u(\vec{p}_1, \lambda_1) \\ \times(-2p_{2_\mu}p_4^\mu) &\int \frac{Imf_+^0(t')}{(t'-4m_N^2)(t'-2m_\pi^2)} P_\sigma(t,t')dt' \end{aligned} \tag{3.32}$$

with $P_\sigma(t,t')$ given by eq. (3.28). Now, since the TOPT propagator $P_\sigma(t,t')$ as well as the pre-factor $-2p_{2_\mu}p_4^\mu = -2\omega_2\omega_4 + \vec{p}_2\vec{p}_4$ are defined off energy shell, the whole expression (3.32) can be extended to the off-shell region.

One more step has to be done, namely a regularization of the obtained potential, since V_σ from (3.32) even without V_0 does not fall off rapidly enough to ensure a convergence of the integrals when solving the Lippmann-Schwinger equation. Therefore we introduce form factors in the form

$$F(p2,p4) = \frac{\Lambda^2}{\Lambda^2+\vec{p}_2^{\,2}} \cdot \frac{\Lambda^2}{\Lambda^2+\vec{p}_4^{\,2}} \tag{3.33}$$

This particular form of the form factor has the following advantages:

- it does not depend on energy.
- it does not modify strongly the on-shell potential (which is assumed to be fully determined by the dispersion integrals) as long as the energy is not too high.
- it does not change the t-dependence of the potential.

The product of $V_\sigma(\vec{k}', \lambda', \vec{k}, \lambda)$ from (3.32) and the form factor $F(p_2,p_4)$ is the final expression for the correlated $\pi\pi$-exchange potential in σ channel.

3.4 Correlated $\pi\pi$-exchange potential in ρ channel

The construction of the ρ-exchange potential is done along the same line as for the σ-exchange potential. But first another "equivalent" transformation of one of the dispersion integrals is needed. As was pointed out in [70] the combination (cf. eq. (3.19))

$$\frac{1}{t-4m_N^2}\left(\frac{m_N}{\sqrt{2}}f_-^1(t)-f_+^1(t)\right)=\frac{A_\rho^{(-)}(s,t)}{24\pi(s+\frac{1}{2}t-m_N^2-m_\pi^2)} \tag{3.34}$$

is analytic at $t=4m_N^2$, because the invariant amplitude $A_\rho^{(-)}(s,t)$ must be free of kinematical singularities. Therefore we can write a dispersion relation equivalent to (3.16) but for the quantity (3.34). The equivalence is broken after we drop the integral along the left-hand cut. The new expression for $A_\rho^{(-)}(s,t)$ is now given by

$$A_\rho^{(-)}(s,t)=12\big(s+t/2-m_N^2-m_\pi^2\big)\int\frac{Im(\sqrt{2}m_N f_-^1(t')-2f_+^1(t'))}{(t'-t)(t'-4m_N^2)}dt'. \tag{3.35}$$

The advantage of this representation of $A_\rho^{(-)}(s,t)$ over that from (3.19) is that the integral converges more rapidly, but the main point is that we get rid of the artificial pole factor $\frac{1}{t-4m_N^2}$ which cannot appear, if we deal with an effective Lagrangian based potential.

We can now write an expression for the total ρ-exchange on-shell potential

$$\begin{aligned} V_\rho(\vec{k}',\lambda',\vec{k},\lambda) &= -\kappa\Bigg[12\big(s+t/2-m_N^2-m_\pi^2\big) \\ &\times\int\frac{Im(\sqrt{2}m_N f_-^1(t')-2f_+^1(t'))}{(t'-t)(t'-4m_N^2)}dt'\bar{u}(\vec{p}_3,\lambda_3)u(\vec{p}_1,\lambda_1) \\ &+6\sqrt{2}\int\frac{Im f_-^1(t')dt'}{t'-t}\bar{u}(\vec{p}_3,\lambda_3)\hat{Q}u(\vec{p}_1,\lambda_1)\Bigg]\vec{\tau}\vec{t} \end{aligned} \tag{3.36}$$

To define this potential off energy shell we follow the procedure described in the previous chapter. We take the interaction Lagrangian for the ρ-meson in the form

$$\mathcal{L}=-g_v\bar{\Psi}\big(\gamma_\mu\vec{\rho}^\mu-\frac{g_t/g_v}{2m_N}\sigma_{\mu\nu}\partial^\nu\vec{\rho}^\mu\big)\frac{\vec{\tau}}{2}\Psi-g_{\rho\pi\pi}(\vec{\pi}\times\partial^\mu\vec{\pi})\vec{\rho}^\mu \tag{3.37}$$

The πN potential produced by this Lagrangian corresponding to a stable ρ-exchange is given in appendix B. In order to identify this potential with the one coming from a dispersion relation, we change it to

$$V_\rho^{st}(m_\rho^2) = -\kappa g_{\rho\pi\pi}\bar{u}(\vec{p}_3,\lambda_3)\left[(g_v+g_t)\gamma^\mu - \frac{g_t}{4m_N}(p_1+p_3)^\mu\right]u(\vec{p}_1,\lambda_1)$$
$$\times\left(\frac{1}{2\omega_q(Z-\omega_q-E_3-\omega_2)}+\frac{1}{2\omega_q(Z-\omega_q-E_1-\omega_4)}\right)(p_2+p_4)_\mu\vec{\tau}\vec{t} \quad (3.38)$$

which is equivalent to the expression given in appendix B on energy shell. After some manipulations one gets

$$\begin{aligned} V_\rho^{st}(m_\rho^2) &= V_A(m_\rho^2)+V_B(m_\rho^2) \\ V_A(m_\rho^2) &= -\kappa\frac{g_{\rho\pi\pi}g_t}{2m_N}(p_1+p_3)^\mu Q_\mu\bar{u}(\vec{p}_3,\lambda_3)u(\vec{p}_1,\lambda_1)P_\rho(t,m_\rho^2)\vec{\tau}\vec{t} \\ V_B(m_\rho^2) &= -\kappa g_{\rho\pi\pi}(g_v+g_t)\bar{u}(\vec{p}_3,\lambda_3)\hat{Q}u(\vec{p}_1,\lambda_1)P_\rho(t,m_\rho^2)\vec{\tau}\vec{t}, \end{aligned} \quad (3.39)$$

where $P_\rho(t,m_\rho^2) = \dfrac{1}{2\omega_q(Z-\omega_q-E_3-\omega_2)}+\dfrac{1}{2\omega_q(Z-\omega_q-E_1-\omega_4)}$. The terms V_A and V_B are analogs of the invariant amplitudes A and B. Noticing that on energy shell $(p_1+p_3)^\mu Q_\mu = s+t/2-m_N^2-m_\pi^2$ and $P_\rho(t,m_\rho^2) = \dfrac{1}{t-m_\rho^2}$ one can again represent the on-shell correlated $\pi\pi$-exchange potential (3.36) as an exchange by a stable ρ with masses m_ρ weighted by spectral functions $\rho_A(m_\rho^2)$ and $\rho_B(m_\rho^2)$

$$V_\rho(\vec{k}',\lambda',\vec{k},\lambda) = \frac{1}{\pi}\int dm_\rho^2\rho_A(m_\sigma^2)V_A(m_\rho^2)+\frac{1}{\pi}\int dm_\rho^2\rho_B(m_\sigma^2)V_B(m_\rho^2), \quad (3.40)$$

$$\rho_A(m_\rho^2\equiv t') = \frac{24\pi m_N}{g_{\rho\pi\pi}g_t}\frac{Im\big(\sqrt{2}m_N f_-^1(t')-2f_+^1(t')\big)}{t'-4m_N^2}, \quad (3.41)$$

$$\rho_B(t') = -\frac{6\pi\sqrt{2}}{g_{\rho\pi\pi}(g_v+g_t)}Im f_-^1(t') \quad (3.42)$$

Finally, the off-shell extention of the ρ-exchange potential is given by

$$\begin{aligned} V_\rho(\vec{k}',\lambda',\vec{k},\lambda) &= \kappa\Bigg[12(p_1+p_3)^\mu Q_\mu \\ &\times\int\frac{Im(\sqrt{2}m_N f_-^1(t')-2f_+^1(t'))}{t'-4m_N^2}P_\rho(t,t')dt'\bar{u}(\vec{p}_3,\lambda_3)u(\vec{p}_1,\lambda_1) \\ &+ 6\sqrt{2}\int Im f_-^1(t')P_\rho(t,t')dt'\bar{u}(\vec{p}_3,\lambda_3)\hat{Q}u(\vec{p}_1,\lambda_1)\Bigg]\vec{\tau}\vec{t} \end{aligned} \quad (3.43)$$

The form factors at the ρ-exchange potential are taken to be of the same form as for the σ-exchange (3.33).

Chapter 4

Three-body singularities

In this chapter we discuss problems related to the numerical solution of the Lippmann-Schwinger equation, and in particular those arising from the three-particle singularities of the t or u-channel propagators in the potential. First we explain how the logarithmic singularities show up in the potential in JLS basis. Then we study the position of those singularities in the complex plane in more detail, and how the singularities can be treated numerically with the contour rotation technic. Finally we discuss a possible violation of unitarity in our model due to 3-body intermediate states.

4.1 Logarithmic singularities in the partial wave potential

First let us rewrite the Lippmann-Schwinger equation (2.30), keeping explicitly only the momentum dependence of the potential and of the T-matrix and the particle indices

$$T_{\mu\nu}(k', k) = V_{\mu\nu}(k', k) + \sum_{\gamma} \int k''^2 dk'' V_{\mu\gamma}(k', k'') \frac{1}{Z - E_\gamma(k'') + i\epsilon} T_{\gamma\nu}(k'', k). \quad (4.1)$$

We are going to solve eq. (4.1) via a numerical integration over k'' by the discretization of the integral. If one can choose an integration scheme for eq. (2.30) with the same mesh points for all k', then one will get a closed system of linear

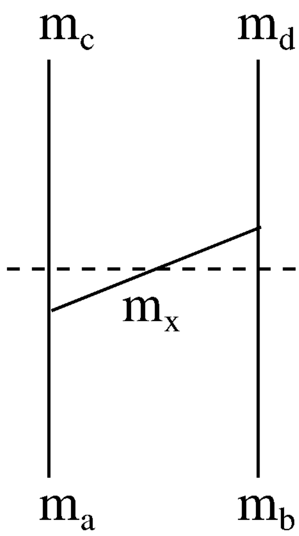

Figure 4.1: Typical s or u-exchange diagram. Dashed line shows the three-body intermediate state.

equations, which can be easily solved numerically. However this method will not work in the presence of singularities in the integrand.

There are two sources of such singularities: those coming from poles of the Green's function, i.e. of $(Z - E_\gamma(k'') + i\epsilon)^{-1}$, and those coming from the potential $V(k', k'')$. The latter originate from three-body propagators of t and u exchange diagrams. The poles of the two-particle propagator do not cause severe problems, because their position is fixed in k'', and they can be removed by a simple transformation [71–73], or integrated out [74]. The 3-body singularities of the potential can not be overcome so easily, because their position in k'' depends on the momentum k' as will be shown below.

Let us consider simultaneously u and t-exchange diagrams. Both can be depicted like the one in fig. 4.1. Let m_a, m_b be the masses of the final particles, m_c, m_d the masses of the intermediate particles, and m_x the mass of the exchanged particle. Consider for example only one time ordering, corresponding to the bcx intermediate state, as shown in fig. 4.1. Then, the 3-body propagator in the potential is given by

$$\frac{1}{Z - E_b(k') - E_c(k'') - E_x(q) + i\epsilon}, \tag{4.2}$$

where $E_b(k'), E_c(k''), E_x(q)$ are the on-shell energies of the particles, and $\vec{q} = \vec{k'} - \vec{k''}$ (we could also define $\vec{q} = \vec{k'} + \vec{k''}$, it will not affect the result). The denominator of the propagator can be equal to zero at some k', k'', if the c.m. energy is above the 3-body threshold ($Z > m_b + m_c + m_x$). If we fix k' and k'', then the expression (4.2) has the pole at some value of the scattering angle $\cos\theta = y(Z, k', k'')$. To obtain the potential in JLS basis one needs therefore to perform an integration of the type (see Appendix.D)

$$\int_{-1}^{1} \frac{R(\cos\theta) d\cos\theta}{y - \cos\theta - i\epsilon} = P.V. \int_{-1}^{1} \frac{R(\cos\theta)}{y - \cos\theta} d\cos\theta + i\pi \int_{-1}^{1} \delta(y - \cos\theta) R(\cos\theta), \tag{4.3}$$

where $R(\cos\theta)$ denotes the regular part of the integrand. After the integration the poles turn into logarithmic singularities at $y = \pm 1$, because for those values of y the position of the pole coincides with the limit of the principle value integral. The partial wave potential will have a cut in the complex k'' plane (at fixed k') corresponding to y moving from -1 to 1. The position of the cut depends on k' and will be studied in the next section.

4.2 The method of contour rotation

One of the ways to deal with 3-body singularities is the method of rotating the integration contour into the complex plane, introduced in [75–77]. It consists of the following steps [78]:

First one makes the substitution $k' = \rho' e^{-i\phi}$ in (4.1) thereby defining the T-matrix for complex k'

$$\begin{aligned} T_{\mu\nu}(\rho' e^{-i\phi}, k) &= V_{\mu\nu}(\rho' e^{-i\phi}, k) \\ &+ \sum_{\gamma} \int_{0}^{\infty} k''^2 dk'' V_{\mu\gamma}(\rho' e^{-i\phi}, k'') \frac{1}{Z - E_\gamma(k'') + i\epsilon} T_{\gamma\nu}(k'', k). \end{aligned} \tag{4.4}$$

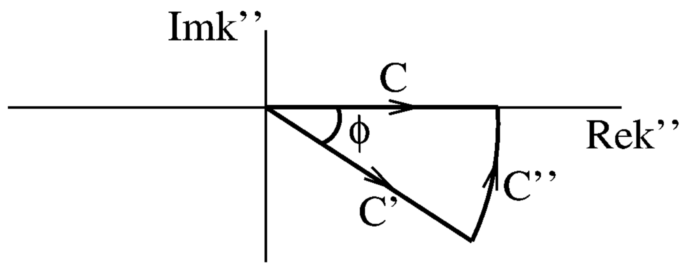

Figure 4.2: Deformation of integration contour in eq. (4.5)

Then the contour of integration in (4.4) can be deformed as shown in fig. 4.2 from C to C' provided that the integral along the infinitely remote arc C'' vanishes (this is satisfied, since the integrand drops fast enough at large k''), and that there are no singularities inside the contour $C'C''C^{-1}$. It is easy to check that the potential $V_{\mu\gamma}(\rho' e^{-i\phi}, k'')$ indeed contains no singularities in this region for sufficiently small ϕ. The same statement can be proved for the T-matrix $T_{\mu\nu}(k'', k)$ [79]. The 2-body Green's function has a pole at $k'' = \frac{1}{2Z}\lambda^{1/2}(Z^2, m_c^2, m_d^2) + i\epsilon$ (where $\lambda(x_1, x_2, x_3) = x_1^2 + x_2^2 + x_3^2 - 2x_1x_2 - 2x_1x_3 - 2x_2x_3$ is a triangle function), and lies above the considered region. Therefore we can change the contour of integration in eq. (4.4) to C'.

$$
\begin{aligned}
T_{\mu\nu}(\rho' e^{-i\phi}, k) &= V_{\mu\nu}(\rho' e^{-i\phi}, k) + \sum_\gamma \int_0^\infty (\rho'' e^{-i\phi})^2 e^{-i\phi} d\rho'' \\
&\times V_{\mu\gamma}(\rho' e^{-i\phi}, \rho'' e^{-i\phi}) \frac{1}{Z - E_\gamma(\rho'' e^{-i\phi}) + i\epsilon} T_{\gamma\nu}(\rho'' e^{-i\phi}, k). \qquad (4.5)
\end{aligned}
$$

Now equation (4.5) can be solved numerically without any problem. The next step is to use eq. (4.5) to obtain the T-matrix for real momenta, putting the final momentum back on the real axis:

$$
\begin{aligned}
T_{\mu\nu}(k', k) &= V_{\mu\nu}(k', k) + \sum_\gamma \int_0^\infty (\rho'' e^{-i\phi})^2 e^{-i\phi} d\rho'' \\
&\times V_{\mu\gamma}(k', \rho'' e^{-i\phi}) \frac{1}{Z - E_\gamma(\rho'' e^{-i\phi}) + i\epsilon} T_{\gamma\nu}(\rho'' e^{-i\phi}, k). \qquad (4.6)
\end{aligned}
$$

The integral can be readily evaluated numerically if, again, the contour of integration does not cross any singularities of the integrand. Really dangerous singularities can appear from the cuts in the potential $V_{\mu\gamma}(k', \rho'' e^{-i\phi})$ discussed in the previous section.

Let us fix k' and look at the position of the cuts in the complex k'' plane. They will correspond to the solution of equation

$$Z - E_b(k') - E_c(k'') - E_x(q) = 0 \tag{4.7}$$

with respect to k'' while $\cos\theta = y$ changes from -1 to 1. It is convenient to introduce the off-shell energy $\tilde{E}_a = Z - E_b$ and off-shell mass $\tilde{m}_a^2 = \tilde{E}_a^2 - k'^2$ of the particle "a". Then eq. (4.7) can be written as conservation of the 4-momentum $q^\mu = \tilde{p}_a^\mu - p_c^\mu$. Squaring gives

$$m_x^2 = \tilde{m}_a^2 + m_c^2 - 2\tilde{E}_a E_c + 2k'k''y. \tag{4.8}$$

Solving this equation one gets

$$k'' = \frac{k'(\tilde{m}_a^2 + m_c^2 - m_x^2)y \pm \tilde{E}_a \sqrt{\lambda(\tilde{m}_a^2, m_c^2, m_x^2) + 4m_c^2 k'^2 (y^2 - 1)}}{2(\tilde{m}_a^2 + k'^2(1 - y^2))} \tag{4.9}$$

Next we consider the expression under the radical in (4.9) (henceforth we will call it $r(y)$). Let us first find such k' at which $r(y)$ is positive for all $y \subset (-1, 1)$. For that purpose one has to solve the equation $r(y = 0) = 0$, since $r(y)$ is maximal at $y = 0$. The solution is

$$k_{c1} \equiv \frac{\lambda((Z - m_c)^2, m_x^2, m_b^2)^{1/2}}{2Z}. \tag{4.10}$$

This expression represents the possibility for the particle "d" with momentum $k'' = 0$ and virtual mass $Z - m_c$ to decay into the system "$x + b$" with the c.m. momentum k'. For $k' < k_{c1}$ the cuts lie on the real axis, as shown in fig. 4.3a and one can safely rotate the contour of integration in the lower half-plane. For $k' > k_{c1}$ the cuts start to move partly away from the real axis as in fig. 4.3b. In this situation the simple deformation of the contour described above does not work. At the moment we do not consider such cases in our model. However at k' above some value (let us call it k_{c2} in the following) the cuts are entirely off the real axis, as plotted in fig. 4.3c or in fig. 4.3d. Then the rotation of the contour is possible again. To evaluate k_{c2} we need to set $r(y = 1) = \lambda(\tilde{m}_a^2, m_c^2, m_x^2) = 0$.

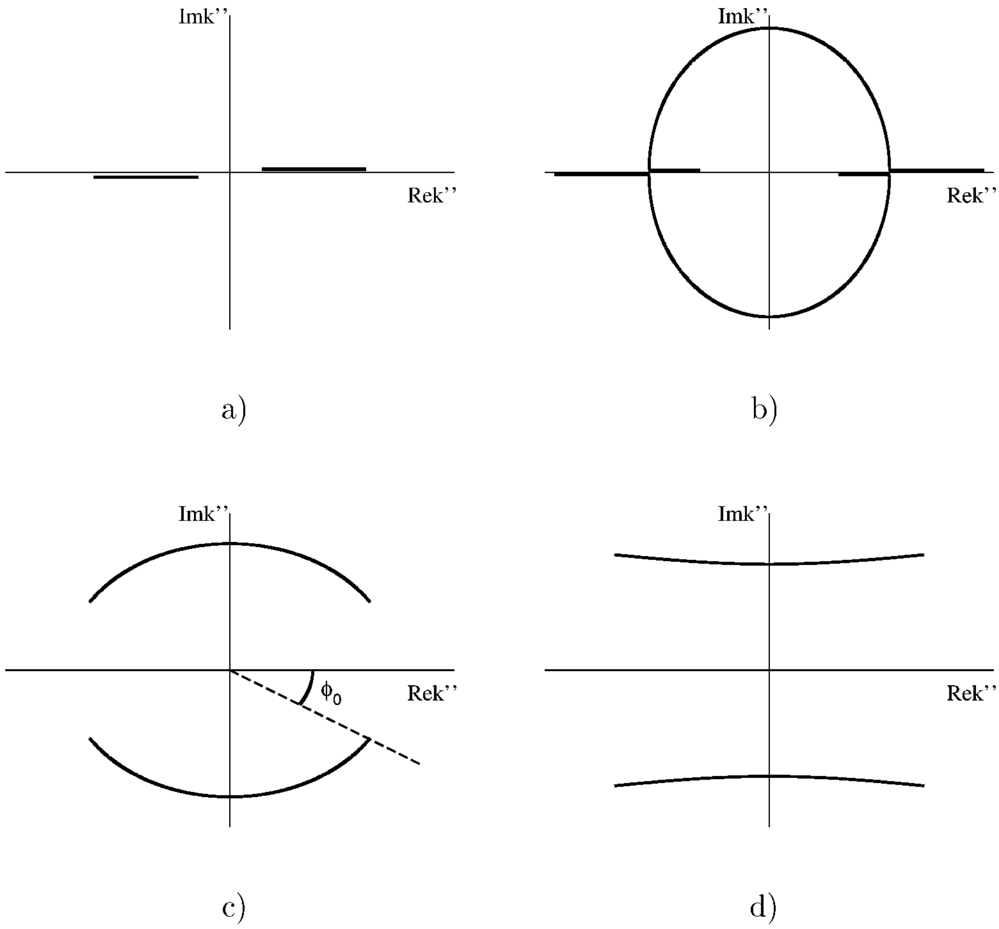

Figure 4.3: The position of the singularities coming from the 3-body propagator in the complex k'' plane. Explanations can be found in the text.

Choosing the solution $\tilde{m}_a^2 = (m_c + m_x)^2$ one gets

$$\begin{aligned} k_{c2} &= \frac{\lambda(Z^2, (m_c + m_x)^2, m_b^2)^{1/2}}{2Z} \\ &= \frac{\left[(Z^2 - (m_b + m_c + m_x)^2)(Z^2 - (m_b - m_c - m_x)^2)\right]^{1/2}}{2Z}. \qquad (4.11) \end{aligned}$$

The physical meaning of k_{c2} is that for $k' > k_{c2}$ ($\tilde{m}_a < m_c + m_x$) the decay process $a \to c + x$ is forbidden. Note that values of k' corresponding to the case $\tilde{m}_a^2 < (m_c - m_x)^2$, at which k'' from (4.9) formally can be real, do not generate any poles in the propagator (4.2), because those k'' do not lie on the sheet that we choose for the complex valued function (4.2) (defined by $ReE_c \geq 0, ReE_x \geq 0$).

In cases when one needs to evaluate the on-shell T-matrix for the processes like $\pi N \to \pi N$ or $\pi N \to \eta N$ transitions, we simply have to set $\tilde{m}_a = m_a$ where m_a is the physical mass of the particle. Then, of course, for stable particles the relation $m_a < m_c + m_x$ always holds, and one deals with the situations like in fig. 4.3c,d. The moment of the transition from fig. 4.3c to fig. 4.3d can be found e.g. from the condition $\frac{dRek''(y=1)}{dy} = 0$, that gives

$$\tilde{m}_a^2 = (m_c/\sqrt{2} \pm \sqrt{m_x^2 - m_c^2/2})^2. \tag{4.12}$$

The cuts as in fig. 4.3d are realized e.g. in the case of nucleon exchange in the $\pi N \to \pi N$ potential, where the physical mass of the nucleon lies in between of the two values of $\tilde{m}_a$ in (4.12).

The contour of integration has to be chosen in such a way that it is not located too close to the real axes, where the 2-body Green's function has singularities, and not too close to the nearest singularity of the potential. The nearest singularities turn out to be those that come from the $\pi\pi N$ intermediate state of the π-exchange diagrams in the $\pi N \to \sigma N$ and $\pi N \to \rho N$ potentials. They appear already at energies above one pion production threshold. The angle ϕ in (4.6) should be therefore taken less then ϕ_0 (cf. fig. 4.3c), defined as $\tan(\phi_0) = \left|\frac{Imk''}{Rek''}\right|_{y=1}$. For energies up to $Z = 1.9$GeV we obtain stable numerical results with $\tan\phi = 0.18$.

One should mention here, that there are poles in the complex k'' plane originating from u and t channel form factors, proportional to $\frac{1}{\vec{q}^2 + \Lambda^2}$. These poles are located at

$$k'' = k' \cos\theta \pm i\sqrt{\Lambda^2 + k'^2 \sin\theta^2}, \tag{4.13}$$

lying on the part of the circle $(Rek'')^2 + (Imk'')^2 = \Lambda^2 + k'^2$, similar to the curve in fig. 4.3c. The critical angle ϕ_0 that bounds the singularities from above(in the lower half-plane) is given by $\tan(\phi_0) = \Lambda/k' \gtrsim 1$, and therefore does not cause any problems for the integration along the contour. The same remark concerns singularities from kinematical factors like $1/E_x(q)$, etc.

Finally let us consider the situation, when we have an unstable system in the final state, e.g. σN. The σ does not have a sharp mass, but is rather distributed in a mass range starting from the $\pi\pi$ threshold. Therefore, to calculate the σ-meson production amplitude one has to deal with cuts as those in fig. 4.3a and in fig. 4.3b (that we presently are not able to do). A similar situation occurs for the $\pi N \rightarrow \pi\Delta$ reaction. However, in the case of the $\pi N \rightarrow \rho N$ transition the difference between k'_{c1} and k'_{c2} (in the π-exchange diagram) is rather small, and for the most part of the ρ mass distribution we are in the situation of fig. 4.3a. Therefore the calculation e.g. of the $\pi N \rightarrow \rho N$ cross section is possible in our approach, as long as we do not include the tail of the resonance (which obviously should be a bad approximation for the σ-meson).

4.3 Violation of three-body unitarity

Another problem closely related to the 3-body intermediate states is a unitarity constraint [28]. The potential of our model is hermitian below the first ($\pi\pi N$) three-particle threshold. This ensures unitarity for the diagonal part of the $\mathcal{T}$-operator defined in (2.17) ($\mathcal{T}$ is diagonal in JLS basis for $\pi N \rightarrow \pi N$ transition):

$$i(\mathcal{T}_{ii} - \mathcal{T}_{ii}^{\dagger}) = \sum_j (2\pi)\delta(E_i - E_j)\mathcal{T}_{ij}\mathcal{T}_{ji}^{\dagger}. \tag{4.14}$$

Above the $\pi\pi N$ threshold the imaginary part of the potential is not zero, because of the three body propagator (4.2)

$$Im \frac{1}{Z - E_b(k') - E_c(k'') - E_x(q) + i\epsilon} = -i\pi\delta(Z - E_b - E_c - E_x). \tag{4.15}$$

This is not yet a problem, because eq. (4.14) simply changes to

$$i(\mathcal{T}_{ii} - \mathcal{T}_{ii}^{\dagger}) < \sum_j (2\pi)\delta(E_i - E_j)\mathcal{T}_{ij}\mathcal{T}_{ji}^{\dagger}, \tag{4.16}$$

where inequality is due to the fact that the sum in (4.16) does not include 3-body states (since we do not calculate 3-particle production cross sections). This inequality, however, holds only if the imaginary part of the potential is negative. Here we give a schematic explanation why a problem can arise.

Fig. 4.4a shows the contribution to the imaginary part of the potential from two time orderings of some t channel diagram (the treatment of u-channel diagrams

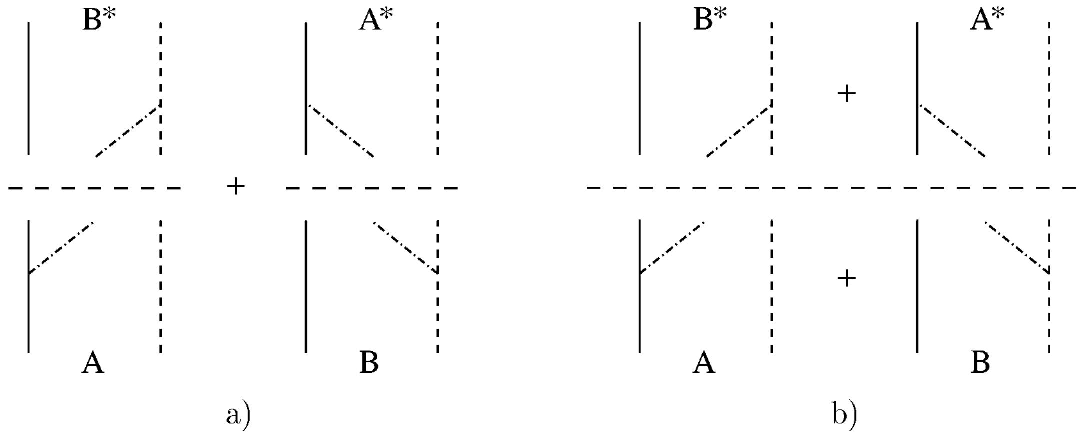

Figure 4.4: Unitarity cuts for t-channel exchange diagrams.

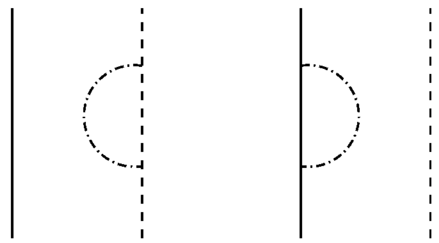

Figure 4.5: Additional diagrams restoring unitarity.

in this respect is similar). The figure should be understood as an expression $A \times B^* + B \times A^*$ multiplied by the δ-function (4.15), where A and B are the vertices. This quantity does not have a definite sign. The correct answer obeying unitarity constrains corresponds to the diagram in fig. 4.4b, because $(A + B)(A^* + B^*)$ is always positive. This would require the inclusion of additional diagrams in the potential, shown in fig. 4.5. In principle we had to include them in the begining, because these diagrams contain three particles in the intermediate state, satisfying the condition that we impose on the potential. The vertices entering into such diagrams are the same as in the usual t-channel exchange graphs. The reason, why we neglected them is just their technical complexity, especially when having to consider correlated $\pi\pi$ exchange. Note, that the quantity $A \times B^* + B \times A^*$ does not have to be necessarily negative, but unfortunately in some cases it is. Luckily the violation of unitarity is extremely small until one moves to higher energies. In

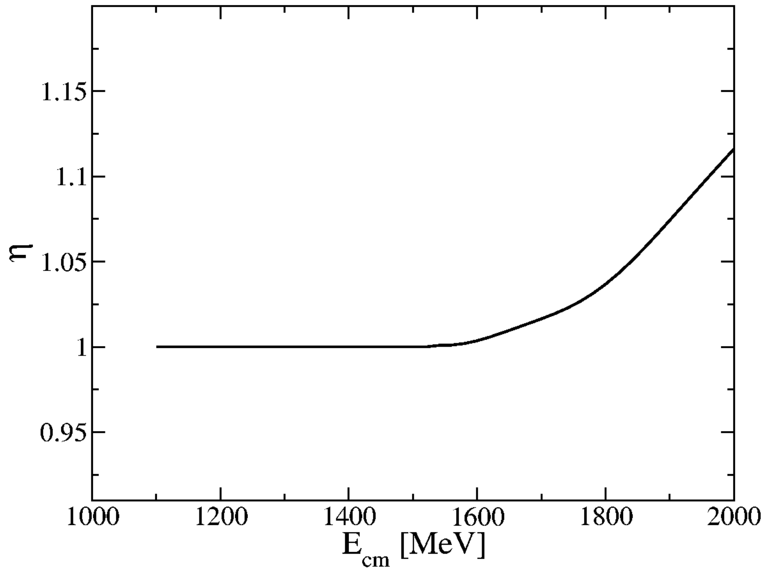

Figure 4.6: Inelasticity parameter η for σ-exchange.

the potential of our model only in one case namely for the t-channel σ exchange (calculated by means of a dispersion relation method) unitarity is violated sizably already at energies 1.85-1.9GeV. If we look at the inelasticity parameter η of the $\pi N \to \pi N$ amplitude calculated with σ-exchange alone, then we see that it starts to exceed one in the above mentioned region. This is another reason why we stop our analysis at energies around 1.9GeV.

Chapter 5

Results

In this chapter we present the results of our model for πN elastic scattering and for the $\pi N \to \pi\eta$ transition in the energy range from πN threshold up to 1.9 GeV. The chapter is organized as follows. First we discuss the parameters of the model, i.e. how they are fixed, and which of them are really crucial for the fit and which are not. Then we survey the results of the fit for πN phase shifts and inelasticities. In particular, the role of the background and of the resonance contributions is analyzed. We also compare the results with those of the previous version of the model. Furthermore, we briefly discuss the results for the $\pi N \to \rho N$ cross section. After that we look at the $\pi N \to \eta N$ total cross section and angular distributions and discuss the role of the background in this process.

5.1 Parameters of the model

Our model is based on the effective potential, which was described in section 2.4. It contains a number of parameters, some of which are well known physical quantities, some were taken from the literature and the rest was determined by a fit to the data.

The masses of all the particles appearing in the model are collected in table 5.1 Here one should pay attention to the mass of the σ meson. While the σ exchange in the $\pi N \to \pi N$ potential is evaluated using a dispersion relation, we have another

Mesons				Baryons	
m_π	138.03	m_ω	782.6	m_N	938.926
m_η	547.45	m_{a_0}	982.7	m_Δ	1232.0
m_σ	650.0	m_{a_1}	1260.0		
m_ρ	769.0				

Table 5.1: Masses of mesons and baryons (in MeV) used in the calculations.

t-channel σ exchange in the $\sigma N \to \sigma N$ potential. In this case we choose the value $m_\sigma = 650$ MeV, which was extracted from a Breit-Wigner parameterization of the correlated $\pi\pi$-exchange in ref. [57] .

Table 5.2 contains coupling constants and cutoff parameters of the form factors for the vertices entering into t and u-exchange diagrams and into contact terms, i.e. those, which constitute the background.

Vertex	Type of the diagram	Coupling constant	Ref.	Cutoff Λ [MeV]
correlated $\pi\pi$–exchange:				
	ρ–channel			*1000*
	σ–channel	$A_0 = \mathit{25}$ MeV$/F_\pi^2$		*900*
$NN\pi$	N exchange	$\frac{f_{NN\pi}^2}{4\pi} = 0.0778$	[80]	*1100*
$N\Delta\pi$	Δ exchange	$\frac{f_{N\Delta\pi}^2}{4\pi} = 0.36$	[80]	*1800*
$NN\rho$	N exchange	$\frac{g_{NN\rho}^2}{4\pi} = 0.84$	[80]	*1600*
		$\kappa = 6.1$	[80]	
$NN\rho\pi$	contact term	$\sim f_{NN\pi} g_{NN\rho}$		*1100*
$NN\pi$	π exchange	$\sim f_{NN\pi}$		*900*
$\pi\pi\rho$	π exchange	$\frac{g_{\pi\pi\rho}^2}{4\pi}$		900
$NN\omega$	ω exchange	$\frac{g_{NN\omega}^2}{4\pi} = 11.0$	[80]	*1200*
$\omega\pi\rho$	ω exchange	$\frac{g_{\omega\pi\rho}^2}{4\pi} = 10.0$	[81,82]	*1200*
NNa_1	a_1 exchange	$\sim f_{NN\pi}$		*1600*
$a_1\pi\rho$	a_1 exchange	$\sim g_{NN\rho}$		1600
$NN\rho$	ρ exchange	$g_{NN\rho}, \kappa$		*1400*

$\rho\rho\rho$	ρ exchange	$\sim g_{NN\rho}$		1400
$NN\rho\rho$	contact term	$\sim g^2_{NN\rho}\kappa$		*1200*
$N\Delta\pi$	N exchange	$\frac{f^2_{N\Delta\pi}}{4\pi} = 0.36$	[80]	*1600*
$\Delta\Delta\pi$	Δ exchange	$\frac{f^2_{\Delta\Delta\pi}}{4\pi} = 0.252$	[83, 84]	*1800*
$N\Delta\rho$	ρ exchange	$\frac{f^2_{N\Delta\rho}}{4\pi} = 20.45$	[80]	*1400*
$\Delta\Delta\rho$	ρ exchange	$\frac{g^{V\,2}_{\Delta\Delta\rho}}{4\pi} = 4.69,$	[83, 84]	*1400*
		$\frac{g^T_{\Delta\Delta\rho}}{g^V_{\Delta\Delta\rho}} = 6.1$	[83, 84]	
$\pi\pi\rho$	ρ exchange	$\frac{g^2_{\rho\pi\pi}}{4\pi} = 2.90$	[85]	*1400*
$NN\sigma$	N exchange	$\frac{g^2_{NN\sigma}}{4\pi} = 13$	[57]	*1800*
$\pi\pi\sigma$	π exchange	$\frac{g^2_{\pi\pi\sigma}}{4\pi} = 0.25$	[86]	1050
$NN\sigma$	σ exchange	$\sim g_{NN\sigma}$		*1700*
$\sigma\sigma\sigma$	σ exchange	$\frac{g^2_{\sigma\sigma\sigma}}{4\pi} = \mathit{0.275}$		1700
$NN\eta$	N exchange	$\frac{f^2_{NN\eta}}{4\pi} = 0.00934$	[23]	*1500*
NNa_0	a_0 exchange	$\frac{g_{NNa_0} g_{\pi\eta a_0}}{4\pi} = 8.0$	[23]	*1500*
$\pi\eta a_0$	a_0 exchange			1500

Table 5.2: Parameters of the vertices which enter into the background diagrams. Free parameters are given in italics. The most important contributions are underlined.

The parameters which are not fixed from other sources are shown in italics. These are the purely phenomenological coupling constant at the triple σ vertex, $g_{\sigma\sigma\sigma}$, and the subtraction constant A_0 for the dispersion relation in the σ channel (which could be also called a "bare Σ term"). In addition the cutoff masses are treated as free parameters and they are to be determined by the fit. Here we should emphasize that we restrict ourselves to values of the cutoff masses of about 1-1.5 GeV (in some cases up to 1.8 GeV for heavy exchanged particles), i.e. values in line with typical hadronic scales, as was already discussed in section 2.5. Some diagrams contribute very little to the potential. In this case the fit is practically insensitive to the parameters on which such diagrams depend. This type of diagrams is not underlined in table 5.2. The role which other diagrams play for the final result is discussed below.

Parameters of the pole diagrams (bare masses and coupling constants) are given

		$f^2/(4\pi)$			
Resonance	Bare mass [MeV]	πN	$\pi\Delta$	ρN	ηN
$N^*_{S_{11}}(1535)$	2051	0.00045	1.09(-)		0.0247
$N^*_{S_{11}}(1650)$	1919	0.0067		0.046[1]	
$N^*_{P_{13}}(1720)$	1910	0.0031	0.0085(-)		0.079(-)
$N^*_{D_{13}}(1520)$	2263	0.00037	0.0118	0.609	0.0008
$\Delta(1232)$	1459	0.163			
$\Delta_{S_{31}}(1620)$	2419	0.0154	2.91(-)		
$\Delta_{P_{31}}(1910)$	2121	0.0043	0.007(-)		
$\Delta_{D_{33}}(1700)$	2252	0.00038	0.03(-)	0.011	

Table 5.3: Parameters of the pole graphs: bare masses and coupling constants. The minus sign in parenthesis indicates that the coupling constant is negative.

in table 5.3. Recall that bare nucleon mass and bare coupling constant $f^B_{\pi NN}$ are not free parameters, because they are fixed by the physical values of the same quantities (see section 2.7). However, the cutoff at the πNN vertex was allowed to vary, in order to fit the P_{11} partial wave. The resulting parameters for the nucleon pole are:

$$M_0 = 1239 \ MeV, \quad \frac{(f^B_{NN\pi})^2}{4\pi} = 0.0166, \quad \Lambda = 1950 \ MeV. \tag{5.1}$$

The cutoff masses for other resonances were all set to 2 GeV, because in this case the result depends weakly on the choice of the cutoff. Its effect can be always compensated by a corresponding change in the coupling constant. The largeness of the resonance cutoff is motivated by the employed specific form of the resonance form factor which falls off with momentum rather rapidly even for such a large cutoff mass (see section 2.6).

By default we adopt a positive value for the sign of the bare coupling constants. However, we use negative coupling constants when demanded by the data. In the case of the $N^*_{P_{13}}(1720)\eta N$ vertex, we changed the sign of the coupling constant in order to get a better description of the $\pi N \to \eta N$ differential cross section via

[1] $g^2/(4\pi)$

an interference of the P_{13} with other partial waves. At this point we would like to remark that among the three phase shift analyses whose results are shown in figures we use the energy independent analysis from ref. [45] as a central one for our fit, because this analysis relies on the smallest number of assumptions about behavior of the amplitudes.

5.2 πN elastic scattering

We start the discussion of the elastic πN data by first looking at the phase shifts in the c.m energy range up to 1.9 GeV as they result from the original model of O. Krehl [1] (cf. figs. 5.1 and 5.2). In general the quality of the fit is rather good, but there are some unsatisfactory points, that we would like to stress here.

Let us consider the deviations of the model results from the data in different partial waves. Those occur mostly in P_{13}, S_{31}, and D_{33}. Of course, the deviation is caused by the presence of resonances in these partial waves, which are not yet included in the model. However, it is easy to see, that the inclusion of those resonances will not help in the case of P_{13} and S_{31}. This is because those resonance contributions must disappear above the position of the resonance within the energy range given roughly by the width (and the phase shift must turn back to the background or change by 180°), whereas, as one can see from figs. 5.1 and 5.2, in the P_{13} partial wave the background goes in the opposite direction to the data, and in S_{31} partial wave the deviation from the data at energies above the position of the resonance is huge. The situation in the D_{33} partial wave is not that bad, and the inclusion of a resonance seems to be possible.

The second problem of the existing πN model is the presence of a long tail of the $S_{11}(1650)$ resonance. This leads to the unpleasant feature, that the low energy S_{11} phase shift is strongly determined by the influence of this resonance. Of course, this influence has simply the effect of a contact term, but its strength is related to the parameters of the resonance. Therefore the tail of the $S_{11}(1650)$ resonance is modified (becomes stronger or weaker) if one changes something in the dynamics of the S_{11} partial wave, e.g. adds additional channels coupled to the $S_{11}(1650)$ resonance. Thus, this problem leads also to technical difficulties apart

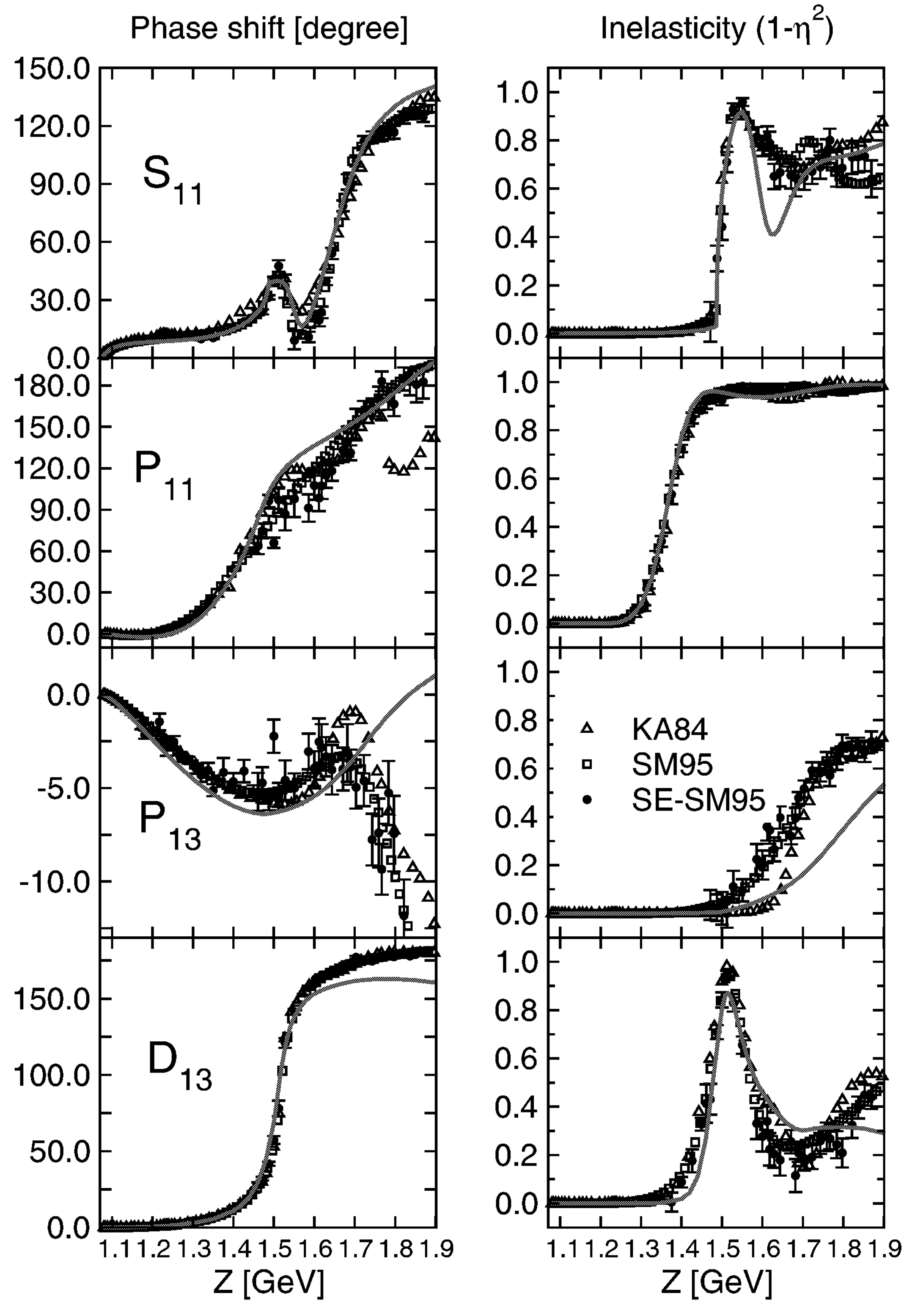

Figure 5.1: Description of the phase shifts and inelasticities by the πN model of O. Krehl [1] (solid curves) for the isospin $I = 1/2$ partial waves. The data are from the phase sift analyses KA84 [44], SM95 [45], and SE-SM95 [45].

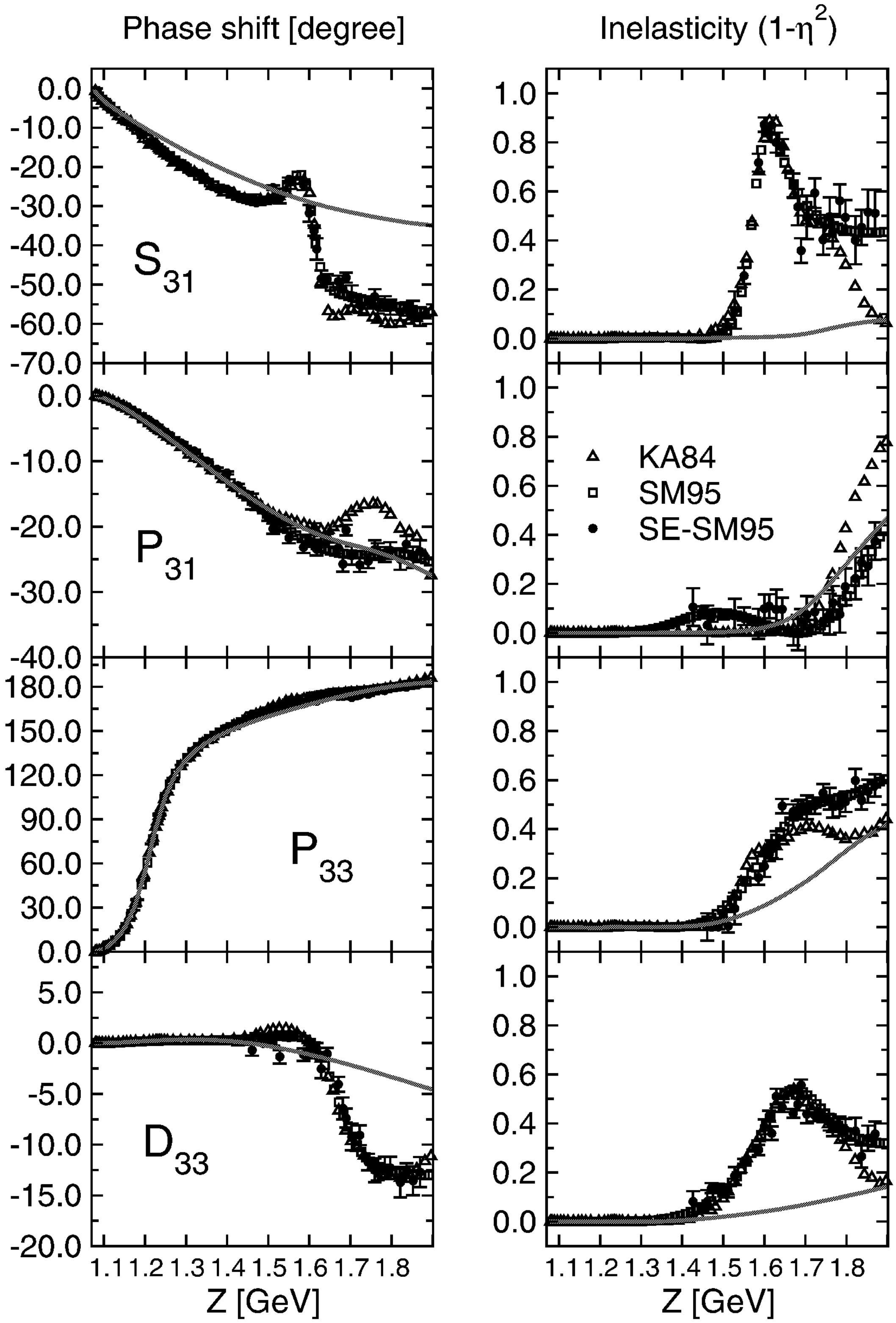

Figure 5.2: Description of the phase shifts and inelasticities by the πN model of O. Krehl [1] (solid curves) for the isospin $I = 3/2$ partial waves. The data are as in fig. 5.1.

from the fact, that it is hard to justify this behaviour physically[2]. Fig. 5.3 shows the discussed effect. One can see that the low energy S_{11} phase shift even changes its sign when all couplings to the $S_{11}(1650)$ resonance are switched off. On the other hand the influence of the $N^*(1535)$ resonance is more localized.

We analyzed the source of this problem. It turned out, that the long tail of the $S_{11}(1650)$ resonance is mostly due to rather hard form factors used in the model and, in particular, in diagrams of the $\pi N \to \rho N$ transition potential (there is a direct coupling of the ρN channel to the $S_{11}(1650)$). As was mentioned before we tried to avoid the use of extremely large cutoff masses. Another feature that allows us to greatly reduce the near threshold contribution from the $S_{11}(1650)$ resonance is that we choose the derivative coupling for the $N^*_{S_{11}}N\pi$ (see appendix B) vertex in analogy with the $NN\pi$ coupling. Finally we need to compensate for the absence of a resonance tail at threshold. We do this by exploiting an additional freedom in the correlated $\pi\pi$-exchange in the σ-channel, namely by introducing a subtraction constant in the dispersion relation (it was set to zero by hand in the old model). This procedure was described in chapter 3.

Now, let us consider how the background of the new model is constructed. First one should note that the main contribution to the background at low energies comes, of course, from the elastic πN channel. That is why it is interesting to see the importance of various πN graphs for the different partial waves. There are five diagrams in the $\pi N \to \pi N$ potential: σ and ρ t-channel exchanges, nucleon and Δ u-channel exchanges, and the nucleon (s-channel) pole diagram. Their contributions to the potential are shown in fig. 5.4 (the nucleon pole, which contributes only to the P_{11} partial wave, is omitted, because in this case the potential depends on the bare parameters which do not have any physical meaning). One can notice that the contribution from the Δ-exchange is very small in all partial waves. This justifies that we do not include u-channel graphs involving heavier resonances. The s waves are dominated by the ρ and σ exchanges. The nucleon exchange becomes important in higher partial waves. Note also, that the ρ-exchange alone provides such a strong attraction in the P_{11} partial wave that it is almost sufficient

[2] As was shown by Weinberg and Tomozawa [87,88] the isovector s-wave πN scattering length is fully determined to leading order by the pion mass m_π and pion decay constant F_π. Therefore, appearance of parameters, related to the $N^*(1650)$ resonance is unnatural

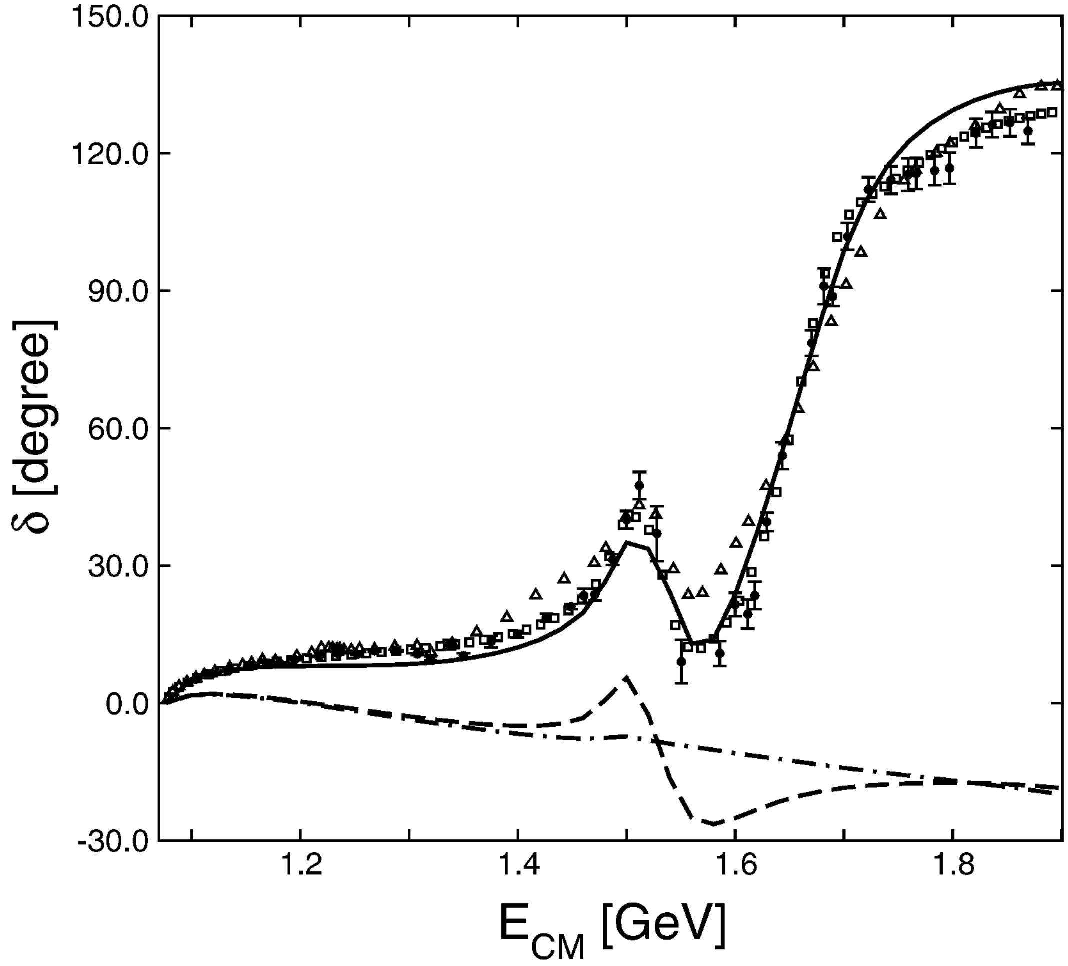

Figure 5.3: The phase shift in the S_{11} partial wave. The curves correspond to the full model of O. Krehl [1] (solid line), the full model with the contribution of the $S_{11}(1650)$ resonance switched off (dashed line), and with both $S_{11}(1650)$ and $S_{11}(1535)$ resonance contributions switched off (dash-dotted line). The data are as in fig. 5.1.

for the formation of a resonance. However it is partly cancelled by the contribution from the nucleon pole. One should emphasize here that, in contrast with the old model, we do not have much freedom in the ρ and σ exchanges (except for one subtraction constant) since their low energy on-shell potential is fixed due to our choice of the form factors (see chapter 3). Thus, the simultaneous description of the background (in the sense discussed above) in seven partial waves with such a small number of parameters is to be considered as a success of our model (cf. dashed lines in fig. 5.5 and fig. 5.6). We have not included the P_{11} partial wave in these consideration, because there the coupling to the σN-channel plays a rather important role.

The next step is the inclusion of the inelastic channels (cf. the solid lines in fig. 5.5 and fig. 5.6). The most important of them are those, that model the effect of the $\pi\pi N$ channel namely ρN, σN and $\pi\Delta$. The σN channel couples dominantly to the P_{11} πN partial wave. This happens because, due to the parity differences, the P_{11} partial wave corresponds to a relative s-wave in the σN system. In the course of fitting the parameters attraction is introduced into the σN channel and also a strong $\pi N \to \sigma N$ transition potential results. This, in turn, provides additional attraction in the πN channel via coupled-channels effects and eventually leads to a dynamical generation of the Roper resonance $N^*(1440)$ in the P_{11} partial wave. This effect was explored in detail in previous studies [1, 23]. The channels ρN and $\pi\Delta$ are responsible for the inelasticities at high energies in all partial waves, in particular in D_{13}, P_{31}, and P_{33}. In the P_{33} partial wave it is the only source of inelasticity, because there are no P_{33} resonances in this energy region that couple strongly to the πN system [89]. The most important diagrams that give contributions to the P_{33} inelasticity are the ρ-exchange in the $\pi N \to \pi\Delta$ potential and, partly, the nucleon exchange in the $\pi N \to \rho N$ potential. One should mention here also the π-exchange diagram in the $\pi N \to \rho N$ transition. It turns out to be much too strong in the P_{13} and S_{11} partial waves independent of the cutoff used. Its contribution alone produces a very strong cusp in the region of the ρN threshold in the S_{11}, and destroys the behavior of the P_{13} phase shift, bending it upwards. Luckily the π-exchange contribution is mostly cancelled by the $\pi N \to \rho N$ contact term from the Wess-Zumino Lagrangian, and also by the ω-exchange diagram. In the end, the phase shifts as a whole are not affected too much by the inelastic channels.

The final step in the description of the elastic πN data consists in adding the resonance terms. Of course, this has to be done simultaneously with adjusting the parameters of the resonance couplings to other channels (in our case to the ηN channel), and describing the transition cross sections. In this section we only show the impact of the resonances on the πN phase shifts and inelasticities. We included resonances in all partial waves except for the P_{11} where the resonance is generated dynamically via a strong coupling to the σN channel. In the S_{11} partial wave there are two resonances, namely $N^*(1535)$ and $N^*(1650)$. The former dominates the near threshold $\pi N \to \eta N$ cross section. As can be seen from the parameters given in table 5.3, among the effective $\pi\pi N$ channels, the $\pi\Delta$ channel is allowed to couple to most of the resonances. This is done because it opens at rather low energies (in contrast to the ρN channel) and can contribute to both ($I = 1/2$ and $I = 3/2$) isospin channels. Since we cannot calculate $\pi N \to \pi\pi N$ observables directly at the moment – which would allow to further constrain the relative importance of the different $\pi\pi N$ channels – we choose this as the simplest possibility to describe the $\pi\pi$ part of the πN inelasticity. However, in addition the ρN channel needs to be coupled to some resonances namely to $D_{13}(1520)$, $S_{11}(1650)$, and $D_{33}(1700)$. In those cases the different energy behavior resulting from the ρN channel is required for a satisfactory description of the data.

The position of the $P_{31}(1910)$ resonance is located above our region of interest (which is from πN threshold up to ~ 1.9 GeV), but nevertheless it was included because its tail still influences some noticeable part of this region.

Notice that, among others, the inelasticity in the P_{13} partial wave shows an incorrect trend at high energies, and the data are underestimated. A similar, but less pronounced deficiency can be found in the D_{13} inelasticity. Some authors claim, that there must be a sizable contribution from the ωN channel, which opens at around 1.7 GeV, to these particular partial waves [16]. Therefore, the inclusion of the ωN channel might improve the description of these data.

The correct description of the isospin $I = 3/2$ resonances is not important for a calculation of the $\pi N \to \eta N$ cross section (as well as for the $\pi N \to K\Lambda$ or $\pi N \to \omega N$ transitions). However, it is needed for the self-consistency of the

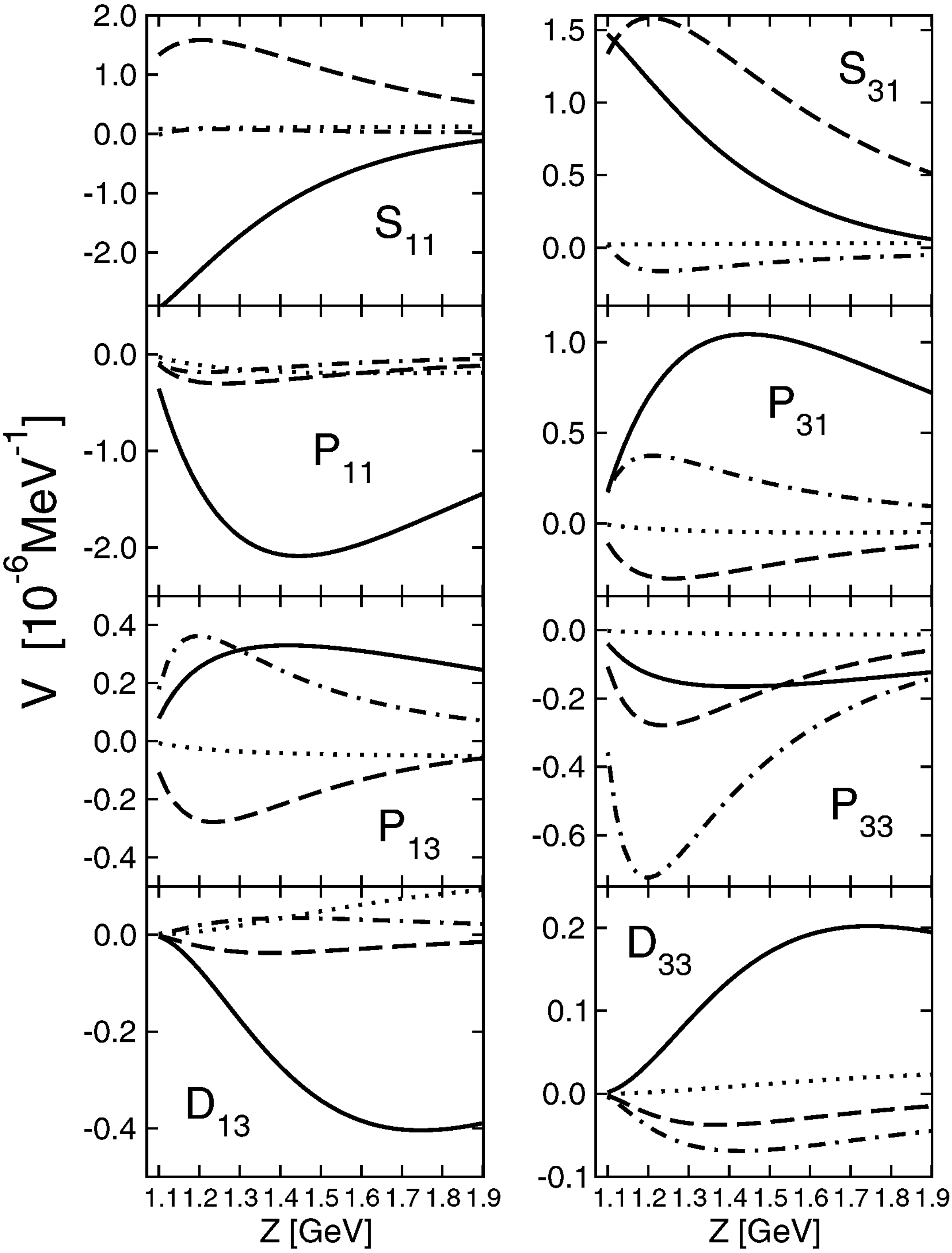

Figure 5.4: Contributions of different diagrams to the $\pi N \to \pi N$ potential. The ρ-exchange is denoted by the solid line, σ-exchange by the dashed line, nucleon exchange by the dash-dotted line, and Δ-exchange by the dotted line.

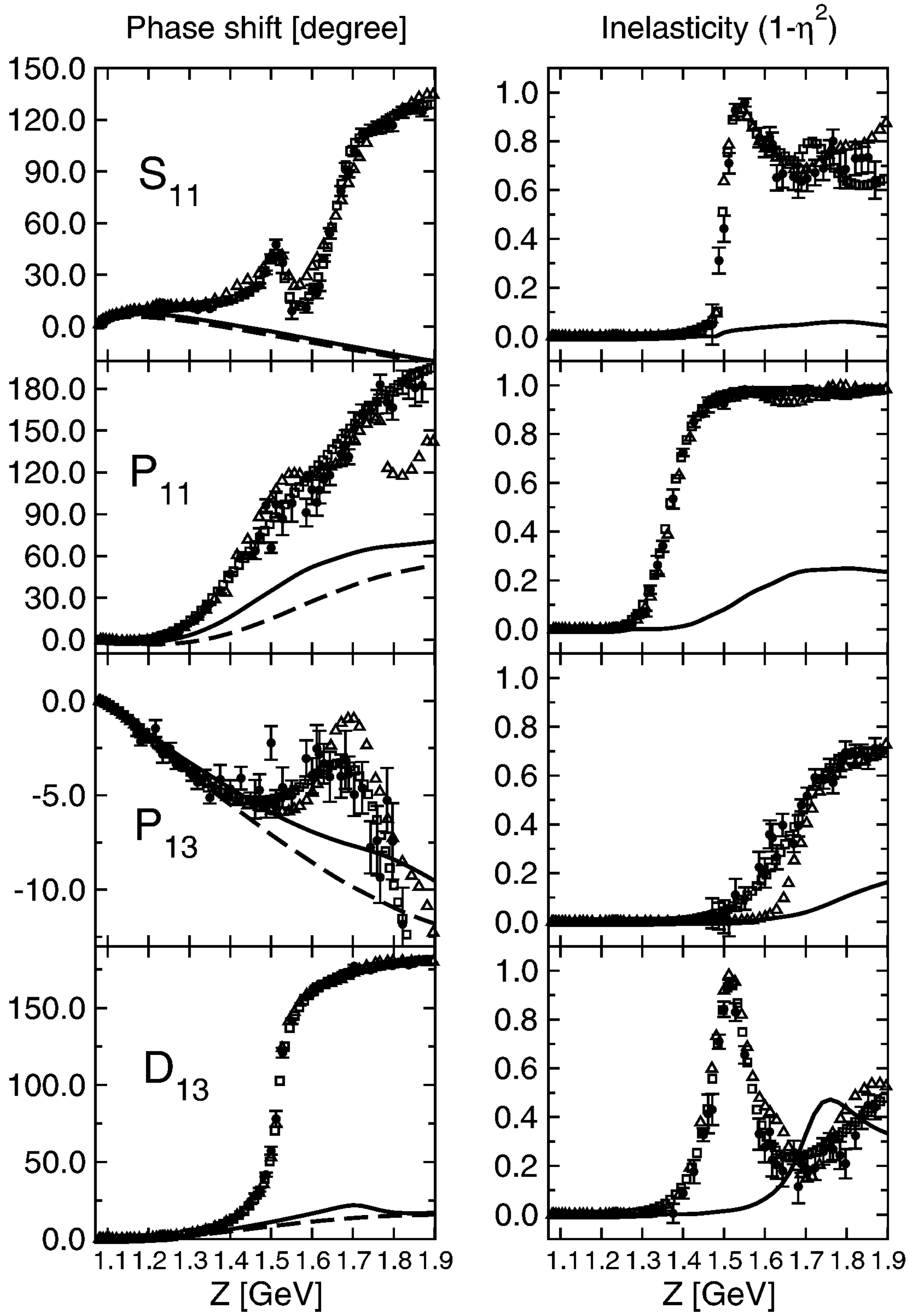

Figure 5.5: Background contribution to the πN phase shifts and inelasticities for the isospin $I = 1/2$ partial waves. The solid line includes the couplings to all channels, except σN, which contributes noticeably to the P_{11} partial wave only. The dashed line corresponds to a calculation based on the $\pi N \to \pi N$ contribution alone. The data are as in fig. 5.1.

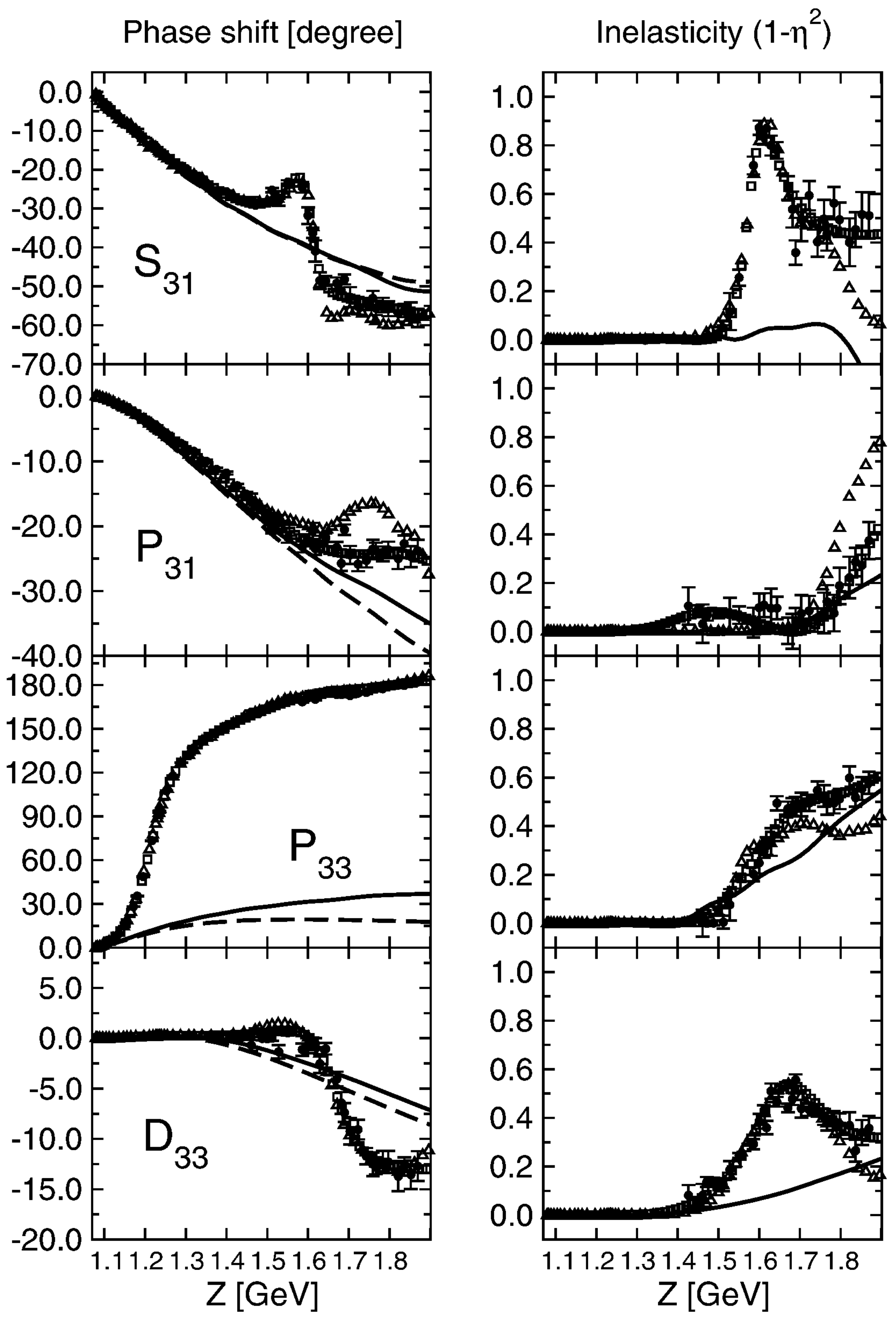

Figure 5.6: Background contribution to the πN phase shifts and inelasticities for the isospin $I = 3/2$ partial waves. The solid line includes the coupling to all channels. The dashed line corresponds to a calculation based on the $\pi N \to \pi N$ contribution alone. The data are as in fig. 5.1.

model, and, of course, for the planned inclusion of the $K\Sigma$ channel.

Figs. 5.9 and 5.10 show another popular representation for the partial wave decomposition, namely in terms of the real and imaginary parts of the partial wave amplitude τ.

In order to get an overall picture for the agreement of our model with the πN data and also to see how far in energy we can go in the description of πN observables without worrying about higher partial waves, we show results for the total and elastic cross sections in the $\pi^- p$ and $\pi^+ p$ channels in fig. 5.11 and fig. 5.12. (Also shown is $\pi^- p \to \pi^0 n$ cross section , because this is the only inelastic channel below the laboratory momentum $p_{lab} \sim 0.4$ GeV/c.) One can see that for the $\pi^- p$ reactions the cross sections calculated within our model start to strongly underestimate the data around $p_{lab} \sim 0.7 - 0.8$ GeV/c, which correspond to c.m. energies $Z \sim 1.5 - 1.6$ GeV. On the other hand in case of the $\pi^+ p$ reactions (which correspond to pure $I = 3/2$ scattering) the deviation from the data is smaller and starts at $p_{lab} \sim 0.9 - 1.0$ GeV/c ($Z \sim 1.7$ GeV). This fact is easy to understand if one looks at the partial wave amplitudes for $J = 5/2$ (fig. 5.13). In the region below $Z = 1.9$ GeV the $I = 1/2$ partial waves have much stronger manifestations of resonances (which are not included in our model). We will come back to this point when we discuss the $\pi N \to \rho N$ cross section. One should also mention here that, although we did not fit the background for $J = 5/2$ partial waves, we automatically obtained a good description of it in the sense that it enables us to include corresponding resonances.

Finally, let us assure ourselves that the low energy parameters of the πN scattering are in a reasonable agreement with available data, as it should be, since we fit our model to the phase shift analyses. The s and p-wave scattering lengths and volumes are collected in table 5.4.

5.3 The $\pi N \to \rho N$ cross section

As we already mentioned before, the calculation of the ρN production cross section is technically possible in our present scheme in contrast to, e.g., $\pi\Delta$ or σN production. A good approximation for calculating the $\pi N \to \rho N$ cross section

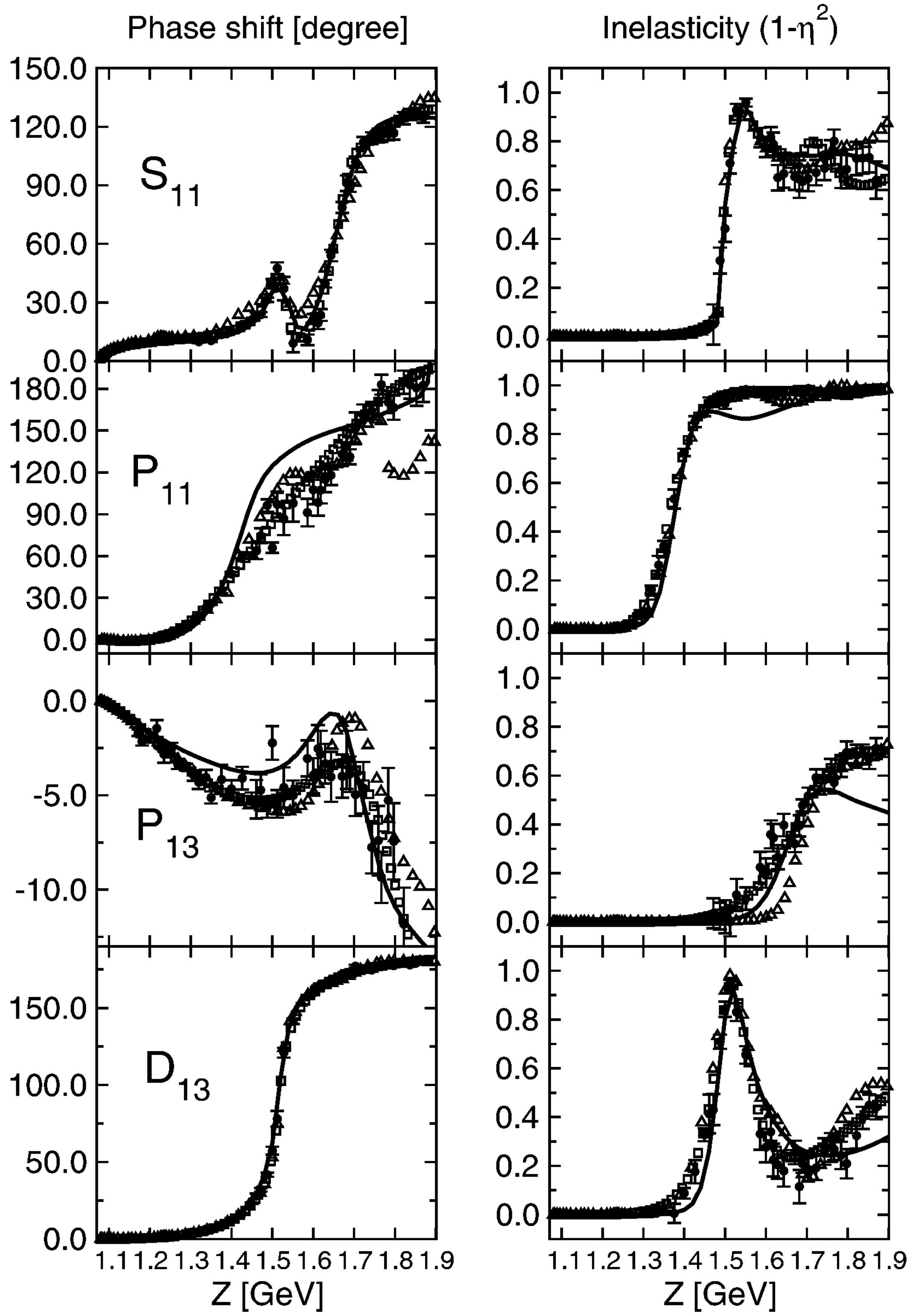

Figure 5.7: Full model results for the πN phase shifts and inelasticities in the $I = 1/2$ channel. The data are as in fig. 5.1.

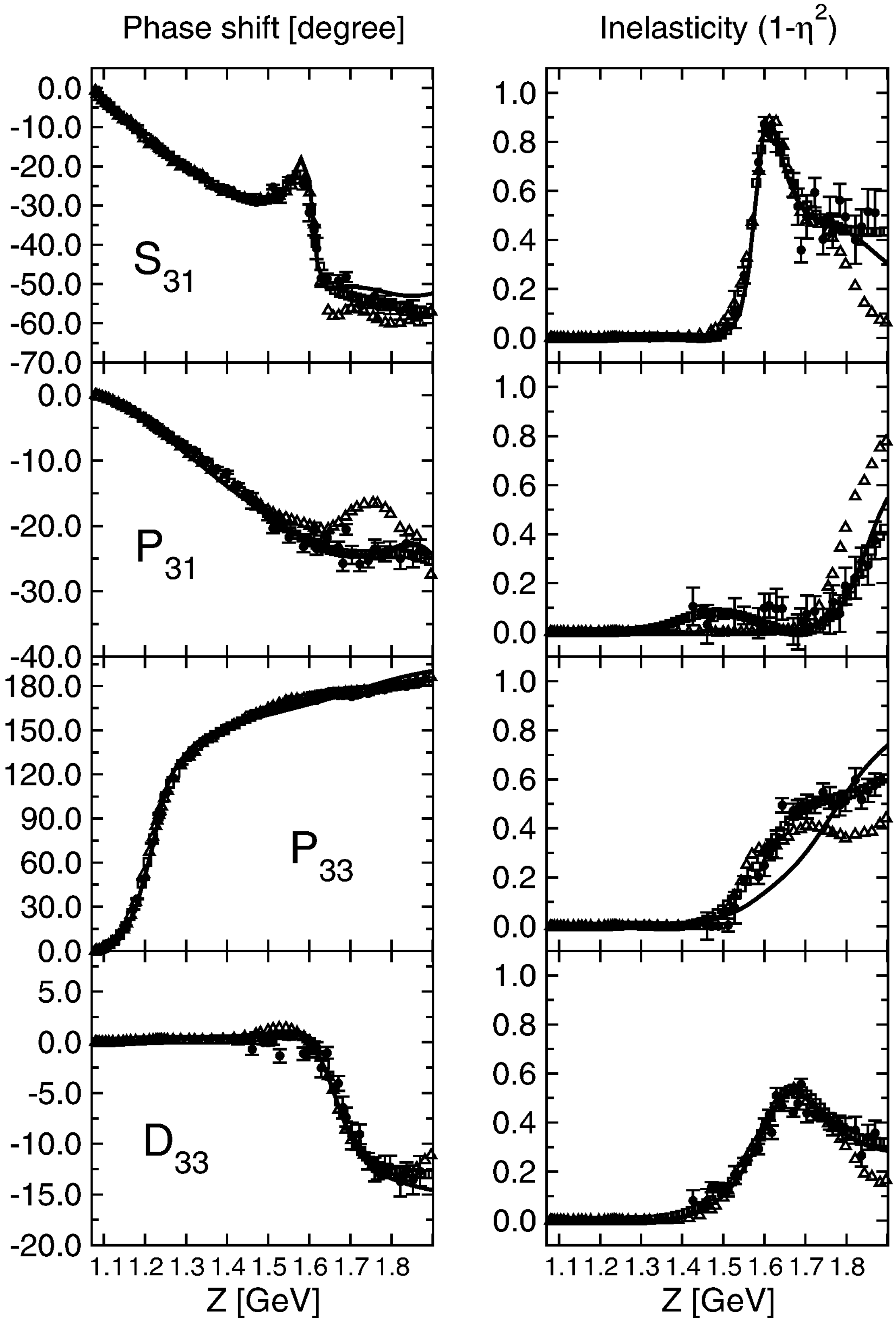

Figure 5.8: Full model results for the πN phase shifts and inelasticities in the $I = 3/2$ channel. The data are as in fig. 5.1.

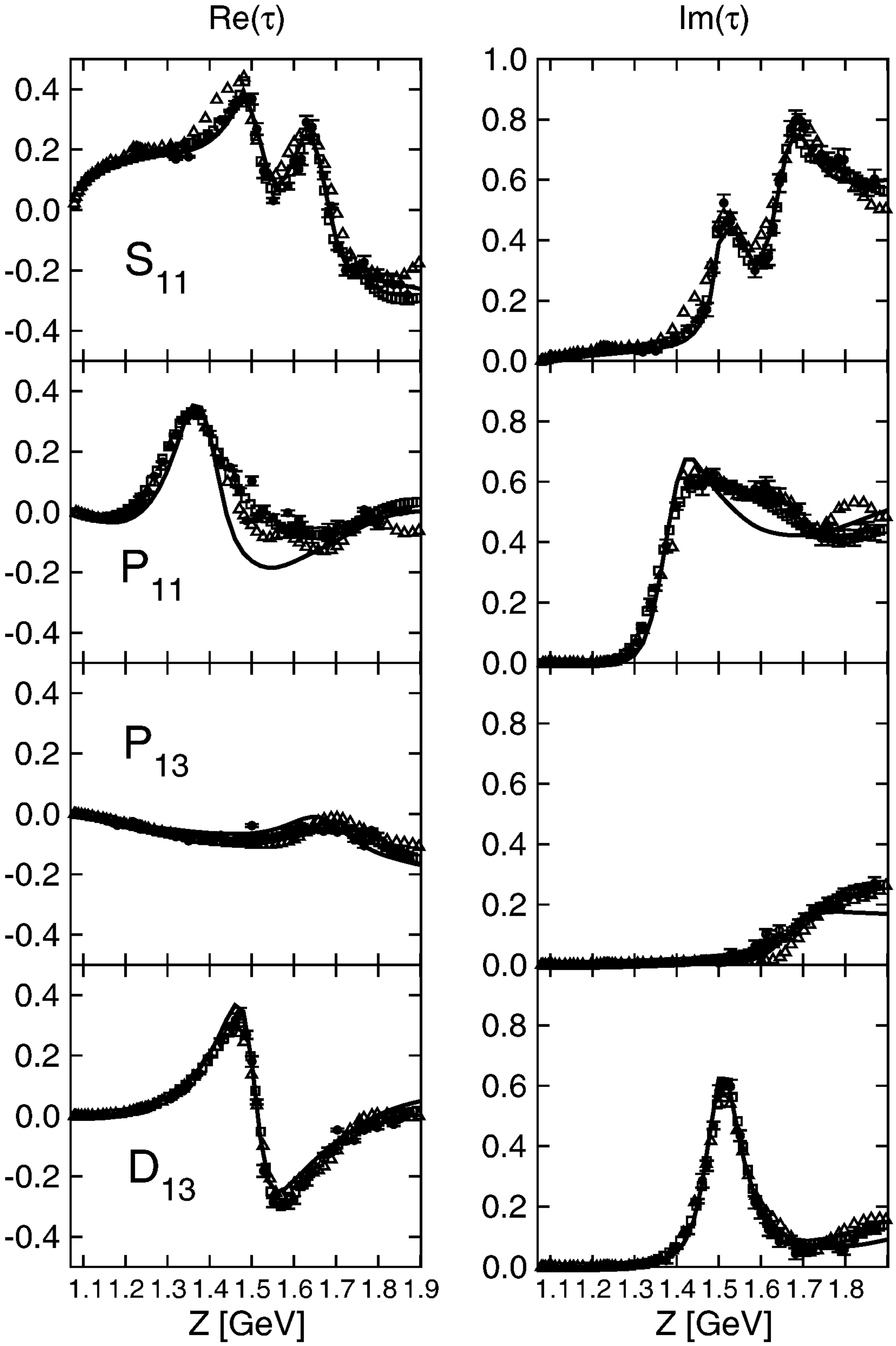

Figure 5.9: Results of the full model for the real and imaginary parts of the πN partial wave amplitudes. The $I = 1/2$ case. The data are as in fig. 5.1.

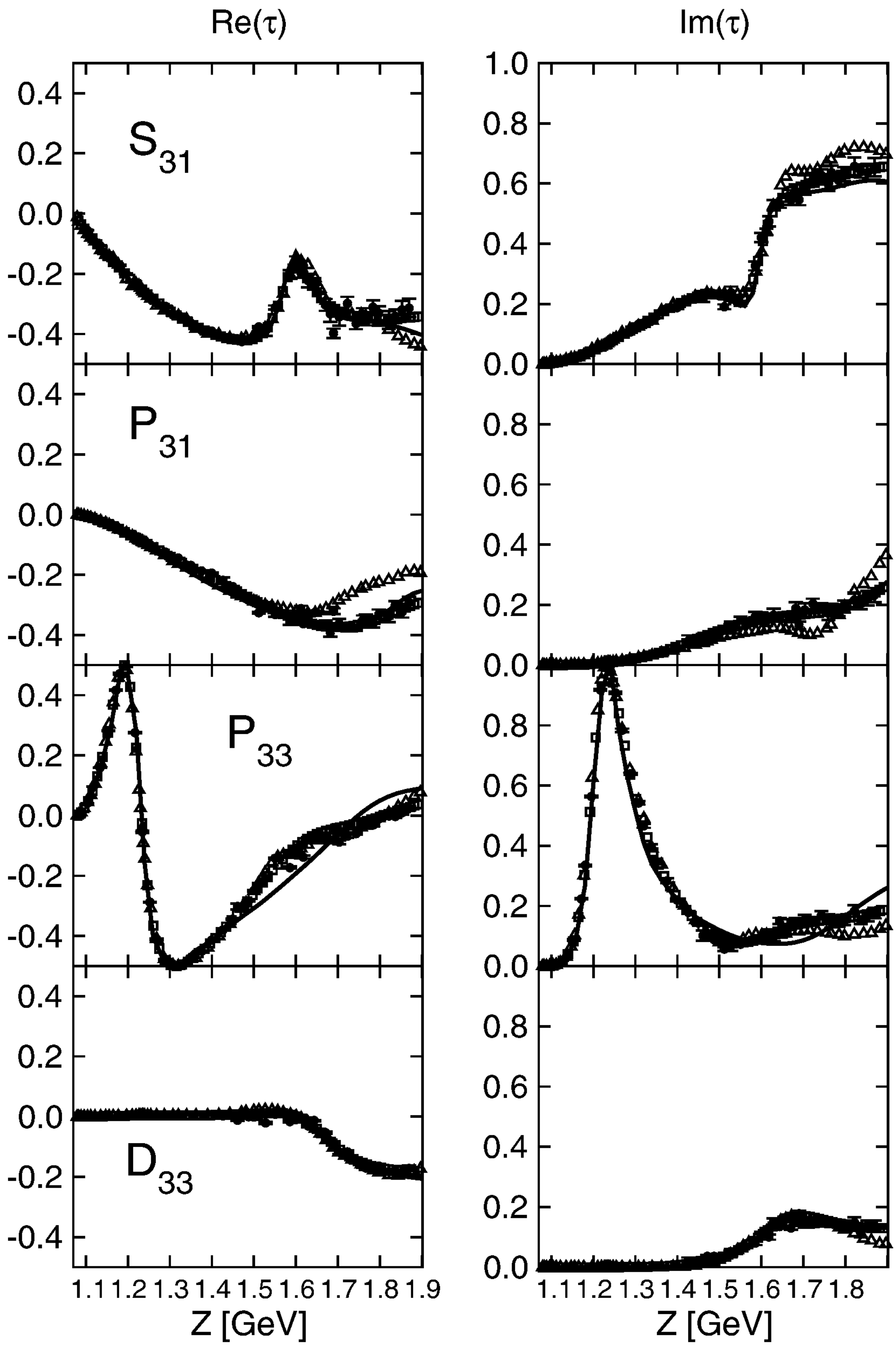

Figure 5.10: Results of the full model for the real and imaginary parts of the πN partial waves amplitude. The $I = 3/2$ case. The data are as in fig. 5.1.

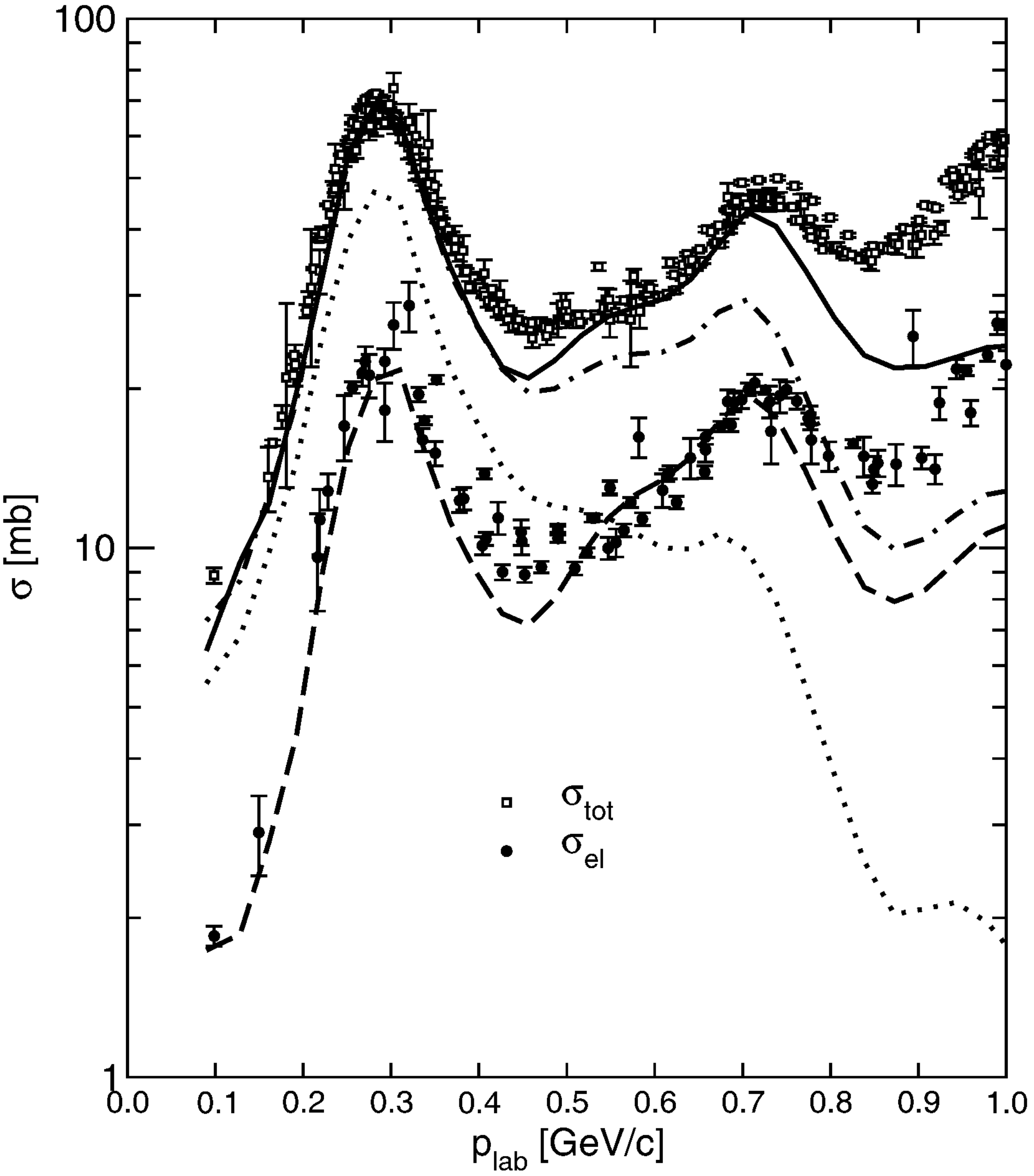

Figure 5.11: Cross sections for $\pi^- p$ scattering. The solid and dashed lines show the total and elastic cross sections, respectively. The dotted line corresponds to the $\pi^- p \to \pi^0 n$ cross section and the dash-dotted line to the sum of the $\pi^- p \to \pi^0 n$ and elastic cross sections. The data are from ref. [89].

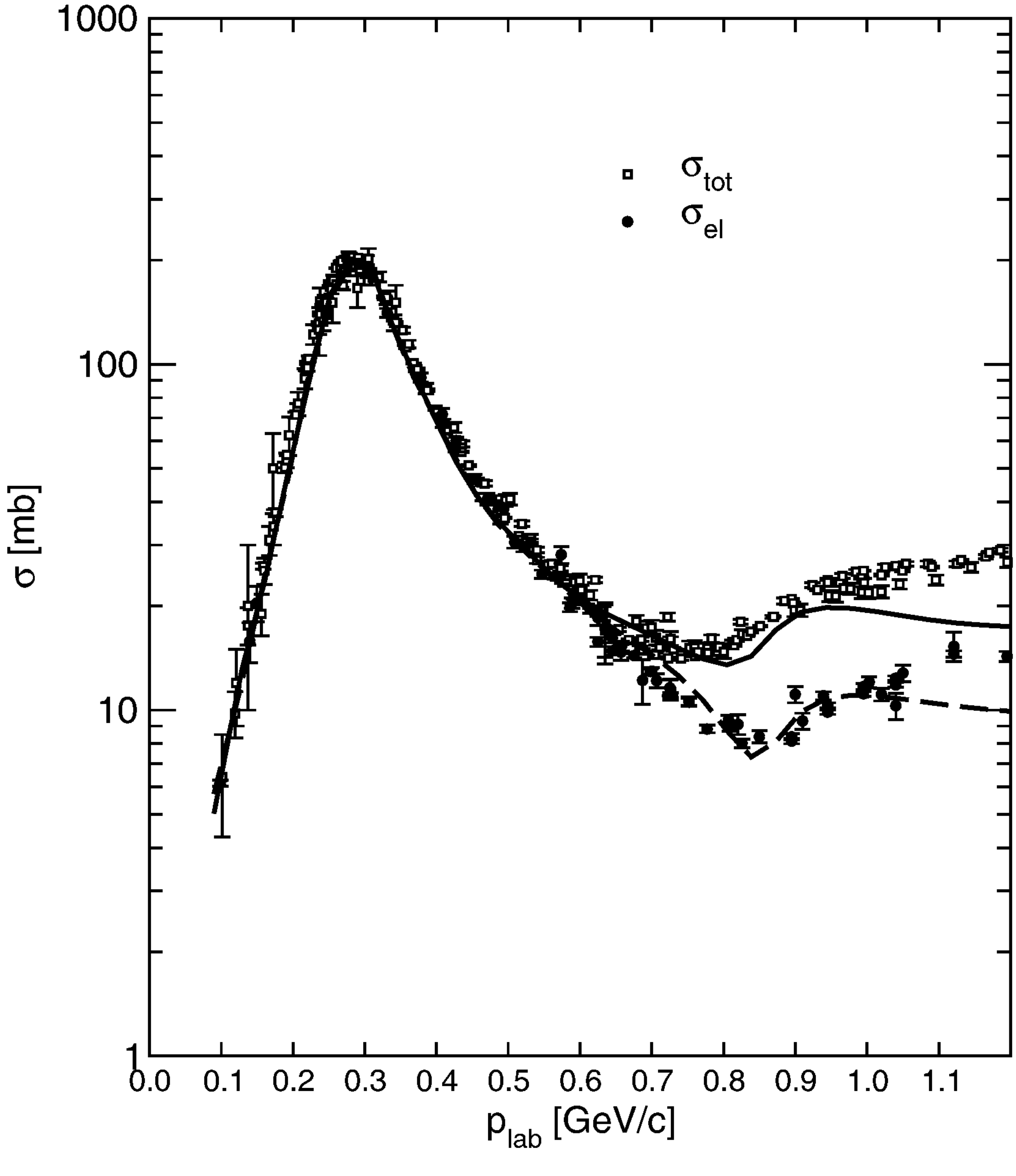

Figure 5.12: Cross sections for $\pi^+ p$ scattering. The solid and dashed lines denote the total and elastic cross sections, respectively. The data are from ref. [89].

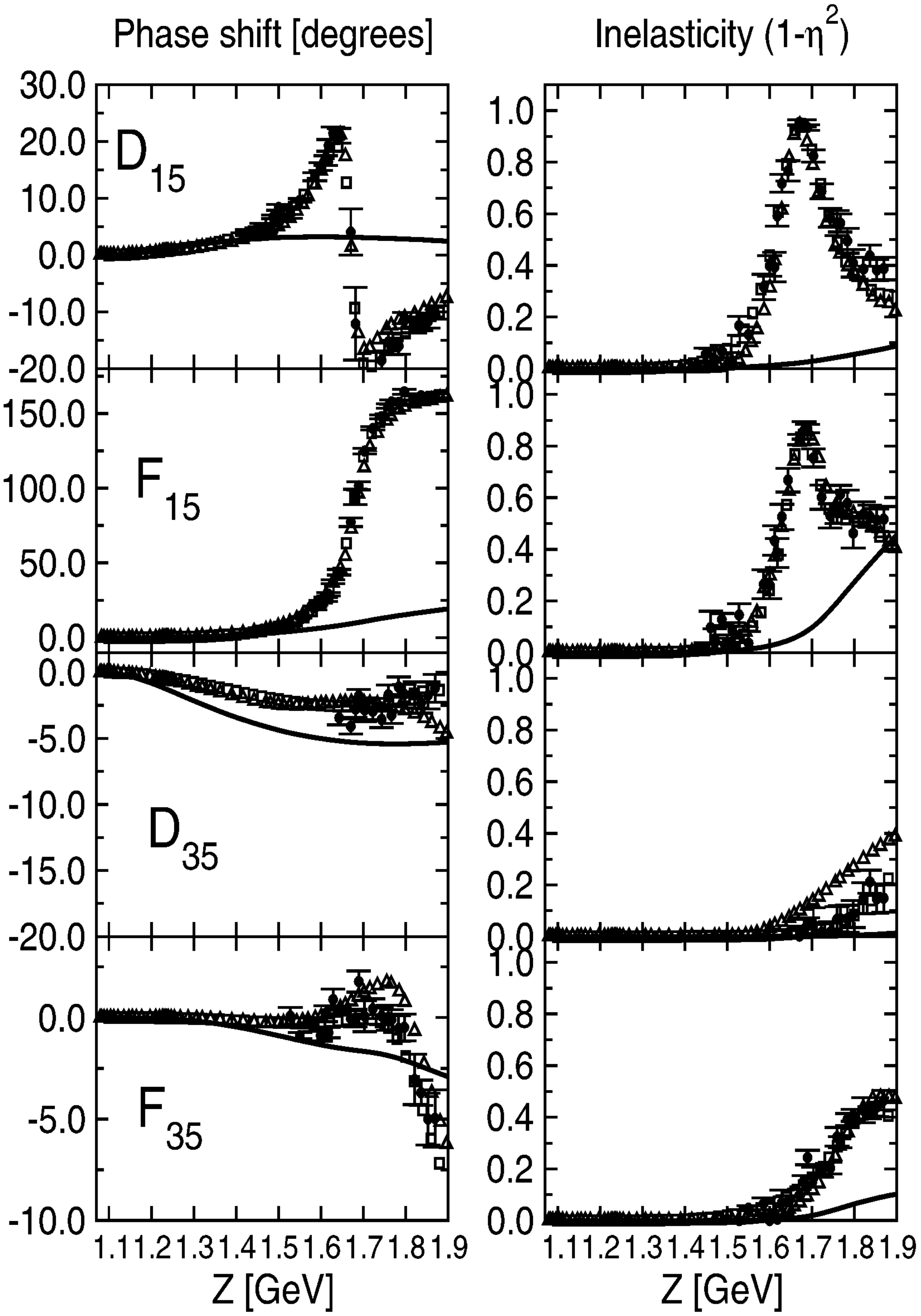

Figure 5.13: Phase shifts and inelasticity for πN partial waves with $J = 5/2$. The curves correspond to the full model. The data are as in fig. 5.1.

	this work	ref. [90]	SM95 [45]
S_{11}	0.195	0.173 ± 0.003	0.175
S_{31}	–0.110	–0.101 ± 0.004	–0.087
P_{11}	–0.089	–0.081 ± 0.002	–0.068
P_{31}	–0.046	–0.045 ± 0.002	–0.039
P_{13}	–0.031	–0.030 ± 0.002	–0.022
P_{33}	0.209	0.214 ± 0.002	0.209

Table 5.4: The s and p-wave πN scattering lengths and volumes in terms of $m_{\pi^+}^{-(2L+1)}$.

should be to consider the production of the ρ meson with a fixed mass, because its width is not so large. In this case one can rotate the contour in the way discussed in section 4.2. We do not take into account this cross section in the fitting procedure, because this would require a consistent treatment of (at least) the $J = 5/2$ partial waves in the πN sector, since those can couple already to the relative p-wave in the ρN system. However, we can check if there is at least qualitative agreement with the data. Fig. 5.14a shows that for both channels for which data are available, $\pi^+ p \to \rho^+ p$ and $\pi^- p \to \rho^0 n$, the description is rather satisfactory. In fig. 5.14b we included the contribution from the $J = 5/2$ partial waves. The $\pi^- p \to \rho^0 n$ cross section becomes now too large. This, however, does not worry us too much, because one should remember, that in the $I = 1/2$ channel there is a number of resonances, not taken into account. The inclusion of them is expected to reduce the $\pi^- p \to \rho^0 n$ cross section via coupled channels effects (e.g. flux from the πN system could then go into other channels than ρN to a larger extend).

5.4 Description of the ηN channel

The reaction $\pi N \to \eta N$ at the ηN threshold is closely related to the properties of the $N^*(1535)$ resonance. The total cross section of this reaction has a very pronounced peak structure at the position of the resonance (cf. fig. 5.15). In

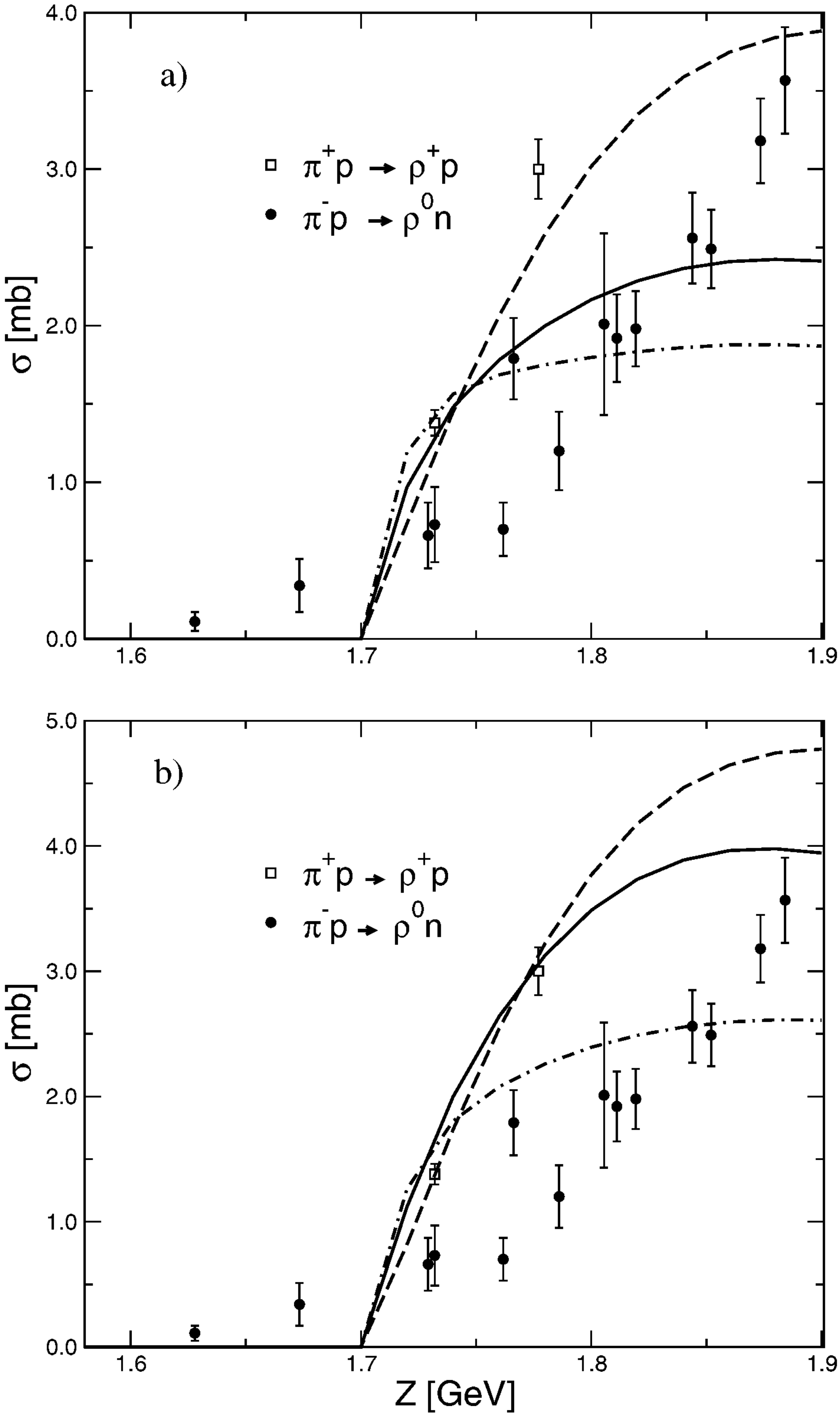

Figure 5.14: The $\pi N \to \rho N$ cross section. The solid lines denote the cross section for the $\pi^- p \to \rho^0 n$ reaction. The dashed lines stand for the $\pi^+ p \to \rho^+ p$ and dash-dotted lines for the $\pi^- p \to \rho^- p$ cross section. Fig. b) includes also the contributions from $J = 5/2$ partial waves. The data are from [91, 92]

the previous version of the Jülich πN model the total $\pi^- p \to \eta n$ cross section was overestimated by about 20-30% at the position of the peak. The reason for this deficiency is that only the πN and ηN channels were allowed to couple to $N^*(1535)$. Therefore, in order to describe the S_{11} πN amplitude one had to associate nearly the whole inelasticity in this partial wave with the ηN channel. The S_{11} part of the inelastic $\pi^- p$ cross section is given (see appendix E) by

$$\sigma_{in} = \frac{2\pi}{3k_1^2}(1-\eta^2), \tag{5.2}$$

that is equal to $\sigma_{in} \sim 3.5$mb at the maximum, and this value overshoots the experimental $\pi^- p \to \eta n$ cross section. This is an indication of the fact, that there should be some contribution of other channels (only the $\pi\pi N$ channel is open at this energy) to the S_{11} inelasticity. That is why we introduced a coupling of the $\pi\Delta$ channel to the $N^*(1535)$ resonance. This allows one to describe simultaneously the total $\pi^- p \to \eta n$ cross section and the inelasticity in the S_{11} partial wave in the resonance region (cf. figs. 5.15 and 5.7).

The inclusion of an $N^*\Delta\pi$ coupling helps also in describing the S_{11} inelasticity above the position of the $N^*(1535)$ resonance. In fig. 5.1 one can see a strong dip in the S_{11} inelasticity, produced by the old model, which corresponds to a similar dip in the s-wave $\pi^- p \to \eta n$ cross section. We found that the origin of this behavior is essentially a unitarity constraint from the πN channel. It can be easily understood schematically, if we assume a two-channel problem with only πN and ηN channels being coupled. We also assume that, apart from the $N^*(1535)$ resonance (whose contribution dies quickly when one moves away from its peak) there is some background contribution to the $\pi N \to \eta N$ transition potential, and that (which is the crucial point) at the same time the direct $\eta N \to \eta N$ potential is negligibly small. (These conditions were satisfied in the old model.) Then the $\pi N \to \eta N$ T-matrix (we consider only the S_{11} partial wave) is given by

$$T_{\pi N \to \eta N} = V_{\pi N \to \eta N} G T_{\pi N \to \pi N}, \tag{5.3}$$

that can be re-expressed in the form (see e.g. [99])

$$T_{\pi N \to \eta N} = ((\beta + ik_1)\frac{\eta e^{2i\delta} - 1}{2ik_1} + 1)V_{\pi N \to \eta N}\,. \tag{5.4}$$

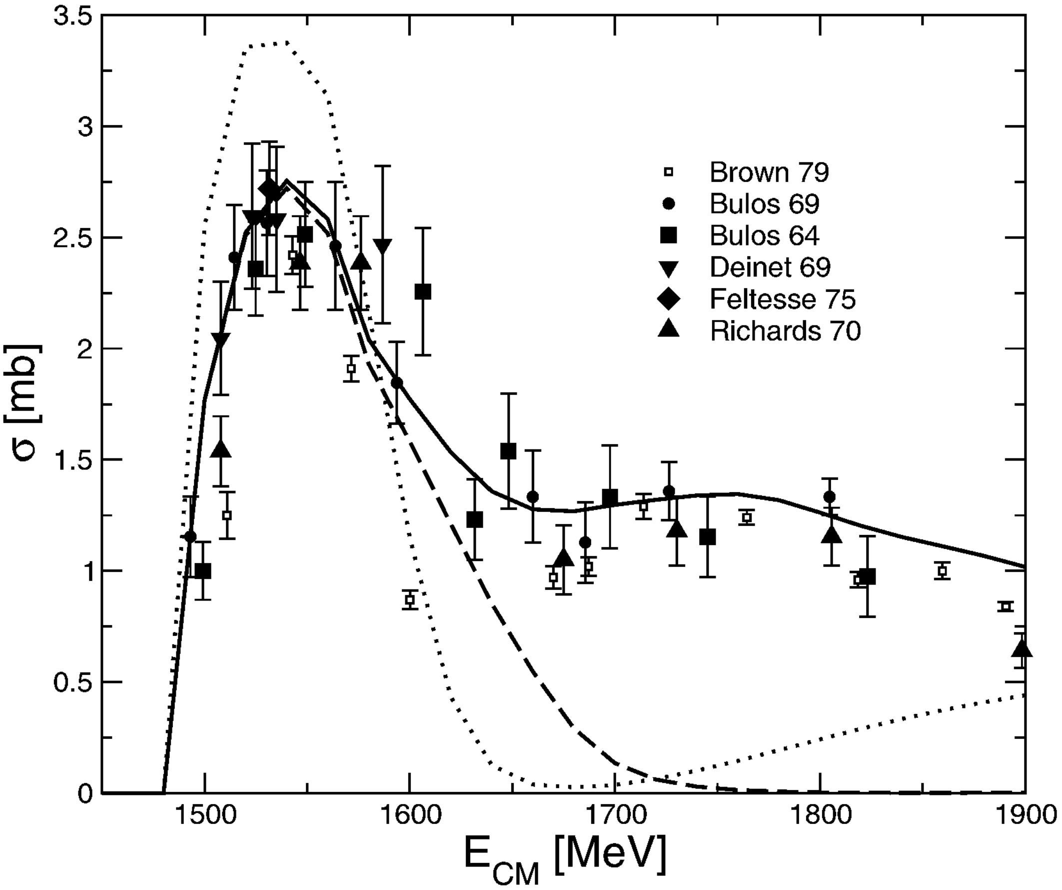

Figure 5.15: Total $\pi^- p \to \eta n$ cross section. The solid line corresponds to the full calculation. The dashed line indicates the pure s-wave contribution. The results of the old model are shown as a dotted line (only s-wave). The data are from [93–98].

Here β is the inverse of the characteristic radius of interaction, which is determined by the principal value integral, δ and η are the S_{11} phase shift and inelasticity parameter and k_1 is the on-shell momentum in the πN channel . Let us now study under what circumstances we can have $T_{\pi N \to \eta N} = 0$. Given our simplifying model assumption, at this point $\eta = 1$, and then β is purely real. Then, it is convenient to rewrite eq. (5.4) as

$$T_{\pi N \to \eta N} = e^{i\delta} \sqrt{1 + \beta^2 / k_1^2} \sin(\gamma - \alpha) V_{\pi N \to \eta N}, \tag{5.5}$$

where $\gamma = \arctan(\beta / k_1)$ and $\alpha = \delta - \pi/2$. Note that in the specific situation we discuss the phase δ crosses $\pi/2$ ($\alpha = 0$), due to the presence of the $N^*(1650)$ resonance in the $\pi N \to \pi N$ interaction, and then continues to rise rapidly, whereas β is a smooth function of k_1 and has a typical value in the order of several hundreds MeV (the exact value is, of course, model dependent), so that in the region of interest $\gamma \lesssim 1$. It is thus easy to convince oneself that the expression (5.5) gets equal to zero at some energy above (but not far from) the position of the $N^*(1650)$ resonance. Expanding $T_{\pi N \to \eta N}$ in powers of $Z - Z_0$, where Z_0 is the position of the "zero", one can see, that the $\pi^- p \to \eta n$ cross section is proportional to $(Z - Z_0)^2$ - which explains the structure of the dip in the cross section given by the old model in fig. 5.15. It is interesting to note, that the same effect can be found in other models, e.g. in ref. [100] (cf. fig. 7). In the general case when there are more than two channels β becomes complex and the cross section at the dip will be finite but still small (provided that the inelasticity is not too large).

In our model the S_{11} inelasticity in this energy region is partly determined by the $N^*(1535)\Delta\pi$ coupling, because in this case the $\Delta\pi$ system is in a pure d-wave, and the maximum of the $\pi N \to \pi\Delta$ cross section is shifted to somewhat higher energies.

Concerning the background contribution, which is provided by the a_0 exchange, we do not need it to be as strong as it was in the old model, since it will be suppressed at energies above the $N^*(1535)$ resonance anyway due to the mechanism discussed above. Moreover, its large contribution was caused mostly by the large value of the cutoff mass (2500 MeV) which we avoid in the present model.

Let us now look at the differential $\pi^- p \to \eta n$ cross section and at the energy dependence of the total cross section not too close to threshold, to see the importance of higher partial waves. To include the effect of higher partial waves we introduced the coupling of the ηN system to the $P_{13}(1720)$ and $D_{13}(1520)$ resonances. Those are the most pronounced resonances in the energy region below 1.9 GeV that couple strongly to the πN system. Note that there are other 3-stars N^* resonances [89] in this region that we do not include, because their coupling to the πN channel is very weak and they cannot be well constrained from the πN data.

At energies below 1.6 GeV the slight deviation of the differential cross section from the flat distribution can be easily described by the interference of the D_{13} resonance with the s-wave amplitude (cf. fig. 5.16). For the total cross section the D_{13} contribution is of minor importance. One can describe the shape of the total cross section above 1.6 GeV by introducing the ηN coupling to the $P_{13}(1720)$ resonance as shown in fig. 5.15. However, as one one can see from fig. 5.17, this is insufficient to get a good agreement with the data for the differential cross section in this energy region. Certainly, that points to missing contributions from higher partial waves, and, may be, specifically from the already discussed $J = 5/2$ resonances. At present, we do not aim to include those. We would like to remark also that the existing data do not allow one to discriminate between different partial-wave contributions – one would need to know polarization observables for this purpose.

Finally let us present the result for the ηN scattering length, that is predicted by our model:

$$a_{\eta N} = (0.40 + i0.25) fm. \tag{5.6}$$

This quantity is very important when studying the effect of the ηN interaction in various reactions, or searching for the η-nucleus bound states. For a more thorough discussion see e.g., [102]. Note that our value for the ηN scattering length is slightly lower than the one of the previous version of the model ($0.42 + i0.34$ fm), but is still consistent with the recent analysis of the reaction $\gamma d \to np\eta$ [102].

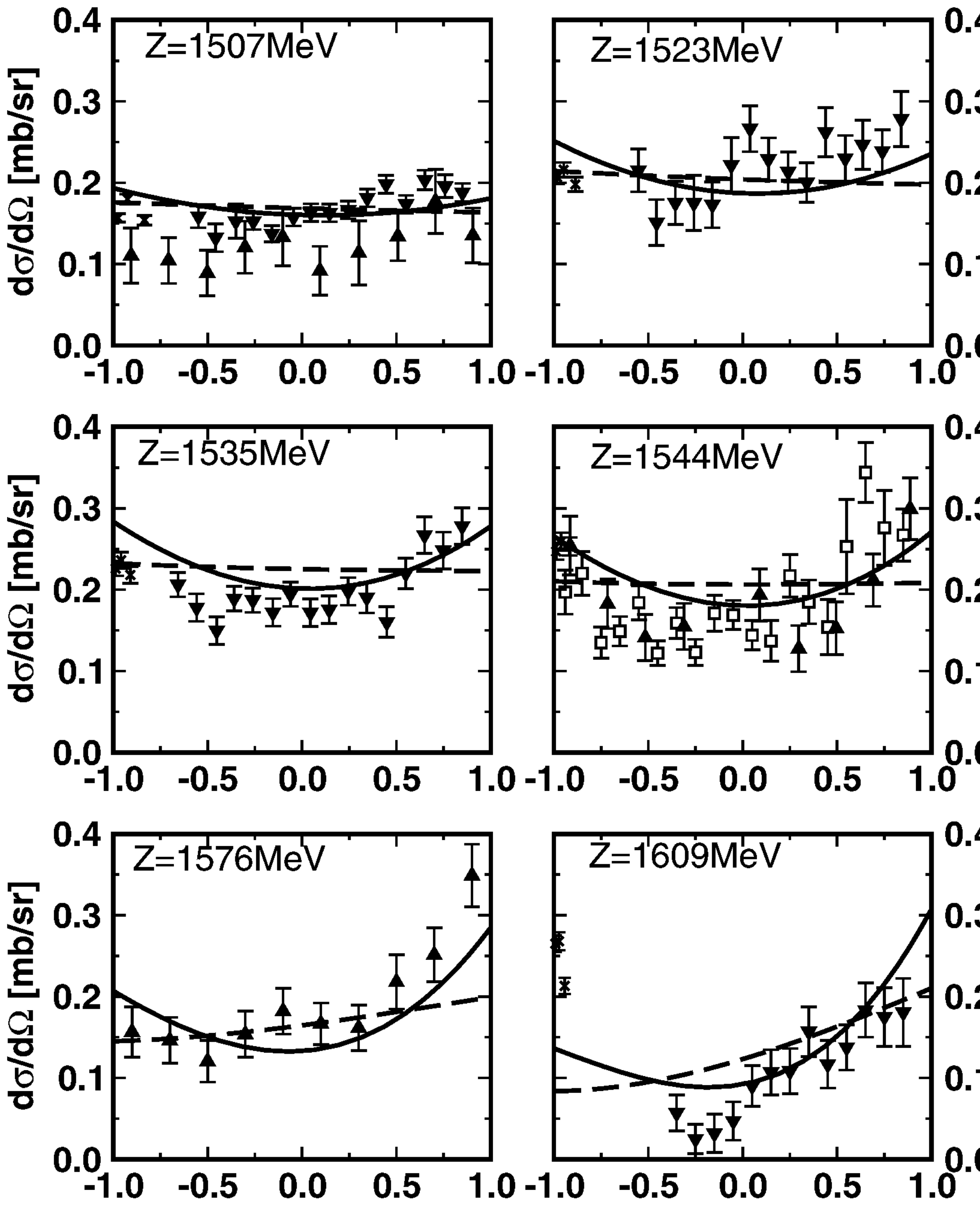

Figure 5.16: Differential $\pi^- N \to \eta n$ cross section at energies close to the ηN threshold. The solid curve corresponds to the full result. The dashed line corresponds to the case when the D_{13} partial wave is switched off. The data are from [93](□), [96](▼), [98](▲), [101](×).

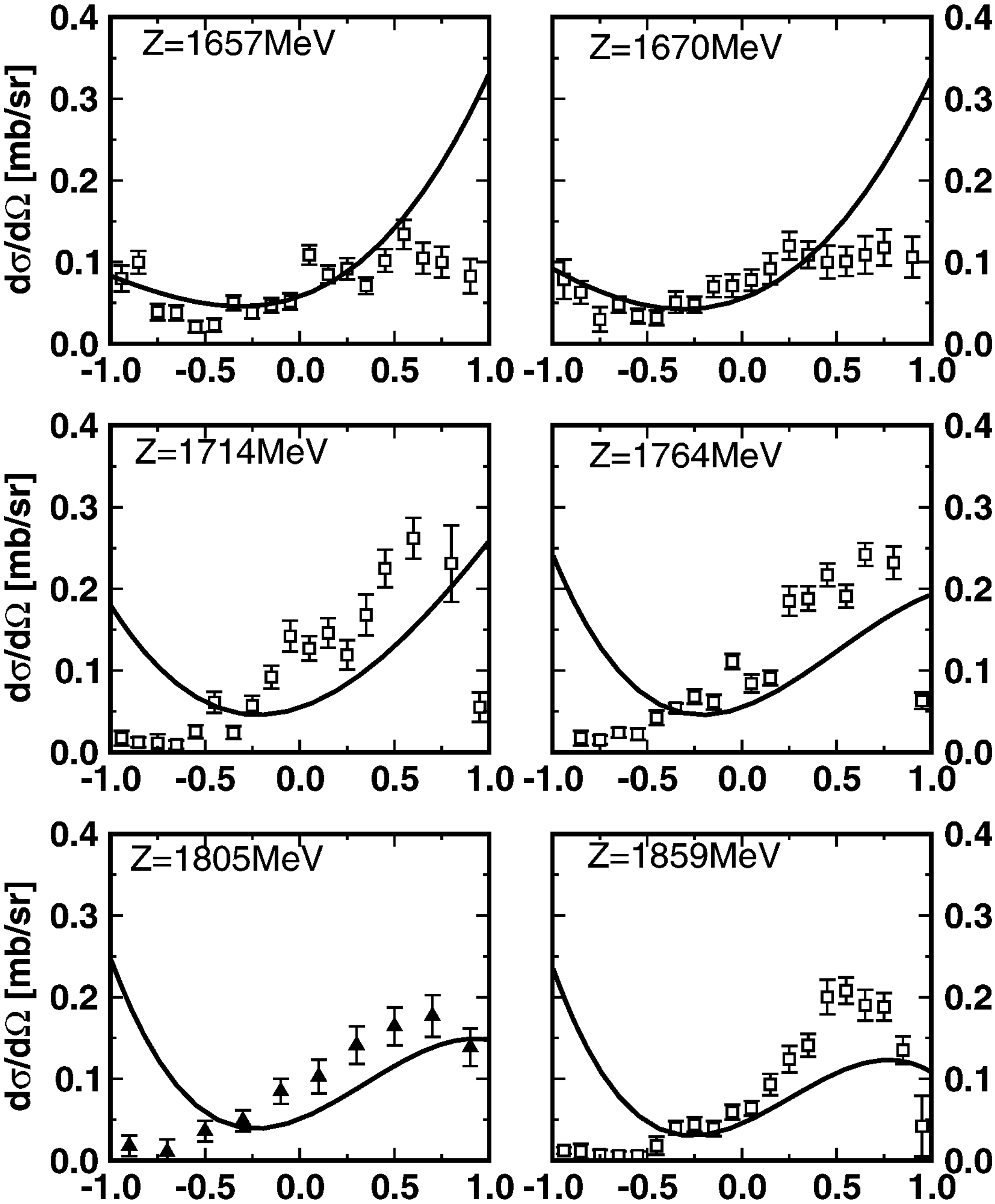

Figure 5.17: Differential $\pi^- N \to \eta n$ cross section at higher energies. The data are from [93](□), [96](▼), [98](▲), [101](×).

Chapter 6

Summary

The present work was dedicated to a further extension and improvement of the Jülich πN model.

The constructed model is based on the meson exchange potential which is derived in its main part from the phenomenological Wess-Zumino Lagrangian, consistent with chiral symmetry. The πN potential in the scalar-isoscalar and vector-isovector channels was calculated by means of dispersion relations. That allows one to minimize the number of parameters. In this work we reduced the freedom in the treatment of dispersion relations, by a choice of the form factors that do not modify the potential on energy shell at small energies.

The potential built in this way was unitarized in a coupled channels Lippmann-Schwinger equation to obtain reaction amplitudes for various processes. At present the following channels were included: πN, σN, ρN, $\pi\Delta$, and ηN. The channels σN, ρN, $\pi\Delta$ were introduced to effectively model the physical $\pi\pi N$ state.

The first and main aim was to describe the elastic πN amplitude in the energy region up to 1.9 GeV and for total angular momenta $J \leq 3/2$ in both isospin channels. First we analyzed the background contribution which comes from the $\pi N \to \pi N$ potential in the $J = 1/2$ and $J = 3/2$ partial waves. Having only a few free parameters we were able to obtain the correct low energy behavior of the πN phase shifts and, at the same time, could describe their high energy trend, having improved noticeably the results of the previous version of the model. The channels ρN, $\pi\Delta$ provided the inelasticity at high energies in some partial waves.

The σN channel played the main role in generating dynamically the P_{11} Roper resonance. Note that the correct description of the background in the $J = 5/2$ partial waves was obtain automatically.

With the background amplitude constructed using this strategy, it was an easy task to include resonance graphs in all partial waves where needed - something that would have been very difficult if not impossible in the old model of O. Krehl. Thus the description of the πN amplitudes in the lowest partial waves has become complete.

Although we did not actually fit the $\pi N \to \rho N$ transition cross section, the results which we obtained for it proves to be in reasonable agreement with the experiment for all isospin channels. The $\pi^- p \to \rho^0 n$ cross section is somewhat overestimated by our model if we switch on the $J = 5/2$ part of the amplitude. However, one has to keep in mind that our model does not describe the $J = 5/2$ πN phase shifts and, therefore, one can argue that this overestimation would not happen in a consistent coupled channels treatment of the $J = 5/2$ partial wave.

The physics connected with the ηN interaction is rather important for various reasons. One of the interesting issues concerns the value of the ηN scattering length and its relation to the existence of η-nucleus bound states. Another important point is provided by possible effects of the strong ηN final state interaction in η-production processes in NN [103–105] and γd collisions [102]. The πN dynamics in the S_{11} partial wave is also strongly affected by the ηN channel in the region close to the ηN threshold. Therefore, we studied the ηN channel in more detail and with particular care. First of all we found that the discrepancy of the old model with the data for the $\pi^- p \to \eta n$ total cross section in the region of $N^*(1535)$ (which appears if one wants to correctly describe the inelasticity in the S_{11} partial wave) can be removed , by an additional flux from the πN to $\pi\Delta$ channel. Furthermore, the inclusion of the ηN coupling to the $P_{13}(1720)$ resonance turned out to lead to a significant improvement of the total cross section at higher energies. At the same time the puzzle of the dip in the S_{11} inelasticity, present in the old model, was solved. The origin of this deficiency turned out to be an almost model independent effect of coupled channels unitarity constraints. We also improved the description of the differential $\pi^- p \to \eta n$ cross section. However, at high energies there is still a persisting discrepancy with the data, most likely because some higher partial wave contributions are still missing in our model. A detailed partial wave analysis of this reaction at such energies is impossible without data on polarization observables.

The model in its present form enables a straightforward inclusion of further channels, and specifically those nearest in energy namely $K\Lambda$, $K\Sigma$, and ωN. An extension of the present model in this direction is planned for the near future.

Appendix A

Definitions and notations

Below we collect the conventions and notations used in this work.

1. The metric tensor is defined as

$$g_{\mu\nu} = g^{\mu\nu} = \begin{pmatrix} 1 & 0 & 0 & 0 \\ 0 & -1 & 0 & 0 \\ 0 & 0 & -1 & 0 \\ 0 & 0 & 0 & -1 \end{pmatrix} . \tag{A.1}$$

2. For the γ–matrices we use the following representation

$$\begin{aligned} \gamma^0 &= \begin{pmatrix} I_2 & 0 \\ 0 & -I_2 \end{pmatrix} , \; \vec{\gamma} = \begin{pmatrix} 0 & \vec{\sigma} \\ -\vec{\sigma} & 0 \end{pmatrix} , \\ \gamma^5 &= i\gamma^0\gamma^1\gamma^2\gamma^3 = \begin{pmatrix} 0 & I_2 \\ I_2 & 0 \end{pmatrix}, \\ \sigma^{\mu\nu} &= \frac{i}{2}(\gamma^\mu\gamma^\nu - \gamma^\nu\gamma^\mu) \end{aligned} \tag{A.2}$$

where

$$I_2 = \begin{pmatrix} 1 & 0 \\ 0 & 1 \end{pmatrix}$$

and

$$\sigma_1 = \begin{pmatrix} 0 & 1 \\ 1 & 0 \end{pmatrix} , \; \sigma_2 = \begin{pmatrix} 0 & -i \\ i & 0 \end{pmatrix} , \; \sigma_3 = \begin{pmatrix} 1 & 0 \\ 0 & -1 \end{pmatrix} \tag{A.3}$$

3. totally antisymmetric Levi-Civita tensor

$$\epsilon_{\mu\alpha\lambda\nu} = \begin{cases} -1 & \text{for even permutations of } 0123 \\ 1 & \text{for odd permutations of } 0123 \\ 0 & \text{otherwise} \end{cases} . \tag{A.4}$$

4. "baryon first" phase convention:

   In this work we follow the standard "baryon first" phase convention (see e.g. [106]) for meson-baryon systems. In this convention, baryons always appear before mesons in all spin and isospin Clebsch-Gordan coefficients. Furthermore, angles are always measured with respect to the first particle i.e. to the baryon.

5. Spin-$\frac{1}{2}$ spinors
   In this work we consider spin-$\frac{1}{2}$ spinors in the helicity basis:

$$u(\vec{k},\lambda) = \sqrt{\frac{E_k+m}{2E_k}} \begin{pmatrix} 1 \\ \frac{2\lambda k}{E_k+m} \end{pmatrix} |\lambda\rangle, \tag{A.5}$$

where m is the mass of the particle with momentum $\vec{k}$ and energy $E_k = \sqrt{\vec{k}^{\,2}+m^2}$. The two dimensional spinors $|\lambda\rangle$ are eigenstates of the helicity operator

$$\frac{\vec{\sigma}\vec{k}}{2k}|\lambda\rangle = \lambda|\lambda\rangle, \tag{A.6}$$

where λ takes the values $\pm\frac{1}{2}$. The explicit form of these spinors is given by

$$|\lambda = +\frac{1}{2}\rangle = \begin{pmatrix} \cos\frac{\theta}{2}\exp(-i\frac{\phi}{2}) \\ \sin\frac{\theta}{2}\exp(i\frac{\phi}{2}) \end{pmatrix}, \tag{A.7}$$

$$|\lambda = -\frac{1}{2}\rangle = \begin{pmatrix} -\sin\frac{\theta}{2}\exp(-i\frac{\phi}{2}) \\ \cos\frac{\theta}{2}\exp(i\frac{\phi}{2}) \end{pmatrix}. \tag{A.8}$$

For the antiparticle the helicity spinor takes the form

$$v(\vec{k},\lambda) = \sqrt{\frac{E_k+m}{2E_k}} \begin{pmatrix} \frac{-k}{E_k+m} \\ 2\lambda \end{pmatrix} |-\lambda\rangle. \tag{A.9}$$

6. Spin-1 polarization vectors:

   The polarization 4-vector of the first particle with spin 1 in the helicity basis, moving with momentum $\vec{k}$ is defined as

$$\epsilon^\mu(\vec{k}, \lambda = \pm 1) = \frac{1}{\sqrt{2}} \begin{pmatrix} 0 \\ \mp \cos\theta \cos\phi + i \sin\phi \\ \mp \cos\theta \sin\phi - i \cos\phi \\ \pm \sin\theta \end{pmatrix}, \tag{A.10}$$

$$\epsilon^\mu(\vec{k}, \lambda = 0) = \frac{1}{m} \begin{pmatrix} k \\ E_k \sin\theta \cos\phi \\ E_k \sin\theta \sin\phi \\ E_k \cos\theta \end{pmatrix}. \tag{A.11}$$

   For the second particle moving with momentum $-\vec{k}$ one takes

$$\epsilon^\mu(-\vec{k}, \lambda = \pm 1) = \frac{1}{\sqrt{2}} \begin{pmatrix} 0 \\ \pm \cos\theta \cos\phi + i \sin\phi \\ \pm \cos\theta \sin\phi - i \cos\phi \\ \mp \sin\theta \end{pmatrix}, \tag{A.12}$$

$$\epsilon^\mu(-\vec{k}, \lambda = 0) = \frac{1}{m} \begin{pmatrix} -k \\ E_k \sin\theta \cos\phi \\ E_k \sin\theta \sin\phi \\ E_k \cos\theta \end{pmatrix}, \tag{A.13}$$

   where we adopt the phase convention of ref. [42].

7. Rarita-Schwinger spinors:

   The Rarita-Schwinger spinor for a spin-3/2 particle is constructed from a spin-1/2 spinor and spin-1 polarization vector as

$$u^\mu(\vec{k}, \lambda) = \sum_{\lambda_1, \lambda_2} \langle 1 \lambda_1 \frac{1}{2} \lambda_2 | \frac{3}{2} \lambda \rangle \epsilon^\mu(\vec{k}, \lambda_1) u(\vec{k}, \lambda_2). \tag{A.14}$$

   For the Δ-exchange we use the Rarita-Schwinger propagator with the numerator of the form

$$P^{\mu\nu}(k) = (\hat{k} + m) \left[-g^{\mu\nu} + \frac{1}{3}\gamma^\mu \gamma^\nu + \frac{2}{3m^2} k^\mu k^\nu - \frac{1}{3m}(k^\mu \gamma^\nu - k^\nu \gamma^\mu) \right], \tag{A.15}$$

   where the abbreviation $\hat{k} = k_\mu \gamma^\mu$ is used.

Appendix B

Potential

In this chapter we list the effective Lagrangian of our model and the potential that one obtains from this Lagrangian using the rules, described in chapter 2. In the end we give the expressions for vertex functions in the pole graphs.

B.1 Effective Lagrangian

First we define the field operators, for the nucleon and the Δ (all other spin-1/2 and spin-3/2 fields are defined in the same way):

$$\begin{aligned}
\Psi(x) &= (2\pi)^{-3/2}\int d^3k \sum_{\lambda}\left[b_N(\vec{k},\lambda)u(\vec{k},\lambda)e^{-ik^\mu x_\mu} + d_N^\dagger v(\vec{k},\lambda)(\vec{k})e^{ik^\mu x_\mu}\right] \\
\Delta^\nu(x) &= (2\pi)^{-3/2}\int d^3k \sum_{\lambda}\left[b_\Delta(\vec{k},\lambda)u^\nu(\vec{k},\lambda)e^{-ik^\mu x_\mu} + d_\Delta^\dagger v^\nu(\vec{k},\lambda)(\vec{k})e^{ik^\mu x_\mu}\right],
\end{aligned}$$

and also for scalar, pseudoscalar, vector, and axial mesons:

$$\begin{aligned}
\Psi_s(x) &= (2\pi)^{-3/2}\int d^3k \frac{1}{\sqrt{2\omega_k}}\left[a_s(\vec{k})e^{-ik^\mu x_\mu} + a_s^\dagger(\vec{k})e^{ik^\mu x_\mu}\right] \\
\Psi_p(x) &= (2\pi)^{-3/2}\int d^3k \frac{1}{\sqrt{2\omega_k}}\left[a_p(\vec{k})e^{-ik^\mu x_\mu} + a_p^\dagger(\vec{k})e^{ik^\mu x_\mu}\right] \\
\Psi_v^\nu(x) &= (2\pi)^{-3/2}\int d^3k \sum_{\lambda}\frac{1}{\sqrt{2\omega_k}}\left[\epsilon^\nu(\vec{k},\lambda)a_v(\vec{k},\lambda)e^{-ik^\mu x_\mu}\right] + \text{h.c.} \\
\Psi_a^\nu(x) &= (2\pi)^{-3/2}\int d^3k \sum_{\lambda}\frac{1}{\sqrt{2\omega_k}}\left[\epsilon^\nu(\vec{k},\lambda)a_a(\vec{k},\lambda)e^{-ik^\mu x_\mu}\right] + \text{h.c.},
\end{aligned} \tag{B.1}$$

where ω_k is the on-shell energy of the meson. The annihilation operators $a(\vec{k},\lambda)$,$b(\vec{k},\lambda')$, and $d(\vec{k},\lambda')$ obey (anti)commutation relations

$$[a(\vec{k},\lambda),a^\dagger(\vec{k}',\lambda')]_- = \delta_{\lambda,\lambda'}\delta(\vec{k}-\vec{k}')$$

$$[b(\vec{k},\lambda),b^\dagger(\vec{k}',\lambda')]_+ = \delta_{\lambda,\lambda'}\delta(\vec{k}-\vec{k}') \tag{B.2}$$

$$[d(\vec{k},\lambda),d^\dagger(\vec{k}',\lambda')]_+ = \delta_{\lambda,\lambda'}\delta(\vec{k}-\vec{k}') \tag{B.3}$$

All interaction terms of the Lagrangian of our model are collected in table B.1.

Vertex	$\mathcal{L}_{int}$
$NN\pi$	$-\frac{f_{NN\pi}}{m_\pi}\bar{\Psi}\gamma^5\gamma^\mu\vec{\tau}\partial_\mu\vec{\pi}\Psi$
$N\Delta\pi$	$\frac{f_{N\Delta\pi}}{m_\pi}\bar{\Delta}^\mu\vec{S}^\dagger\partial_\mu\vec{\pi}\Psi + \text{h.c.}$
$\rho\pi\pi$	$-g_{\rho\pi\pi}(\vec{\pi}\times\partial_\mu\vec{\pi})\vec{\rho}^\mu$
$NN\rho$	$-g_{NN\rho}\bar{\Psi}[\gamma^\mu - \frac{\kappa_\rho}{2m_N}\sigma^{\mu\nu}\partial_\nu]\vec{\tau}\vec{\rho}_\mu\Psi$
$NN\sigma$	$-g_{NN\sigma}\bar{\Psi}\Psi\sigma$
$\sigma\pi\pi$	$\frac{g_{\sigma\pi\pi}}{2m_\pi}\partial_\mu\vec{\pi}\partial^\mu\vec{\pi}\sigma$
$\sigma\sigma\sigma$	$-g_{\sigma\sigma\sigma}m_\sigma\sigma\sigma\sigma$
$NN\rho\pi$	$\frac{f_{NN\pi}}{m_\pi}g_\rho\bar{\Psi}\gamma^5\gamma^\mu\vec{\tau}\Psi(\vec{\rho}_\mu\times\vec{\pi})$
NNa_1	$-\frac{f_{NN\pi}}{m_\pi}m_{a_1}\bar{\Psi}\gamma^5\gamma^\mu\vec{\tau}\Psi\vec{a}_\mu$
$a_1\pi\rho$	$-\frac{g_\rho}{m_{a_1}}\left[\partial_\mu\vec{\pi}\times\vec{a}_\nu - \partial_\nu\vec{\pi}\times\vec{a}_\mu\right]\left[\partial^\mu\vec{\rho}^\nu - \partial^\nu\vec{\rho}^\mu\right]$
	$+\frac{g_\rho}{2m_{a_1}}\left[\vec{\pi}\times(\partial_\mu\vec{\rho}_\nu - \partial_\nu\vec{\rho}_\mu)\right]\left[\partial^\mu\vec{a}^\nu - \partial^\nu\vec{a}^\mu\right]$
$NN\omega$	$-g_{NN\omega}\bar{\Psi}\gamma^\mu\omega_\mu\Psi$
$\omega\pi\rho$	$\frac{g_{\omega\pi\rho}}{m_\omega}\epsilon_{\alpha\beta\mu\nu}\partial^\alpha\vec{\rho}^\beta\partial^\mu\vec{\pi}\omega^\nu$
$N\Delta\rho$	$-i\frac{f_{N\Delta\rho}}{m_\rho}\bar{\Delta}^\mu\gamma^5\gamma^\nu\vec{S}^\dagger\vec{\rho}_{\mu\nu}\Psi + \text{h.c.}$[1]
$\rho\rho\rho$	$\frac{g_\rho}{2}(\vec{\rho}_\mu\times\vec{\rho}_\nu)\vec{\rho}^{\mu\nu}$
$NN\rho\rho$	$\frac{\kappa_\rho g_\rho^2}{8m_N}\bar{\Psi}\sigma^{\mu\nu}\vec{\tau}\Psi(\vec{\rho}_\mu\times\vec{\rho}_\nu)$
$\Delta\Delta\pi$	$\frac{f_{\Delta\Delta\pi}}{m_\pi}\bar{\Delta}_\mu\gamma^5\gamma^\nu\vec{T}\Delta^\mu\partial_\nu\vec{\pi}$
$\Delta\Delta\rho$	$-g_{\Delta\Delta\rho}\bar{\Delta}_\tau\left(\gamma^\mu - i\frac{\kappa_{\Delta\Delta\rho}}{2m_\Delta}\sigma^{\mu\nu}\partial_\nu\right)\vec{\rho}_\mu\vec{T}\Delta^\tau$
$NN\eta$	$-\frac{f_{NN\eta}}{m_\pi}\bar{\Psi}\gamma^5\gamma^\mu\partial_\mu\eta\Psi$
NNa_0	$g_{NNa_0}m_\pi\bar{\Psi}\vec{\tau}\Psi\vec{a}_0$
$\pi\eta a_0$	$g_{\pi\eta a_0}m_\pi\eta\vec{\pi}\vec{a}_0$
$N^*(S_{11})N\pi$	$\frac{f_{N^*N\pi}}{m_\pi}\bar{\Psi}_{N^*}\gamma^\mu\vec{\tau}\Psi\partial_\mu\vec{\pi} + \text{h.c.}$

[1] $\vec{\rho}_{\mu\nu} = \partial_\mu\vec{\rho}_\nu - \partial_\nu\vec{\rho}_\mu$

$N^*(S_{11})N\eta$	$\frac{f_{N^*N\eta}}{m_\pi}\bar{\Psi}_{N^*}\gamma^\mu\Psi\partial_\mu\eta + \text{h.c.}$
$N^*(S_{11})N\rho$	$g_{N^*N\rho}\bar{\Psi}_{N^*}\gamma^5\gamma^\mu\vec{\tau}\vec{\rho}_\mu\Psi + \text{h.c.}$
$N^*(S_{11})\Delta\pi$	$\frac{f_{N^*\Delta\pi}}{m_\pi}\bar{\Psi}_{N^*}\gamma^5\vec{S}\Delta^\mu\partial_\mu\vec{\pi} + \text{h.c.}$
$N^*(P_{13})N\pi$	$\frac{f_{N^*N\pi}}{m_\pi}\bar{\Psi}^\mu_{N^*}\vec{\tau}\Psi\partial_\mu\vec{\pi} + \text{h.c.}$
$N^*(P_{13})N\eta$	$\frac{f_{N^*N\eta}}{m_\pi}\bar{\Psi}^\mu_{N^*}\Psi\partial_\mu\eta + \text{h.c.}$
$N^*(P_{13})\Delta\pi$	$\frac{f_{N^*\Delta\pi}}{m_\pi}\bar{\Psi}^\mu_{N^*}\gamma^5\gamma^\nu\vec{S}\Delta_\mu\partial_\nu\vec{\pi} + \text{h.c.}$
$N^*(D_{13})N\pi$	$\frac{f_{N^*N\pi}}{m_\pi^2}\bar{\Psi}\gamma^5\gamma^\nu\vec{\tau}\Psi^\mu_{N^*}\partial_\nu\partial_\mu\vec{\pi} + \text{h.c.}$
$N^*(D_{13})N\eta$	$\frac{f_{N^*N\eta}}{m_\pi^2}\bar{\Psi}\gamma^5\gamma^\nu\Psi^\mu_{N^*}\partial_\nu\partial_\mu\eta + \text{h.c.}$
$N^*(D_{13})\Delta\pi$	$i\frac{f_{N^*\Delta\pi}}{m_\pi}\bar{\Psi}_{N^*\nu}\vec{S}\gamma^\mu\Delta^\nu\partial_\mu\vec{\pi} + \text{h.c.}$
$N^*(D_{13})N\rho$	$\frac{f_{N^*N\rho}}{m_\rho}\bar{\Psi}^\mu_{N^*}\gamma^\nu\vec{\tau}\vec{\rho}_{\mu\nu}\Psi + \text{h.c.}$
$\Delta^*(S_{31})N\pi$	$\frac{f_{\Delta^*N\pi}}{m_\pi}\bar{\Delta}^*\gamma^\mu\vec{S}^\dagger\Psi\partial_\mu\vec{\pi} + \text{h.c.}$
$\Delta^*(S_{31})\Delta\pi$	$\frac{f_{\Delta^*\Delta\pi}}{m_\pi}\bar{\Delta}^*\gamma^5\vec{T}\Delta^\mu\partial_\mu\vec{\pi} + \text{h.c.}$
$\Delta^*(P_{31})N\pi$	$-\frac{f_{\Delta^*N\pi}}{m_\pi}\bar{\Delta}^*\gamma^5\gamma^\mu\vec{S}^\dagger\Psi\partial_\mu\vec{\pi} + \text{h.c.}$
$\Delta^*(P_{31})\Delta\pi$	$-\frac{f_{\Delta^*\Delta\pi}}{m_\pi}\bar{\Delta}^*\vec{T}\Delta^\mu\partial_\mu\vec{\pi} + \text{h.c.}$
$N^*(D_{33})N\pi$	$\frac{f_{N^*N\pi}}{m_\pi^2}\bar{\Psi}\gamma^5\gamma^\nu\vec{S}^\dagger\Psi^\mu_{N^*}\partial_\nu\partial_\mu\vec{\pi} + \text{h.c.}$
$N^*(D_{33})\Delta\pi$	$i\frac{f_{N^*\Delta\pi}}{m_\pi}\bar{\Delta}^*\nu\vec{T}\gamma^\mu\Delta^\nu\partial_\mu\vec{\pi} + \text{h.c.}$
$N^*(D_{33})N\rho$	$\frac{f_{N^*N\rho}}{m_\rho}\bar{\Delta}^{*\mu}\gamma^\nu\vec{S}^\dagger\vec{\rho}_{\mu\nu}\Psi + \text{h.c.}$

Table B.1: Effective Lagrangian.

B.2 Calculation of the diagrams

Fig. B.1 shows the notations for the momenta and helicities of initial, final, and intermediate particles in various diagrams. All on-shell meson energies are denoted as

$$\omega_i = \sqrt{\vec{p}_i^{\,2} + m_i^2}, \tag{B.4}$$

and on-shell baryon energies as

$$E_i = \sqrt{\vec{p}_i^{\,2} + m_i^2}, \tag{B.5}$$

where m_i are the masses of the corresponding particles. The 3-momentum $\vec{q}$ of the intermediate particle is equal to $\vec{q} = \vec{p_1} - \vec{p_4}$ for u-channel diagrams, $\vec{q} = \vec{p_1} - \vec{p_3}$ for

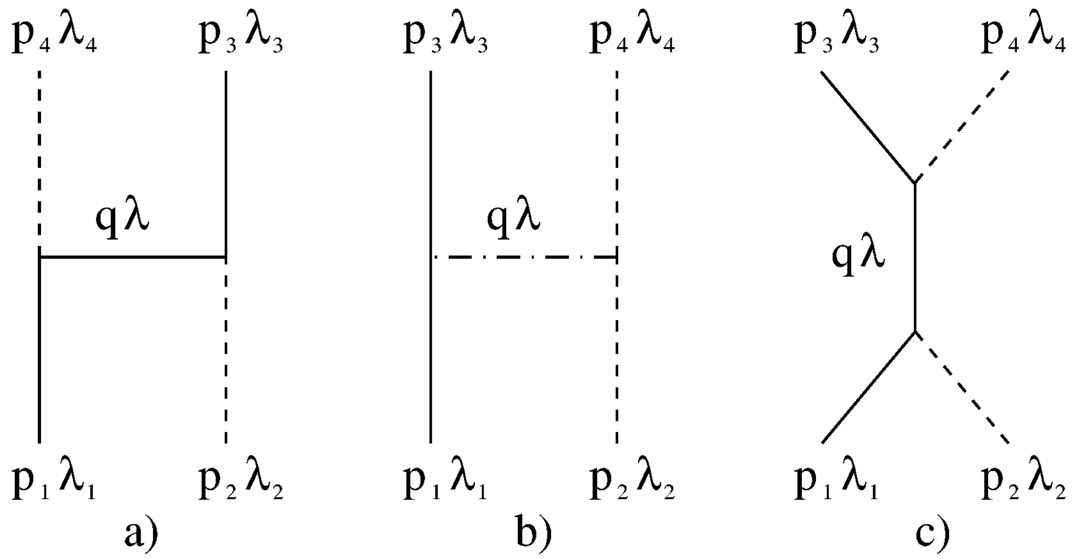

Figure B.1: Notations for the momenta and helicities of the particles in the u, t, and s- channel diagrams, drawn in figs. a), b), and c), respectively.

t channel diagrams, and $\vec{q} = \vec{p_1} + \vec{p_2} = 0$ for s-channel diagrams. The 4-momentum of the intermediate particle for the first time ordering is denoted by q with $q^0 = \omega_q$ (for meson exchanges) or $q^0 = E_q$ (for baryon exchanges). For the second time ordering it is denoted by $\tilde{q}$ with $\tilde{q}^0 = -\omega_q(-E_q)$. For the Δ-exchange diagrams we use the simplified prescription of ref. [65] in order to avoid serious complications, related to the TOPT treatment. In this case we set the zeroth component of the 4-momentum q_Δ equal to $q^0_\Delta = \epsilon_1 - \epsilon_4$, where ϵ_1, ϵ_4 are the on-shell energies ϵ_1, ϵ_4 are given by

$$\epsilon_1 = \frac{Z^2 + m_1^2 - m_2^2}{2Z}, \; \epsilon_4 = \frac{Z^2 - m_3^2 + m_4^2}{2Z}. \tag{B.6}$$

The zeroth components of the initial and final momenta are set to their on-mass-shell values: $p_i^0 = \omega_i(E_i)$. Each diagram contains a kinematical normalization factor

$$\kappa = \frac{1}{(2\pi)^3} \frac{1}{\sqrt{2\omega_2 2\omega_4}}. \tag{B.7}$$

The isospin coefficients, corresponding to $I = 1/2$ and $I = 3/2$ states are denoted as IF and are given in appendix C.

Let us now come to the explicit potential matrix elements. First we list the expressions for the background diagrams in different channels.

$\pi N \to \pi N$

- stable σ exchange

$$\kappa \frac{g_{\sigma\pi\pi}}{2m_\pi} g_{NN\sigma}(-2p_{2_\mu} p_4^\mu) \frac{1}{2\omega_q} \left(\frac{1}{Z - E_q - E_3 - \omega_2} + \frac{1}{Z - E_q - E_1 - \omega_4} \right)$$
$$\bar{u}(\vec{p}_3, \lambda_3) u(\vec{p}_1, \lambda_1) IF_\sigma \quad \text{(B.8)}$$

- stable ρ exchange

$$- i\kappa g_{\rho\pi\pi} g_{NN\rho} \bar{u}(\vec{p}_3, \lambda_3) \left([\gamma^\mu - i\frac{\kappa_\rho}{2m_N}\sigma^{\mu\nu} q_\nu] \frac{1}{2\omega_q(Z - \omega_q - E_3 - \omega_2)} \right.$$
$$\left. + [\gamma^\mu - i\frac{\kappa_\rho}{2m_N}\sigma^{\mu\nu} \tilde{q}_\nu] \frac{1}{2\omega_q(Z - \omega_q - E_1 - \omega_4)} \right) u(\vec{p}_1, \lambda_1)(p_2 + p_4)_\mu IF_\rho \quad \text{(B.9)}$$

For simplicity reasons we always use this prescription for the ρ (and also ω) propagator instead of the TOPT expression, including contact term. These two prescriptions are equivalent on energy shell. The resulting difference between them turns out to be small [1].

- nucleon exchange

$$\kappa \frac{f_{NN\pi}^2}{m_\pi^2} \bar{u}(\vec{p}_3, \lambda_3)\gamma_5 \hat{p}_2 \frac{1}{2E_q} \left(\frac{\hat{q} + m_N}{Z - E_q - \omega_2 - \omega_4} + \frac{\hat{\tilde{q}} + m_N}{Z - E_q - E_1 - E_3} \right)$$
$$\gamma_5 \hat{p}_4 u(\vec{p}_1, \lambda_1) IF_{Nu} \quad \text{(B.10)}$$

- Δ exchange

$$\kappa \frac{f_{N\Delta\pi}^2}{m_\pi^2} \bar{u}(\vec{p}_3, \lambda_3) p_{2_\mu} P^{\mu\nu}(q_\Delta) \left(\frac{1}{2E_q(Z - E_q - \omega_2 - \omega_4)} + \right.$$
$$\left. \frac{1}{2E_q(Z - E_q - E_1 - E_3)} \right) p_{4_\nu} u(\vec{p}_1, \lambda_1) IF_{\Delta u} \quad \text{(B.11)}$$

$\pi N \to \rho N$

- nucleon exchange

$$
\begin{aligned}
& -i\kappa g_{NN\rho}\frac{f_{NN\pi}}{m_\pi}\bar{u}(\vec{p}_3,\lambda_3)\gamma_5\hat{p}_2\left(\frac{\hat{q}+m_N}{Z-E_q-\omega_2-\omega_4}+\frac{\hat{\tilde{q}}+m_N}{Z-E_q-E_1-E_3}\right)\\
&\qquad \frac{1}{2E_q}[\hat{\epsilon}^*(\vec{p}_4,\lambda_4)-i\frac{\kappa_\rho}{2m_N}\sigma^{\mu\nu}p_{4_\nu}\epsilon^*_\mu(\vec{p}_4,\lambda_4)]u(\vec{p}_1,\lambda_1)IF_{Nu} \qquad (B.12)
\end{aligned}
$$

- $NN\pi\rho$ contact term

$$
-\kappa g_\rho\frac{f_{NN\pi}}{m_\pi}\bar{u}(\vec{p}_3,\lambda_3)\gamma^5\hat{\epsilon}^*(\vec{p}_4,\lambda_4)u(\vec{p}_1,\lambda_1)IF_{ct} \qquad (B.13)
$$

- π exchange

$$
\begin{aligned}
& -\kappa g_{\rho\pi\pi}\frac{f_{NN\pi}}{m_\pi}\bar{u}(\vec{p}_3,\lambda_3)\gamma^5\left(\frac{\tilde{q}_\mu(p_2-q)_\nu}{2\omega_q(Z-\omega_q-E_3-\omega_2)}\right.\\
&\qquad \left.+\frac{\tilde{q}_\mu(p_2-\tilde{q})_\nu}{2\omega_q(Z-\omega_q-E_1-\omega_4)}-\gamma^0\delta^0_\nu\right)\epsilon^{*,\nu}(\vec{p}_4,\lambda_4)u(\vec{p}_1,\lambda_1)IF_\pi
\end{aligned} \qquad (B.14)
$$

- ω exchange

$$
\begin{aligned}
& \kappa g_{NN\omega}\frac{g_{\omega\pi\rho}}{m_\omega}\bar{u}(\vec{p}_3,\lambda_3)\left([\gamma^\nu-i\frac{\kappa_\omega}{2m_N}\sigma^{\nu\tau}q_\tau]\frac{1}{2\omega_q(Z-\omega_q-E_3-\omega_2)}\right.\\
&\qquad \left.+[\gamma^\nu-i\frac{\kappa_\omega}{2m_N}\sigma^{\nu\tau}\tilde{q}_\tau]\frac{1}{2\omega_q(Z-\omega_q-E_1-\omega_4)}\right)\\
&\qquad\qquad u(\vec{p}_1,\lambda_1)\epsilon_{\alpha\beta\mu\nu}p_4^\alpha\epsilon^{*,\beta}(\vec{p}_4,\lambda_4)p_2^\mu IF_\omega \qquad (B.15)
\end{aligned}
$$

- a_1 exchange

$$
\begin{aligned}
&2\kappa g_\rho \frac{f_{NN\pi}}{m_\pi}\bar{u}(\vec{p}_3,\lambda_3)\gamma^5\gamma_\mu \left(\frac{-g^{\mu\nu}+\frac{q^\mu q^\nu}{m_{a_1}^2}}{2\omega_q(Z-\omega_q-E_3-\omega_2)} \right.\\
&\qquad [(p_2+\frac{q}{2})_\tau p_4^\tau \epsilon_\nu^*(\vec{p}_4,\lambda_4)-(p_2+\frac{q}{2})^\tau \epsilon_\tau^*(\vec{p}_4,\lambda_4)p_{4_\nu}]\\
&\qquad +[(p_2+\tilde{q}/2)_\tau p_4^\tau \epsilon_\nu^*(\vec{p}_4,\lambda_4)-(p_2+\tilde{q}/2)^\tau \epsilon_\tau^*(\vec{p}_4,\lambda_4)p_{4_\nu}]\\
&\qquad \frac{-g^{\mu\nu}+\frac{\tilde{q}^\mu \tilde{q}^\nu}{m_{a_1}^2}}{2\omega_q(Z-\omega_q-E_1-\omega_4)}\\
&\qquad \left. +\frac{1}{m_{a_1}^2}\delta_\mu^0[p_{2\nu}p_4^\nu \epsilon_0^*(\vec{p}_4,\lambda_4)-p_2^\nu \epsilon_\nu^*(\vec{p}_4,\lambda_4)p_{4_0}] \right) u(\vec{p}_1,\lambda_1)IF_{a_1}
\end{aligned}
\tag{B.16}
$$

$\rho N \to \rho N$

- nucleon exchange

$$
\begin{aligned}
&\kappa g_{NN\rho}^2 \bar{u}(\vec{p}_3,\lambda_3)[\gamma^\mu + i\frac{\kappa_\rho}{2m_N}\sigma^{\mu\nu}p_{2_\nu}]\epsilon_\mu(\vec{p}_2,\lambda_2)\\
&\qquad \frac{1}{2E_q}\left(\frac{\hat{q}+m_N}{Z-E_q-\omega_2-\omega_4} + \frac{\hat{\tilde{q}}+m_N}{Z-E_q-E_1-E_3} \right)\\
&\qquad [\gamma^\tau - i\frac{\kappa_\rho}{2m_N}\sigma^{\tau\nu}p_{4_\nu}]\epsilon_\tau^*(\vec{p}_4,\lambda_4)u(\vec{p}_1,\lambda_1)IF_{Nu}
\end{aligned}
\tag{B.17}
$$

- $NN\rho\rho$ contact term

$$
\kappa g_{NN\rho}\frac{f_{NN\rho}}{2m_N}\bar{u}(\vec{p}_3,\lambda_3)\sigma^{\mu\nu}\epsilon_\mu(\vec{p}_2,\lambda_2)\epsilon_\nu^*(\vec{p}_4,\lambda_4)u(\vec{p}_1,\lambda_1)IF_{ct} \tag{B.18}
$$

- ρ exchange

$$- i\kappa \frac{g_\rho^2}{2} \Bigg(\bar{u}(\vec{p}_3, \lambda_3)[\gamma^\mu - i\frac{\kappa_\rho}{2m_N}\sigma^{\mu\nu} q_\nu] u(\vec{p}_1, \lambda_1) \frac{1}{2\omega_q(Z - \omega_q - E_3 - \omega_2)}$$
$$[\epsilon^\tau(\vec{p}_2, \lambda_2)\epsilon^*_\tau(\vec{p}_4, \lambda_4)(-p_4 - p_2)_\mu + (q + p_4)^\tau \epsilon_\tau(\vec{p}_2, \lambda_2)\epsilon^*_\mu(\vec{p}_4, \lambda_4) +$$
$$(p_2 - q)^\tau \epsilon^*_\tau(\vec{p}_4, \lambda_4)\epsilon_\mu(\vec{p}_2, \lambda_2)]$$
$$+ [\epsilon^\tau(\vec{p}_2, \lambda_2)\epsilon^*_\tau(\vec{p}_4, \lambda_4)(-p_4 - p_2)_\mu + (\tilde{q} + p_4)^\tau \epsilon_\tau(\vec{p}_2, \lambda_2)\epsilon^*_\mu(\vec{p}_4, \lambda_4) +$$
$$(p_2 - \tilde{q})^\tau \epsilon^*_\tau(\vec{p}_4, \lambda_4)\epsilon_\mu(\vec{p}_2, \lambda_2)]$$
$$\bar{u}(\vec{p}_3, \lambda_3)[\gamma^\mu - i\frac{\kappa_\rho}{2m_N}\sigma^{\mu\nu} \tilde{q}_\nu] u(\vec{p}_1, \lambda_1) \frac{1}{2\omega_q(Z - \omega_q - E_1 - \omega_4)} \Bigg) IF_\rho \tag{B.19}$$

$\pi N \to \pi\Delta$

- nucleon exchange

$$-\kappa \frac{f_{N\Delta\pi} f_{NN\pi}}{m_\pi^2} \bar{u}^\mu(\vec{p}_3, \lambda_3) p_{2_\mu} \frac{1}{2E_q} \left(\frac{\hat{q} + m_N}{Z - E_q - \omega_2 - \omega_4} + \frac{\hat{\tilde{q}} + m_N}{Z - E_q - E_1 - E_3} \right)$$
$$\gamma^5 \hat{p}_4 u(\vec{p}_1, \lambda_1) IF_{Nu} \tag{B.20}$$

- Δ exchange

$$\kappa \frac{f_{\Delta\Delta\pi} f_{N\Delta\pi}}{m_\pi^2} \bar{u}_\mu(\vec{p}_3, \lambda_3)\gamma^5 \hat{p}_2 \frac{P^{\mu\nu}(q_\Delta)}{2E_q}$$
$$\left(\frac{1}{Z - E_q - \omega_2 - \omega_4} + \frac{1}{Z - E_q - E_1 - E_3} \right) p_4^\nu u(\vec{p}_1, \lambda_1) IF_{\Delta u} \tag{B.21}$$

- ρ exchange

$$- i\kappa g_\rho \frac{f_{N\Delta\rho}}{m_\rho} \bar{u}^\mu(\vec{p}_3, \lambda_3)\gamma^5 (q_\mu \gamma_\nu - \hat{q} g_{\mu\nu}) u(\vec{p}_1, \lambda_1) \frac{1}{2\omega_q}$$
$$\left(\frac{1}{Z - \omega_q - \omega_2 - E_3} + \frac{1}{Z - \omega_q - \omega_4 - E_1} \right) (p_2 + p_4)^\nu IF_\rho \tag{B.22}$$

$\pi\Delta \to \pi\Delta$

- nucleon exchange

$$\kappa\frac{f^2_{N\Delta\pi}}{m^2_\pi}\bar{u}^\mu(\vec{p}_3,\lambda_3)p_{2_\mu}\frac{1}{2E_q}\left(\frac{\hat{q}+m_N}{Z-E_q-\omega_2-\omega_4}+\frac{\hat{\tilde{q}}+m_N}{Z-E_q-E_1-E_3}\right)$$
$$p_{4_\nu}u^\nu(\vec{p}_1,\lambda_1)IF_{Nu} \quad \text{(B.23)}$$

- Δ exchange

$$\kappa\frac{f^2_{\Delta\Delta\pi}}{m^2_\pi}\bar{u}_\mu(\vec{p}_3,\lambda_3)\gamma^5\hat{p}_2\frac{P^{\mu\nu}(q_\Delta)}{2E_q}\left(\frac{1}{Z-E_q-\omega_2-\omega_4}+\frac{1}{Z-E_q-E_1-E_3}\right)$$
$$\gamma^5\hat{p}_4u_\nu(\vec{p}_1,\lambda_1)IF_{\Delta u} \quad \text{(B.24)}$$

- ρ exchange

$$i\kappa g_{\Delta\Delta\rho}g_{\rho\pi\pi}\bar{u}^\tau(\vec{p}_3,\lambda_3)\left[\gamma_\mu - i\frac{\kappa_{\Delta\Delta\rho}}{2m_\Delta}\sigma_{\mu\nu}q^\nu\right]u_\tau(\vec{p}_1,\lambda_1)\frac{1}{2\omega_q}$$
$$\left(\frac{1}{Z-\omega_q-\omega_2-E_3}+\frac{1}{Z-\omega_q-\omega_4-E_1}\right)(p_2+p_4)^\mu IF_\rho \quad \text{(B.25)}$$

$\pi N \to \sigma N$

- nucleon exchange

$$-i\kappa g_{NN\sigma}\frac{f_{NN\pi}}{m_\pi}\bar{u}(\vec{p}_3,\lambda_3)\gamma^5\hat{p}_2\frac{1}{2E_q}\left(\frac{\hat{q}+m_N}{Z-E_q-\omega_2-\omega_4}+\frac{\hat{\tilde{q}}+m_N}{Z-E_q-E_1-E_3}\right)$$
$$u(\vec{p}_1,\lambda_1)IF_{Nu} \quad \text{(B.26)}$$

- π exchange

$$i\kappa\frac{f_{NN\pi}}{m_\pi}\frac{g_{\sigma\pi\pi}}{m_\pi}\bar{u}(\vec{p}_3,\lambda_3)\frac{1}{2\omega_q}\left(\frac{\gamma^5\hat{q}q_\mu}{Z-E_q-\omega_2-E_3}\right.$$
$$\left.+\frac{\gamma^5\hat{\tilde{q}}\tilde{q}_\mu}{Z-E_q-\omega_4-E_1}+2\omega_q\gamma^5\gamma^0p_2^0\right)p_2^\mu u(\vec{p}_1,\lambda_1)IF_\pi \quad \text{(B.27)}$$

$\sigma N \to \sigma N$

- nucleon exchange

$$\kappa g^2_{NN\sigma}\bar{u}(\vec{p}_3,\lambda_3)\frac{1}{2E_q}\left(\frac{\hat{q}+m_N}{Z-E_q-\omega_2-\omega_4}+\frac{\hat{\tilde{q}}+m_N}{Z-E_q-E_1-E_3}\right)u(\vec{p}_1,\lambda_1)IF_{Nu} \tag{B.28}$$

- σ exchange

$$\kappa 6 g_{NN\sigma}g_{\sigma\sigma\sigma}m_\sigma\bar{u}(\vec{p}_3,\lambda_3)u(\vec{p}_1,\lambda_1)$$
$$\frac{1}{2\omega_q}\left(\frac{1}{Z-\omega_q-\omega_2-E_3}+\frac{1}{Z-\omega_q-\omega_4-E_1}\right)IF_\sigma \tag{B.29}$$

$\pi N \to \eta N$

- nucleon exchange

$$\kappa\frac{f_{NN\pi}f_{NN\eta}}{m^2_\pi}\bar{u}(\vec{p}_3,\lambda_3)\gamma^5\hat{p}_2\frac{1}{2E_q}\left(\frac{\hat{q}+m_N}{Z-E_q-\omega_2-\omega_4}+\frac{\hat{\tilde{q}}+m_N}{Z-E_q-E_1-E_3}\right)$$
$$\gamma^5\hat{p}_4u(\vec{p}_1,\lambda_1)IF_{Nu} \tag{B.30}$$

- a_0 exchange

$$\kappa g_{NNa_0}g_{\pi\eta a_0}m_\pi\bar{u}_\mu(\vec{p}_3,\lambda_3)u(\vec{p}_1,\lambda_1)$$
$$\frac{1}{2\omega_q}\left(\frac{1}{Z-\omega_q-\omega_2-E_3}+\frac{1}{Z-\omega_q-\omega_4-E_1}\right)IF_{a_0} \tag{B.31}$$

$\eta N \to \eta N$

- nucleon exchange

$$\kappa\frac{f^2_{NN\eta}}{m^2_\pi}\bar{u}(\vec{p}_3,\lambda_3)\gamma^5\hat{p}_2\frac{1}{2E_q}\left(\frac{\hat{q}+m_N}{Z-E_q-\omega_2-\omega_4}+\frac{\hat{\tilde{q}}+m_N}{Z-E_q-E_1-E_3}\right)$$
$$\gamma^5\hat{p}_4u(\vec{p}_1,\lambda_1)IF_{Nu} \tag{B.32}$$

Each pole graph contributes only to one particular partial wave. Moreover, resonance diagrams are factorizable in the JLS basis, and can be fully defined by the vertex functions (see section 2.6). Below we give the expressions for all vertex functions, which enter into the calculation. They are derived from the Lagrangian given in table B.1 and transformed to the JLS basis (cf. chapter D).

We use the following abbreviations here:

$$\tilde{k} = \frac{k}{E_k + m}; \; N(k) = \sqrt{\frac{E_k + m}{E_k \omega_k}}, \tag{B.33}$$

where k is the c.m. momentum of the meson-baryon system, and m is the baryon mass. The isospin factors IF should be understood as the factors corresponding to each vertex. They are given in appendix C. Since the pole diagrams are equal (up to isospin factors) for the resonances that differ only in the isospin quantum number, we give only one expression for both cases. The coupling constant is denoted simply by $f(g)$ without indices.

$S_{11}(S_{31})$

$$\begin{aligned}
v_{\pi N(\eta N)}(k) &= \frac{f}{m_\pi}\frac{1}{\sqrt{8\pi}}N(k)(\omega(k) + k\tilde{k})IF_{\pi N(\eta N)} \\
v_{\pi\Delta}(k) &= \frac{f}{m_\pi}\frac{1}{\sqrt{12\pi}}\frac{1}{m_\Delta}N(k)(\omega(k) + E_k)k\tilde{k}IF_{\pi\Delta} \\
v_{\rho N}^{L=0,S=1/2}(k) &= ig\frac{1}{\sqrt{24\pi}}\frac{1}{m_\rho}N(k)(\omega(k) + k\tilde{k} + 2m_\rho)IF_{\rho N} \\
v_{\rho N}^{L=2,S=3/2}(k) &= ig\frac{1}{\sqrt{24\pi}}\frac{1}{m_\rho}N(k)(\omega(k) + k\tilde{k} - m_\rho)IF_{\rho N}
\end{aligned} \tag{B.34}$$

nucleon (P_{31})

$$\begin{aligned}
v_{\pi N}(k) &= \frac{f}{m_\pi}\frac{1}{\sqrt{8\pi}}N(k)(k + \omega_k\tilde{k})IF_{\pi N} \\
v_{\pi\Delta}(k) &= -\frac{f}{m_\pi}\frac{1}{\sqrt{12\pi}}\frac{1}{m_\Delta}N(k)(\omega(k) + E_k)IF_{\pi\Delta}
\end{aligned} \tag{B.35}$$

$P_{13}(P_{33})$

$$
\begin{aligned}
v_{\pi N(\eta N)}(k) &= \frac{f}{m_\pi}\frac{1}{\sqrt{24\pi}}N(k)kIF_{\pi N(\eta N)} \\
v_{\pi\Delta}^{L=1}(k) &= \frac{f}{m_\pi}\frac{1}{\sqrt{360\pi}}\frac{1}{m_\Delta}N(k)(4k^2\tilde{k}+3E_k\omega_k\tilde{k}-4\omega_k k-5E_k k)IF_{\pi\Delta} \\
v_{\pi\Delta}^{L=3}(k) &= \frac{f}{m_\pi}\frac{1}{\sqrt{40\pi}}\frac{1}{m_\Delta}N(k)(k^2\tilde{k}+2E_k\omega_k\tilde{k}-\omega_k k)IF_{\pi\Delta}
\end{aligned}
\tag{B.36}
$$

$D_{13}(D_{33})$

$$
\begin{aligned}
v_{\pi N(\eta N)}(k) &= \frac{f}{m_\pi^2}\frac{1}{\sqrt{24\pi}}N(k)(k^2+\omega_k k\tilde{k})IF_{\pi N(\eta N)} \\
v_{\pi\Delta}^{L=2}(k) &= -\frac{f}{m_\pi}\frac{1}{\sqrt{72\pi}}\frac{1}{m_\Delta}N(k)(\omega(k)+k\tilde{k})(E_k-m_\Delta)IF_{\pi\Delta} \\
v_{\pi\Delta}^{L=0}(k) &= \frac{f}{m_\pi}\frac{1}{\sqrt{72\pi}}\frac{1}{m_\Delta}N(k)(\omega(k)+k\tilde{k})(E_k+2m_\Delta)IF_{\pi\Delta} \\
v_{\rho N}^{L=2,S=1/2}(k) &= i\frac{f}{m_\rho}\frac{1}{\sqrt{72\pi}}N(k)(-k\tilde{k}+\omega_k-m_\rho)IF_{\rho N} \\
v_{\rho N}^{L=2,S=3/2}(k) &= i\frac{f}{m_\rho}\frac{1}{\sqrt{72\pi}}N(k)(2k\tilde{k}+\omega_k-m_\rho)IF_{\rho N} \\
v_{\rho N}^{L=0,S=3/2}(k) &= i\frac{f}{m_\rho}\frac{1}{\sqrt{72\pi}}N(k)(k\tilde{k}+2\omega_k+m_\rho)IF_{\rho N}
\end{aligned}
\tag{B.37}
$$

Finally, one should note that all the contributions, presented in this chapter are multiplied by a corresponding form factor.

Appendix C

Isospin relations

Because of the isospin invariance of the strong interaction, we calculate the potentials in the isospin basis, thus reducing the number of independent amplitudes. For the nucleon, pion, and Δ wave functions in the isospin space we use the following notation

$$N = \begin{pmatrix} p \\ n \end{pmatrix}, \ \vec{\pi} = \begin{pmatrix} -\pi^+ \\ \pi^0 \\ \pi^- \end{pmatrix}, \ \Delta = \begin{pmatrix} \Delta^{++} \\ \Delta^+ \\ \Delta^0 \\ \Delta^- \end{pmatrix}, \tag{C.1}$$

and similarly for all other particles with isospin $I = 1/2$, 1, and 3/2.

The isospin matrices are defined as

$$\tau_{-1} = \sqrt{2} \begin{pmatrix} 0 & 0 \\ -1 & 0 \end{pmatrix}, \quad \tau_0 = \begin{pmatrix} 1 & 0 \\ 0 & -1 \end{pmatrix}, \quad \tau_{+1} = \sqrt{2} \begin{pmatrix} 0 & 1 \\ 0 & 0 \end{pmatrix} \tag{C.2}$$

for the nucleon,

$$t_{-1} = \begin{pmatrix} 0 & 0 & 0 \\ -1 & 0 & 0 \\ 0 & -1 & 0 \end{pmatrix}, \ t_0 = \begin{pmatrix} 1 & 0 & 0 \\ 0 & 0 & 0 \\ 0 & 0 & -1 \end{pmatrix}, \ t_{+1} = \begin{pmatrix} 0 & 1 & 0 \\ 0 & 0 & 1 \\ 0 & 0 & 0 \end{pmatrix} \tag{C.3}$$

for the pion,

$$S_{-1} = \begin{pmatrix} 1 & 0 & 0 & 0 \\ 0 & \frac{1}{\sqrt{3}} & 0 & 0 \end{pmatrix}, S_0 = \sqrt{\frac{2}{3}} \begin{pmatrix} 0 & 1 & 0 & 0 \\ 0 & 0 & 1 & 0 \end{pmatrix}, S_{+1} = \begin{pmatrix} 0 & 0 & \frac{1}{\sqrt{3}} & 0 \\ 0 & 0 & 0 & 1 \end{pmatrix} \tag{C.4}$$

for the $I = 3/2$ to $I = 1/2$ transition, and

$$
\begin{aligned}
T_{-1} &= \begin{pmatrix} 0 & 0 & 0 & 0 \\ -\sqrt{\frac{2}{3}} & 0 & 0 & 0 \\ 0 & -\frac{2\sqrt{2}}{3} & 0 & 0 \\ 0 & 0 & -\sqrt{\frac{2}{3}} & 0 \end{pmatrix}, \\
T_{0} &= \begin{pmatrix} 1 & 0 & 0 & 0 \\ 0 & \frac{1}{3} & 0 & 0 \\ 0 & 0 & -\frac{1}{3} & 0 \\ 0 & 0 & 0 & -1 \end{pmatrix}, \\
T_{+1} &= \begin{pmatrix} 0 & \sqrt{\frac{2}{3}} & 0 & 0 \\ 0 & 0 & \frac{2\sqrt{2}}{3} & 0 \\ 0 & 0 & 0 & \sqrt{\frac{2}{3}} \\ 0 & 0 & 0 & 0 \end{pmatrix}
\end{aligned} \tag{C.5}
$$

for the Δ. The scalar product for the isospin vectors is given by

$$\vec{A}\vec{B} = \sum_m (-1)^m A_m B_{-m}. \tag{C.6}$$

If we introduce basis states as

$$
\begin{aligned}
(\chi_l)_{l'} &= \delta_{ll'} (l, l' = \pm 1/2) \text{ for } I = 1/2 \text{ particles,} && \text{(C.7)} \\
(\phi_m)_{m'} &= \delta_{m,m'} (m, m' = 0, \pm 1) \text{ for } I = 1 \text{ particles, and} && \text{(C.8)} \\
(\Delta_l)_{l'} &= \delta_{ll'} (l, l' = \pm 1/2, \pm 3/2) \text{ for } I = 3/2 \text{ particles,} && \text{(C.9)}
\end{aligned}
$$

then the expressions for the vertices which appear in the calculations of the isospin

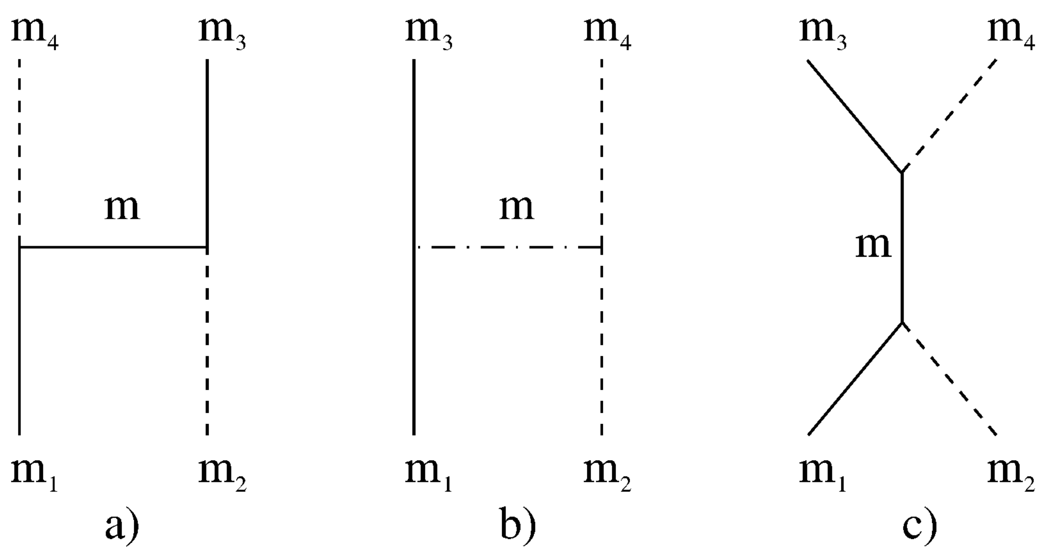

Figure C.1: Isospin indices of the initial, final and intermediate particles for a) u-channel, b) t-channel, and c) s-channel diagrams.

coefficients take the form:

$$
\begin{aligned}
\vec{\phi}_l \vec{\phi}_{l'} &= (-)^l \delta_{l,-l'} \\
\vec{\phi}_l \times \vec{\phi}_{l'} &= \sum_{l''=0,\pm 1} i\sqrt{2} \langle\, 1\, l\, 1\, l' \,|\, 1\, l'' \,\rangle\, \vec{\phi}_{l''} \\
\chi_l^\dagger \chi_{l'} &= \delta_{l,l'} \\
\chi_{l'}^\dagger \vec{\tau} \vec{\phi}_m \chi_l &= \sqrt{3}\, \langle\, \tfrac{1}{2}\, l\, 1\, m \,|\, \tfrac{1}{2}\, l' \,\rangle \\
\Delta_{l'}^\dagger \vec{S}^\dagger \vec{\phi}_m \chi_l &= \langle\, \tfrac{1}{2}\, l\, 1\, m \,|\, \tfrac{3}{2}\, l' \,\rangle \\
\Delta_{l'}^\dagger \vec{T} \vec{\phi}_m \Delta_l &= \sqrt{\frac{5}{3}}\, \langle\, \tfrac{3}{2}\, l\, 1\, m \,|\, \tfrac{3}{2}\, l' \,\rangle
\end{aligned}
\tag{C.10}
$$

The calculation of the isospin coefficients IF for different exchange diagrams consists in constructing the isospin part of the amplitude M^{iso} from two vertices (cf. fig. C.1). E.g. for the nucleon exchange in the $\pi N \to \pi N$ potential:

$$
\langle\, 1/2\, m_3\, 1\, m_4 \,|\, M^{iso} \,| 1/2\, m_1\, 1\, m_2 \rangle = \sum_m \chi_{m_3}^\dagger \vec{\tau} \vec{\phi}_{m_2} \chi_m \; \chi_m^\dagger \vec{\tau} \vec{\phi}_{m_4}^{*} \chi_{m_1} \tag{C.11}
$$

Then the isospin coefficient $IF(I)$ is equal to the matrix element of M^{iso} between initial and final states with fixed total isospin

$$IF(I) \equiv \langle I\, I_z \,|\, M^{iso} \,| I\, I_z\rangle = \sum_{m1,m2} \sum_{m_3,m_4} \langle\, I_3\, m_3\, I_4\, m_4 \,|\, I\, I_z\,\rangle\langle\, I_1\, m_1\, I_2\, m_2 \,|\, I\, I_z\,\rangle$$
$$\times \;\; \langle\, I_3\, m_3\, I_4\, m_4 \,|\, M^{iso} \,| I_1\, m_1\, I_2\, m_2\rangle \tag{C.12}$$

The isospin coefficients for the background diagrams are collected in table C.1.

Reaction channel	Diagram	$IF(\frac{1}{2})$	$IF(\frac{3}{2})$
$\pi N \to \pi N$	N exchange	-1	2
	σ exchange	1	1
	ρ exchange	$2i$	$-i$
	Δ exchange	$\frac{4}{3}$	$\frac{1}{3}$
$\pi N \to \rho N$	N exchange	-1	2
	contact term	$-2i$	i
	π exchange	$-2i$	i
	ω exchange	1	1
	a_1 exchange	$-2i$	i
	Δ exchange	$\frac{4}{3}$	$\frac{1}{3}$
$\rho N \to \rho N$	N exchange	-1	2
	contact term	$-2i$	i
	ρ exchange	$2i$	$-i$
	Δ exchange	$\frac{4}{3}$	$\frac{1}{3}$
$\pi N \to \pi\Delta$	N exchange	$-\sqrt{\frac{8}{3}}$	$\sqrt{\frac{5}{3}}$
	Δ exchange	$-\frac{5}{3}\sqrt{\frac{2}{3}}$	$-\frac{10}{3\sqrt{15}}$
	ρ exchange	$\sqrt{\frac{2}{3}}$	$\sqrt{\frac{5}{3}}$
$\pi\Delta \to \pi\Delta$	N exchange	$\frac{1}{3}$	$-\frac{2}{3}$
	ρ exchange	$\frac{5}{3}$	$\frac{2}{3}$
	Δ exchange	$-\frac{10}{9}$	$\frac{11}{9}$
$\pi N \to \sigma N$	N exchange	$\sqrt{3}$	0
	π exchange	$\sqrt{3}$	0
$\sigma N \to \sigma N$	N exchange	1	0
	σ exchange	1	0

$\pi N \to \eta N$	N exchange	$\sqrt{3}$	0
	a_0 exchange	$\sqrt{3}$	0
$\eta N \to \eta N$	N exchange	1	0

Table C.1: Isospin factors for the background diagrams.

Since the isospin factors for the resonance diagrams factorize, it is convenient to present them for each vertex. They are given in table C.2.

Channel	πN	ρN	$\pi\Delta$	ηN
$IF(I = 1/2)$	$\sqrt{3}$	$\sqrt{3}$	$-\sqrt{2}$	1
$IF(I = 3/2)$	1	1	$\sqrt{\frac{5}{3}}$	0

Table C.2: Isospin coefficients for the resonance vertex functions.

Appendix D

Partial wave decomposition and transformation from helicity basis to JLS-basis

The most appropriate basis to solve the Lippmann-Schwinger equation is the JLS-basis (J-total angular momentum, L orbital angular momentum and S total spin of the two particle system). The reason for that is that due to the rotational symmetry of the Lagrangian (and hence of the potential) the angular momentum is conserved and the T-matrix does not depend on the angular momentum projection J_z on a chosen axis. Moreover L can change only by certain integers, depending on spin and parity of the interacting particles.

Therefore one has to transform the potential from the helicity plain wave basis (cf. appendix B) to the JLS basis.

D.1 Partial wave decomposition

The Lippmann-Schwinger equation in the plain wave helicity basis has the form 2.29

$$\begin{aligned}\langle\lambda_3\lambda_4\vec{k}'|T|\lambda_1\lambda_2\vec{k}\rangle &= \langle\lambda_3\lambda_4\vec{k}'|V|\lambda_1\lambda_2\vec{k}\rangle \\ &+\sum_{\gamma_1\gamma_2}\int d^3q\langle\lambda_3\lambda_4\vec{k}'|V|\gamma_1\gamma_2\vec{q}\rangle G(q)\langle\gamma_1\gamma_2\vec{q}|T|\lambda_1\lambda_2\vec{k}\rangle. \end{aligned}\tag{D.1}$$

Here, the channel and isospin indices were suppressed. The helicity operator commutes with the angular momentum. Therefore one can introduce a basis with fixed J, M (z-projection of J), and λ [42]. The connection between this basis and the plain wave basis for V and T matrices is given by

$$\langle\lambda_3\lambda_4\vec{k}'|T|\lambda_1\lambda_2\vec{k}\rangle = \frac{1}{4\pi}\sum_J(2J+1)D^J_{\lambda\lambda'}(\Omega_{k'k},0)^*\langle\lambda_3\lambda_3 k'|T^J|\lambda_1\lambda_2 k\rangle, \tag{D.2}$$

where $\lambda := \lambda_1-\lambda_2, \lambda' := \lambda_3-\lambda_4$. The $\Omega_{k'k}$ denotes the solid angle between the directions of the vectors $\vec{k}$ and $\vec{k}'$. The quantities $D^J_{\lambda\lambda'}(\Omega_{k'k},0)$ are related to the operator of finite rotations,

$$\mathcal{D}^J(\alpha,\beta,\gamma) = e^{-i\alpha J_z}e^{-i\beta J_y}e^{-i\gamma J_z} \tag{D.3}$$

via

$$D^J_{\lambda\lambda'}(\alpha,\beta,\gamma) = \langle J\lambda'|\mathcal{D}^J(\alpha,\beta,\gamma)|J\lambda\rangle = e^{-i\alpha\lambda'}d^J_{\lambda\lambda'}(\beta)e^{-i\gamma\lambda}\,, \tag{D.4}$$

where $d^J_{\lambda\lambda'}(\beta)$ are the reduced rotation matrices [107]. The α,β,γ are the standard Euler angles. The first two are related to $\Omega_{k'k}$. An arbitrary angle γ can be set to zero. Substituting eq. (D.2) into eq. (D.1) and making use of the orthogonality relations for the functions $D^J_{\lambda\lambda'}(\Omega_{k'k},0)$, we obtain the one-dimensional integral equation.

$$\begin{aligned}\langle\lambda_3\lambda_4 k'|T^J|\lambda_1\lambda_2 k\rangle &= \langle\lambda_3\lambda_4 k'|V^J|\lambda_1\lambda_2 k\rangle \\ &+\sum_{\gamma_1\gamma_2}\int dqq^2\langle\lambda_3\lambda_4 k'|V^J|\gamma_1\gamma_2 q\rangle G(q)\langle\gamma_1\gamma_2 q|T^J|\lambda_1\lambda_2 k\rangle. \end{aligned}\tag{D.5}$$

To calculate the potential in the J, M, λ basis one has to perform the transformation inverse to (D.2):

$$\langle\lambda_3\lambda_4 k'|T^J|\lambda_1\lambda_2 k\rangle = \int d\Omega_{k'k}D^J_{\lambda\lambda'}(\Omega_{k'k},0)\langle\lambda_3\lambda_4\vec{k}'|T|\lambda_1\lambda_2\vec{k}\rangle. \tag{D.6}$$

D.2 Transformation from helicity basis to JLS basis

The two particle state in the J, M, λ basis can be written as a linear combination of the states in JLS basis.

$$|JM\lambda_1\lambda_2 k\rangle = \sum_{LS} \langle JMLS|JM\lambda_1\lambda_2\rangle |JMLS\rangle. \tag{D.7}$$

The transformation matrix can be expressed via Clebsch-Gordan coefficients [42]

$$\langle JMLS|JM\lambda_1\lambda_2\rangle = \left(\frac{2L+1}{2J+1}\right)^{1/2} \langle L0S\lambda|J\lambda\rangle\langle S_1\lambda_1 S_2\lambda_2|S\lambda\rangle, \tag{D.8}$$

where S_1 and S_2 are the spins of the first and the second particles and $\lambda = \lambda_1 - \lambda_2$. The transformation of the potential and of the T-matrix to the JLS basis in matrix notation is given by

$$V_{LS}^{J,L'S'} = U_{\lambda_3\lambda_4}^{L'S'} V_{\lambda_1\lambda_2}^{J,\lambda_3\lambda_4} \left(U_{\lambda_1\lambda_2}^{J,LS}\right)^\dagger, \; T_{LS}^{J,L'S'} = U_{\lambda_3\lambda_4}^{L'S'} T_{\lambda_1\lambda_2}^{J,\lambda_3\lambda_4} \left(U_{\lambda_1\lambda_2}^{J,LS}\right)^\dagger \tag{D.9}$$

with the transformation matrix

$$U_{\lambda_1\lambda_2}^{J,LS} := \langle JMLS|JM\lambda_1\lambda_2\rangle. \tag{D.10}$$

Applying the transformation D.9 to eq. (D.5) one finally gets the Lippmann-Schwinger equation in the JLS basis:

$$\langle L'S'k'|T^J|LSk\rangle = \langle L'S'k'|V^J|LSk\rangle + \\ \sum_{L''S''} \int q^2 dq \langle L'S'k'|V^J|L''S''q\rangle G(q) \langle L''S''q|T^J|LSk\rangle. \tag{D.11}$$

For the calculations we need the coefficients of the transformation matrix $U_{\lambda_1\lambda_2}^{J,LS}$ for the following two-body systems:

- $S_1 = 1/2$, $S_2 = 0$

This case corresponds to the channels πN, σN, and ηN. The coefficients "d" of the transformation

$$\begin{pmatrix} |JM, L = J + \frac{1}{2}, S = \frac{1}{2}\rangle \\ |JM, L = J - \frac{1}{2}, S = \frac{1}{2}\rangle \end{pmatrix} = \underbrace{\begin{pmatrix} d_+^1 & -d_+^1 \\ d_-^1 & d_-^1 \end{pmatrix}}_{U^{J,LS}_{\lambda_1\lambda_2}(\frac{1}{2}\times 0)} \begin{pmatrix} |JM, \lambda_1 = \frac{1}{2}, \lambda_2 = 0\rangle \\ |JM, \lambda_1 = -\frac{1}{2}, \lambda_2 = 0\rangle \end{pmatrix} \quad \text{(D.12)}$$

are equal to

$$d_+^1 = -\frac{1}{\sqrt{2}}, \; d_-^1 = \frac{1}{\sqrt{2}}. \quad \text{(D.13)}$$

- $S_1 = 3/2, S_2 = 0$

  This situation we have for the $\pi\Delta$ channel. The transformation to the JLS basis takes the form

$$\begin{pmatrix} |JM, L = J + \frac{1}{2}, S = \frac{3}{2}\rangle \\ |JM, L = J - \frac{1}{2}, S = \frac{3}{2}\rangle \\ |JM, L = J + \frac{3}{2}, S = \frac{3}{2}\rangle \\ |JM, L = J - \frac{3}{2}, S = \frac{3}{2}\rangle \end{pmatrix} = \underbrace{\begin{pmatrix} e_+^1 & e_+^1 & e_+^2 & e_+^2 \\ e_-^1 & -e_-^1 & e_-^2 & -e_-^2 \\ f_+^1 & -f_+^1 & f_+^2 & -f_+^2 \\ f_-^1 & f_-^1 & f_-^2 & f_-^2 \end{pmatrix}}_{U^{J,LS}_{\lambda_1\lambda_2}(\frac{3}{2}\times 0)} \begin{pmatrix} |JM, \lambda_1 = \frac{1}{2}, \lambda_2 = 0\rangle \\ |JM, \lambda_1 = -\frac{1}{2}, \lambda_2 = 0\rangle \\ |JM, \lambda_1 = \frac{3}{2}, \lambda_2 = -1\rangle \\ |JM, \lambda_1 = -\frac{1}{2}, \lambda_2 = 1\rangle \end{pmatrix}, \quad \text{(D.14)}$$

  with the coefficients given in table D.1

- $S_1 = 1/2, \; S_2 = 1$

Coefficient	Index +	Index −
e^1	$-\frac{1}{2\sqrt{2}}\sqrt{\frac{2J+3}{2J}}$	$-\frac{1}{2\sqrt{2}}\sqrt{\frac{2J-1}{2J+2}}$
e^2	$\sqrt{\frac{3}{8}}\sqrt{\frac{2J-1}{2J}}$	$-\sqrt{\frac{3}{8}}\sqrt{\frac{2J+3}{2J+2}}$
f^1	$\sqrt{\frac{3}{8}}\sqrt{\frac{2J+3}{2J+2}}$	$\sqrt{\frac{3}{8}}\sqrt{\frac{2J-1}{2J}}$
f^2	$-\frac{1}{2\sqrt{2}}\sqrt{\frac{2J-1}{2J+2}}$	$\frac{1}{2\sqrt{2}}\sqrt{\frac{2J+3}{2J}}$

Table D.1: Coefficients of the transformation to the JLS basis for the $\pi\Delta$ system.

The transformation to te JLS basis for the ρN system is given by

$$\begin{pmatrix} |JM, L=J+\frac{1}{2}, S=\frac{1}{2}\rangle \\ |JM, L=J-\frac{1}{2}, S=\frac{1}{2}\rangle \\ |JM, L=J+\frac{3}{2}, S=\frac{3}{2}\rangle \\ |JM, L=J-\frac{3}{2}, S=\frac{3}{2}\rangle \\ |JM, L=J+\frac{1}{2}, S=\frac{3}{2}\rangle \\ |JM, L=J-\frac{1}{2}, S=\frac{3}{2}\rangle \end{pmatrix} =$$

$$\underbrace{\begin{pmatrix} a^2_+ & a^2_+ & a^1_+ & a^1_+ & 0 & 0 \\ a^2_- & -a^2_- & a^1_- & -a^1_- & 0 & 0 \\ b^3_+ & -b^3_+ & b^2_+ & -b^2_+ & b^1_+ & -b^1_+ \\ b^3_- & b^3_- & b^2_- & b^2_- & b^1_- & b^1_- \\ c^3_+ & c^3_+ & c^2_+ & c^2_+ & c^1_+ & c^1_+ \\ c^3_- & -c^3_- & c^2_- & -c^2_- & c^1_- & -c^1_- \end{pmatrix}}_{U^{J,LS}_{\lambda_1\lambda_2}(\frac{1}{2}\times 1)} \begin{pmatrix} |JM, \lambda_1=\frac{1}{2}, \lambda_2=0\rangle \\ |JM, \lambda_1=-\frac{1}{2}, \lambda_2=0\rangle \\ |JM, \lambda_1=-\frac{1}{2}, \lambda_2=-1\rangle \\ |JM, \lambda_1=\frac{1}{2}, \lambda_2=1\rangle \\ |JM, \lambda_1=\frac{1}{2}, \lambda_2=-1\rangle \\ |JM, \lambda_1=-\frac{1}{2}, \lambda_2=1\rangle \end{pmatrix}. \tag{D.15}$$

The coefficients of the matrix $U^{J,LS}_{\lambda_1\lambda_2}$ are collected in table D.2.

D.3 Parity conservation

The fact that parity is conserved in strong interactions enables to further reduce the number of permitted amplitudes. As was stated in the begining of the chapter, only a limited number of different L contribute for a given J. The limitations

Coefficient	Index +	Index −
a^1	$\frac{1}{\sqrt{3}}$	$-\frac{1}{\sqrt{3}}$
a^2	$-\frac{1}{\sqrt{6}}$	$\frac{1}{\sqrt{6}}$
b^1	$-\frac{1}{2\sqrt{2}}\sqrt{\frac{2J-1}{2J+2}}$	$\frac{1}{2\sqrt{2}}\sqrt{\frac{2J+3}{2J}}$
b^2	$\frac{1}{2\sqrt{2}}\sqrt{\frac{2J+3}{2J+2}}$	$\frac{1}{2\sqrt{2}}\sqrt{\frac{2J-1}{2J}}$
b^3	$\frac{1}{2}\sqrt{\frac{2J+3}{2J+2}}$	$\frac{1}{2}\sqrt{\frac{2J-1}{2J}}$
c^1	$\sqrt{\frac{3}{8}}\sqrt{\frac{2J-1}{2J}}$	$-\sqrt{\frac{3}{8}}\sqrt{\frac{2J+3}{2J+2}}$
c^2	$\frac{1}{2\sqrt{6}}\sqrt{\frac{2J+3}{2J}}$	$-\frac{1}{2\sqrt{6}}\sqrt{\frac{2J-1}{2J+2}}$
c^3	$\frac{1}{2\sqrt{3}}\sqrt{\frac{2J+3}{2J}}$	$-\frac{1}{2\sqrt{6}}\sqrt{\frac{2J-1}{2J+2}}$

Table D.2: Coefficients of the transformation to the JLS basis for the ρN system.

depend on the total spin of the system as $|J - S| \leq L \leq J + S$. Therefore, for the systems πN, σN, and ηN $L = J \pm 1/2$, whereas in the case of $\pi\Delta$ and ρN channels $L = J \pm 1/2$, $|J \pm 3/2|$. The total parity of the two-particle system is defined by a product

$$\eta_P = \eta_1 \eta_2 (-1)^L \,, \tag{D.16}$$

where η_1 and η_2 are the intrinsic parities of the particles. For all channels $\eta_1\eta_2 = -1$, except for the σN channel where $\eta_1\eta_2 = 1$. That leads to the following allowed transitions:

$$\begin{aligned} L_{\eta N} &= L_{\pi N}, \\ |L_{\sigma N} - L_{\pi N}| &= 1, \\ |L_{\rho N} - L_{\pi N}| &= 0 \text{ or } 2, \\ |L_{\pi\Delta} - L_{\pi N}| &= 0 \text{ or } 2. \end{aligned} \tag{D.17}$$

Appendix E

Observables

In this chapter we show how the T-matrix, which is the solution of the Lippmann-Schwinger equation, is related to the πN phase shifts and inelasticities, and to total and differential cross sections.

First we define the partial wave amplitude [108] for the transition $i \to f$

$$\tau_{fi}^{JLS} = -\pi\sqrt{\rho_f \rho_i} T_{fi}^{JLS}, \tag{E.1}$$

where

$$\rho_{i,f} = \frac{k_{i,f}}{Z} E(k_{i,f}) \omega(k_{i,f}) \tag{E.2}$$

is a kinematical factor. The $k_{i,f}$ denote initial and final c.m. momenta, and E and ω are the energies of the baryon and meson, respectively. The amplitude τ^{JLS} for $\pi N \to \pi N$ is expressed in terms of the phase shift δ and inelasticity parameter η as

$$\tau = \frac{1}{2i}(\eta e^{2i\delta} - 1). \tag{E.3}$$

The πN scattering lengths and volumes are defined as

$$a_{JLS} = \lim_{q_{\rm on} \to 0} \frac{Re(\tau^{JLS})}{k_1^{2L+1}}, \tag{E.4}$$

where k_1 is the pion c.m. momentum. The elastic πN cross section, averaged over the initial nucleon polarization, is given by

$$\bar{\sigma}_{\rm el} = S\frac{4\pi}{k_1^2} \sum_{JLS} (2J+1) \left|\tau^{JLS}\right|^2, \tag{E.5}$$

where $S = 1/2$ is the averaging factor. The optical theorem relates the total πN cross section and the imaginary part of τ^{JLS}:

$$\bar{\sigma}_{\text{tot}} = S\frac{4\pi}{k_1^2}\sum_{JLS}(2J+1)Im(\tau^{JLS}). \tag{E.6}$$

Then the inelastic cross section $\bar{\sigma}_{\text{in}} = \bar{\sigma}_{\text{tot}} - \bar{\sigma}_{\text{el}}$ becomes

$$\bar{\sigma}_{\text{in}} = S\frac{4\pi}{k_1^2}\sum_{JLS}(2J+1)\frac{1}{4}(1-\eta_{JLS}^2). \tag{E.7}$$

Evidently, $\bar{\sigma}_{\text{in}}$ is fully determined by the parameters η. The transition cross section (e.g. $\pi N \to \rho N$ and $\pi N \to \eta N$) is given by

$$\bar{\sigma} = S\frac{4\pi}{k_1^2}\sum_{JLSL'S'}(2J+1)\left|\tau_{LS}^{JL'S'}\right|^2, \tag{E.8}$$

where the amplitude $\tau_{LS}^{JL'S'}$ corresponds to the transition process. Finally, we give the expression for the differential $\pi N \to \eta N$ cross section:

$$\begin{aligned}\frac{d\bar{\sigma}_{\pi N\to\eta N}}{d\Omega} = \frac{S}{k_1^2}\frac{1}{2}&\left\{\left|\sum_J(2J+1)\left(\tau_{\pi N\to\eta N}^{J\,J-\frac{1}{2}\,\frac{1}{2}} + \tau_{\pi N\to\eta N}^{J\,J+\frac{1}{2}\,\frac{1}{2}}\right)d_{\frac{1}{2}\frac{1}{2}}^J(\theta)\right|^2\right.\\ &\left.+\left|\sum_J(2J+1)\left(\tau_{\pi N\to\eta N}^{J\,J-\frac{1}{2}\,\frac{1}{2}} - \tau_{\pi N\to\eta N}^{J\,J+\frac{1}{2}\,\frac{1}{2}}\right)d_{\frac{-1}{2}\frac{1}{2}}^J(\theta)\right|^2\right\}.\end{aligned} \tag{E.9}$$

Bibliography

[1] O. Krehl, C. Hanhart, S. Krewald and J. Speth, Phys. Rev. C **62**, 025207 (2000).

[2] H. Machner,J. Haidenbauer, J. Phys. G **25**, R231 (1999).

[3] C. Hanhart, J. Haidenbauer, A. Reuber, C. Schütz and J. Speth, Phys. Lett. B **358**, 21 (1995).

[4] V. Baru et al., in preparation.

[5] N. Fettes, U. Meißner, Nucl. Phys. **A693**, 693 (2001).

[6] B. Blankleider and G.E. Walker, Phys. Lett. B **152**, 291 (1985).

[7] R.J. McLeod and I.R. Afnan, Phys. Rev. C **32**, 222 (1985).

[8] M. Fuda, Phys. Rev. C **57**, 2149 (1998).

[9] J. Caro Ramon, N. Kaiser, S. Wetzel, W.Weise, Nucl. Phys. **A672**, 249 (2000).

[10] J. Nieves and E. Ruiz Arriola, Phys. Rev. D **64**, 116008 (2001).

[11] T. Inoue, E. Oset, M.J. Vicente Vacas, Phys. Rev. C **65**, 035204 (2002).

[12] P.F.A. Goudsmit, H.J. Leisi, E. Matsinos, B.L. Birbrair and A.B. Gridnev, Nucl. Phys. **A575**, 673 (1994).

[13] M. Batinić, I. Šlaus, and A. Švarc, Phys. Rev. C **51**, 2310 (1995).

[14] A.B. Gridnev and N.G. Kozlenko, Eur. Phys. J. A **4**, 187 (1999).

[15] T. Feuster and U. Mosel, Phys. Rev. C **59**, 460 (1999).

[16] G.Penner and U. Mosel, Phys. Rev. C **65**, 055202 (2002).

[17] B.C. Pearce and B.K. Jennings, Nucl. Phys. **A528**, 655 (1991).

[18] C. Lee, S.N. Yang and T.-S. H. Lee, J. Phys. G **17**, (1991).

[19] F. Gross and Y. Surya, Phys. Rev. C **47**, 703 (1993).

[20] C.T. Hung, S.N. Yang and T.-S. H. Lee, J. Phys. G **20**, 1531 (1994).

[21] V. Pascalutsa and J.A. Tjon, Phys. Rev. C **61**, 054003 (2002).

[22] C. Schütz, J.W. Durso, K. Holinde and J. Speth, Phys. Rev. C **49**, 2671 (1994).

[23] C. Schütz, J. Haidenbauer, J.W. Durso and J. Speth, Phys. Rev. C **57**, 1464 (1998).

[24] O. Krehl, C. Hanhart, S. Krewald, and J. Speth, Phys. Rev. C **60**, 055206 (1999).

[25] A. Gasparian, J. Haidenbauer, C. Hanhart, L. Kondratyuk, J. Speth, Phys. Lett. B **480**, 273 (2000).

[26] A. Gasparian, J. Haidenbauer, C. Hanhart, L. Kondratyuk, J. Speth, Nucl. Phys. **A684**, 397 (2001).

[27] A. Gasparyan, *Schriften des FZ-Jülich-Matter and Materials* 11, 205 (2002).

[28] R. Aaron, R.D. Amado and J.E. Young., Phys. Rev. **174**, 2022 (1968).

[29] Ulf-G. Meißner, Phys. Rept. **213**, (1998).

[30] B. Borasoy, Ulf-G. Meißner, Int. J. Mod. Phys. **A11**, (1996).

[31] J. Wess and B. Zumino, Phys. Rev. **163**, 1727 (1967).

[32] K. Kawarabayashi and M. Suzuki, Phys. Rev. Lett. **16**, 255 (1966).

[33] Fayyazuddin and Riazuddin, Phys. Rev. **147**, 1071 (1966).

[34] C. Schütz, Jülich report, Nr. 2733 (1993).

[35] V. Bernard, N. Kaiser and U. Meißner, Eur. Phys. J. A **4**, 259 (1999).

[36] S.S. Schweber, *An Introduction to relativistic Quatum Field Theory* (Harper and Row, New York, 1962).

[37] D. Schütte, Nucl. Phys. **A221**, 450 (1974).

[38] K. Kotthoff, K. Holinde, R. Machleidt and D. Schütte, Nucl. Phys. **A242**, 429 (1975).

[39] S. Weinberg, *The quantum Theory of Fields I* (Cambridge University Press, Cambridge, 1996).

[40] M.L. Goldberger and K.M. Watson, *Collision Theory* (John Wiley and Sons, New York, 1964).

[41] J.D. Bjorken and S.D. Drell, *Relativistic Quantum Mechanics* (McGraw-Hill, New York, 1964).

[42] M. Jacob and G.C. Wick, Ann. Phys. (N.Y.) **7**, 404 (1959).

[43] B. A. Lippmann and J. Schwinger, Phys. Rev. **79**, 469 (1950).

[44] R. Koch, Nucl. Phys. **A 448**, 707 (1986).

[45] R.A. Arndt, I.I. Strakovsky, R.L. Workman and M.M. Pavan, Phys. Rev. C **52**, 2120 (1995).

[46] R. Courant, D. Hilbert, *Methods of mathematical physics* (Interscience Publ., New York, 1962).

[47] N. Vinogradov, private communication.

[48] C. Lovelace, Phys. Rev. **135**, 1225 (1964).

[49] R. Machleidt, K. Holinde and Ch. Elster, Phys. Rep. **149**, 1 (1987).

[50] S. Krewald, private communication.

[51] G. Breit and E. Wigner, Phys. Rev. **49**, 519 (1936).

[52] B.C. Pearce and I.R. Afnan, Phys. Rev. C **34**, 991 (1986).

[53] C.D. Froggatt and J.L. Petersen, Nucl. Phys. **B129**, 89 (1977).

[54] W. Ochs, Dissertation, (München, 1973).

[55] B. Hyams et al., Nucl. Phys. **B100**, 205 (1975).

[56] W.N. Cottingham, M. Lacombe, B. Loiseau,J.M. Richard, and R. Vinh Mau, Phys. Rev. D **8**, 800 (1973).

[57] J.W. Durso, A.D. Jackson and B.J. Verwest, Nucl. Phys. **A345**, 471 (1980).

[58] G.E. Brown and A.D. Jackson, *The Nucleon-Nucleon Interaction* (North-Holland, Amsterdam, 1976).

[59] H. Nielsen, G.C. Oades, Nucl. Phys. **B49**, 586 (1990).

[60] G. Höhler and E. Pietarinen, Nucl. Phys. **B95**, 210 (1975).

[61] G. Hohler, F. Kaiser, R. Koch, and E. Pietarinen, Handbook of Pion-Nucleon-Scattering, Physics Data 12-1, Fachinformationszentrum Karlsruhe, 1979 .

[62] S. Mandelstam, Phys. Rev. **112**, 1344 (1958).

[63] W.R. Frazer and J.R. Fulco, Phys. Rev. **117**, 1603 (1960).

[64] P.D.B. Collins and E.J. Squires, *Regge poles in particle physics* (Springer-Verlag, Berlin, 1968).

[65] C. Schütz, K. Holinde, J. Speth, B.C. Pearce and J.W. Durso, Phys. Rev. C **51**, 1374 (1995).

[66] T.P. Cheng, R. Dashen, Phys. Rev. Lett. **26**, 594 (1971).

[67] J. Gasser, H. Leutwyler and M.E. Sainio, Phys. Lett. B **253**, 252 (1991).

[68] M.E. Sainio, LANL preprint hep-ph/0110413 (2001).

[69] O. Krehl, Jülich report, Nr. 3692 (1999).

[70] W.R. Frazer and J.R. Fulco, Phys. Rev. **117**, 1609 (1960).

[71] H.P. Noyes, Phys. Rev. Lett. **15**, 538 (1965).

[72] K.L. Kowalski, Phys. Rev. Lett. **15**, 798 (1965).

[73] D. Cohen et al., Phys. Rev. C **3**, 525 (1971).

[74] T. Mongan, Nuovo Cim. **63B**, 539 (1969).

[75] J.H. Hetherington and L.H. Schick, Phys. Rev. **137B**, 935 (1965).

[76] R. Aaron and R.D. Amado, Phys. Rev. **150**, 857 (1966).

[77] R.T. Cahill and I.H. Sloan, Nucl. Phys. **A165**, 161 (1971).

[78] E.W. Schmid and H.Z. Ziegelmann, *The Quantum Mechanical Three-Body Problem* (Pergamon Press, Oxford, 1972).

[79] D.D. Brayshaw, Phys. Rev. **176**, 1855 (1968).

[80] G. Janßen, K. Holinde and J. Speth, Phys. Rev. C **54**, 2218 (1996).

[81] K. Nakayama, A. Szczurek, C. Hanhart, J. Haidenbauer and J. Speth, Phys. Rev. C **57**, 1580 (1998).

[82] J.W. Durso, Phys. Lett. B **184**, 348 (1987).

[83] C. Schütz, Jülich report, Nr. 3130 (1995).

[84] G.E. Brown and W. Weise, Phys. Rep. **22**, 279 (1975).

[85] G. Janßen, B.C. Pearce, K. Holinde and J. Speth, Phys. Rev. D **52**, 2690 (1995).

[86] O. Krehl and J. Speth, Nucl. Phys. **A623**, 162c (1997).

[87] S. Weinberg, Phys. Rev. Lett. **17**, 616 (1966).

[88] Y. Tomozawa, Nuovo Cim. **46A**, 707 (1966).

[89] K. Hagiwara et al., Phys. Rev. D **66**, 010001 (2002).

[90] R. Koch and E. Pietarinen, Nucl. Phys. **A336**, 331 (1980).

[91] *Handbook of Physics, Landolt–Börnstein*, Hrsg. H. Schopper (Springer Verlag, Berlin, 1987), Vol. 12/a.

[92] A.D. Brody et al., Phys. Rev. D **4**, 2693 (1971).

[93] R.M. Brown et al., Nucl. Phys. **B153**, 89 (1979).

[94] F. Bulos et al., Phys. Rev. Lett. **13**, 486 (1964).

[95] F. Bulos et al., Phys. Rev. **187**, 1827 (1969).

[96] W. Deinet et al., Nucl. Phys. **B11**, 495 (1969).

[97] J. Feltesse et al., Nucl. Phys. **B93**, 242 (1975).

[98] B.W. Richards et al., Phys. Rev. D **1**, 10 (1970).

[99] C. Hanhart, K. Nakayama, Phys. Lett. B **454**, 176 (1999).

[100] G.Penner and U. Mosel, LANL preprint nucl-th/0207066(2002).

[101] N.C. Debenham et al., Phys. Rev. D **12**, 2545 (1975).

[102] A. Sibirtsev, S. Schneider, C. Elster, J. Haidenbauer, S. Krewald and J. Speth, Phys. Rev. C **65**, 044007 (2002).

[103] V. Y. Grishina *et al.*, Phys. Lett. **B475**, 9 (2000).

[104] H. Garcilazo und M. T. Pena, Phys. Rev. **C61**, 064010 (2000).

[105] S. Wycech und A. M. Green, Phys. Rev. **C64**, 045206 (2001).

[106] D.M. Manley, R.A. Arndt, Y. Goradia and V.L. Teplitz, Phys. Rev. D **30**, 904 (1984).

[107] D.M. Brink and G.R. Satchler, *Angular Momentum* (Oxford Library of the Physical Sciences, Oxford, 1968).

[108] C.J. Joachain, *Quantum Collision Theory* (North-Holland Publishing Company, Amsterdam, 1975).

Forschungszentrum Jülich
in der Helmholtz-Gemeinschaft

Jül-4015
November 2002
ISSN 0944-2952

Acknowledgments

I would like to thank Prof. J. Speth for giving me the opportunity to work on this thesis in the Jülich theory group. Owing to a friendly working atmosphere I was able to gain an invaluable (though theoretical) scientific experience.

I am grateful to Leonid Kondratyuk from whom I learned a lot about how to orient myself in the world of theoretical physics and how to analyze extremely complicated problems in a simple way. I also wish to express my thanks to Alexander Kudryavtsev, who opened my eyes to many comic sides of science (and real life), that enabled me to clearly separate the serious part of occurring problems.

My gratitude goes to Dr. J. Haidenbauer, Dr. Ch. Hanhart, Prof. S. Krewald, Prof. L. Kondratyuk, and Prof. A. Kudryavtsev for many fruitful discussions of my work.

I am indebted to Dr. J. Haidenbauer and Dr. Ch. Hanhart for a careful reading of this thesis.

The accomplishment of this work was possible thanks to the financial support of the Forschungszentrum Jülich, and in particular the Institute for Nuclear Physics.

I wish to thank all my Jülich friends – Vadim, Igor, Dima, and others. Meeting them led to a lot of funny situations making workaday routine not hard at all. My special thanks to Andreas for an inestimable contribution to my cultural education.

I want to thank the table tennis club of the Forschungszentrum Jülich and all its members that allowed me to be always in a good physical shape for thinking.

Finally, I would like to say thanks to my family, which has always supported my enthusiasm in science.